Master's thesis

NTNU
Norwegian University of Science and Technology
Faculty of Engineering
Department of Marine Technology

Olav Røthe Kyte

Design of Mooring Systems For Floating Wind Turbines in Shallow Water

Master's thesis in Marine Technology

Supervisor: Kjell Larsen

June 2020

NTNU
Norwegian University of
Science and Technology

Olav Røthe Kyte

Design of Mooring Systems For Floating Wind Turbines in Shallow Water

Master's thesis in Marine Technology
Supervisor: Kjell Larsen
June 2020

Norwegian University of Science and Technology
Faculty of Engineering
Department of Marine Technology

NTNU
Norwegian University of
Science and Technology

NTNU Trondheim
Norges teknisk-naturvitenskapelige universitet
Institutt for marin teknikk

MASTER THESIS SPRING 2020

for

Stud. tech. Olav Røthe Kyte

Design of mooring systems for floating wind turbines in shallow water

Design av forankringssystemer for flytende vindturbiner på grunt vann

Background

In the development of floating wind turbines (FWTs) for utilizing the offshore wind resource, various technologies from the offshore oil and gas (O&G) industry have been adopted, including mooring system solutions. The purpose of the mooring system is to keep the floating wind turbine safely at a required position. It normally consists of three mooring lines of chain. Compared to O&G installations, FWTs tend to be significantly smaller. The external loads are characterized with large mean loads (due to the rotor thrust) in moderate wave conditions and high wave motions in extreme wave conditions.

The importance of the mooring system for a floating wind turbine is crucial. The moorings must be reliable enough to prevent any free drift where cable rupture and collisions are typical consequences and the cost of mooring must be as low as possible in order to make such developments profitable. Optimization of the mooring system is therefore an important task. Mooring systems for shallow water, typically for water depth in the range 50-100m, is a challenging task. Feasibility of such systems will, however, open-up large new areas where fixed turbines of the monopile type become too expensive.

The overall objective of this thesis is to study mooring system design for FWTs and to optimize such systems for shallow water. This includes mooring system concepts and building blocks as well as design methods and requirements stated in rules and regulations.

Scope of Work

1) Review relevant literature and give a brief overview of floating wind turbine concepts. Describe possible mooring and station keeping systems for floating units in general and floating wind turbines in particular. Focus on station keeping principles and main hardware components.

2) Describe the design limit states for mooring systems of floating wind turbines with corresponding acceptance criteria outlined in rules and regulations (use DNVGL-ST-0119).

3) Describe the time-domain analysis methods for mooring systems and how extreme wind turbine motions and line tension can be estimated. Theory to be based on the SIMO/SIMA software suite and respective theory and user manuals.

4) Familiarize with and improve an existing, simplified SIMA model of a CSC 10MW FWT, with the objective of performing numerical time-domain simulations of wind turbine motions

and mooring line tensions. Include a mooring system for a water depth of 80m water depth in the model. The system can be based on the present "Hywind Scotland" mooring system. Perform pull-out and decay tests do document the dynamic system.
Numerical simulations to document the ULS compliance shall also be performed.

5) Optimization and comparison of alternative concepts for a water depth of 80m. Assess if the selected "Hywind Scotland" mooring system can be improved by use of synthetic components and/or clump weights and buoys. The extent of this activity to be agreed with supervisor.

6) Conclusions and recommendations for further work.

General information

All necessary input data for the simulation case is assumed to be provided by NTNU/Equinor. The work scope may prove to be larger than initially anticipated. Subject to approval from the supervisor, topics may be reduced in extent.
In the thesis, the candidate shall present his personal contribution to the resolution of problems within the scope of work.
Theories and conclusions should be based on mathematical derivations and/or logic reasoning identifying the various steps in the deduction.
The candidate should utilise the existing possibilities for obtaining relevant literature.

Report/Delivery
The thesis report should be organised in a rational manner to give a clear exposition of results, assessments, and conclusions. The text should be brief and to the point, with a clear language. Telegraphic language should be avoided.

The thesis report shall be written in English and edited as a research report including literature survey, description of relevant mathematical models together with numerical simulation results, discussion, conclusions and proposal for further work. List of symbols and acronyms, references and (optional) appendices shall also be included. All figures, tables and equations shall be numerated.

The original contribution of the candidate and material taken from other sources shall be clearly defined. Work from other sources shall be properly referenced using an acknowledged referencing system.

The report shall be submitted in Inspera, as specified by the department of Marine Technology. In addition, an electronic copy (pdf) to be sent to the supervisor.

Ownership
NTNU has according to the present rules the ownership of the thesis results. Any use of the thesis results has to be approved by NTNU (or external partner when this applies). The department has the right to use the results as if the work was carried out by a NTNU employee, if nothing else has been agreed in advance.

Thesis supervisor**:**
Prof. II Kjell Larsen, NTNU/Equinor

Deadline: June 10th, 2020

Trondheim, January 31st, 2020

Kjell Larsen (sign)

Olav Røthe Kyte (sign)

Preface

This thesis is the final part of my master's degree in Marin Technology with a specialization in marine hydrodynamics. The thesis has been completed at the Norwegian University of Science and Technology at the Department of Department of Marin Technology with all necessary input data for the simulation case provided by NTNU and Equinor. The last two years have been both challenging and rewarding, and I am today proud of what I have accomplished.

I want the opportunity to express my gratitude to my supervisor, Professor Kjell Larsen, for his guidance and encouragement over the last year. I have truly benefited from our weekly meetings, and I am grateful for the increased insight in hydrodynamics and marine operation you have provided me.

I want to thank George E. Katsikogiannis and Erling Neerland Lone for their help on the SIMO/RIFLEX-model. Last, I must thank my family and friends for the support and encouragement throughout my time as a student.

Trondheim, June 10, 2020

Olav Røthe Kyte

Abstract

The overall objective of this thesis is to study mooring system design for FWTs and to optimize such systems for shallow water. This includes mooring system concepts and building blocks as well as design methods and requirements stated in rules and regulations. The analysis will conducting in the time domain and simulated in SIMA for different load cases determined by the operational state of the turbine. One of the goals in the project has been to simplify an excisiting SIMO/RIFLEX model of the CSC10MW FWT, with the objective of reducing the computational effort needed for each simulation. This has been achieved by removing the wind turbine, and modifying the kinematics of the semi-submersible. The aerodynamic load has successfully been implimented by using a quadratic wind coefficient which encounter for both tower drag and rotor thrust.

A total of eight mooring systems, distributed over four mooring line configuration, is proposed. The initial mooring design, is a chain catenary system based of the present mooring system at Hywind Scotland. The second and third configuration uses polyester mooring line in combination with buoy and clump weight to add geometric stiffness and reduce the risk of slack(zero line tension). To determine the effect of diameter reduction and choice of axial stiffness model, will several sub systems be tested for comparison reasons. The last configuration will be using nylon with a linear axial stiffness model. This configuration consisted only of one buoy to prevent contact between the seabed and the rope, take full advantage of the elastic stiffness.

The weather configurations are based on data Metocean data from the Hywind Buchan Deep operation site, with two load cases during operational state, and two extreme conditions. The extreme weather conditions are determined by the 50 and 10-year return period of mean wind and current speed respectively. The wave condition are based on the 50-year Hs-Tp contour plot.

The feasibility of the systems are mainly determined by the design tension with respect to the ULS requirement outlined in DNVGL-ST-0119 *Floating wind turbine structures*. The dynamic responses has been studied with respect structure motion and top end line tension. The system characteristics in surge and natural period in surge, heave, pitch and yaw, has also been documented.

The results from the analysis show that a mooring system with synthetic ropes are possible for water depth of 80m. The issue with diameter reduction are related to extreme offsets and not design tension. The choice of stiffness model will be off great importance when modelling a polyester system.

Sammendrag

Det overordnede målet med denne oppgaven har vært å studere forankringsdesignet av flytende havvindmøller. Dette inkluder en studie av ulike typer forankring, samt studere ulike design metoder og designkrav. Analysene vil bli utført i tidsdomenet og simulert i SIMA for lasttilfeller basert på den operasjonelle tilstanden på vindturbinen. Et delmål med oppgaven har vært å forenkle en allerede eksisterende SIMO/RIFLEX-modell av CSC10MW havvindmøllen med det formål å redusere tiden det tar å gjennomføre en simulering. Dette er blitt oppnådd ved å fjerne selve vindmøllen for deretter å modifisere kinematikken til den halvt nedsenkbare plattformen. Vindkreftene har med suksess blitt implementert ved bruk av en kvadratisk vindkoeffisient som har høyde for dragkreftene på tårnet og skyvekraften fra rotoren.

Totalt har åtte forankringssystemer, fordelt på fire line konfigurasjoner, litt foreslått. Det første systemet består av kjetting og baserer seg i stor grad på forankringssystemet brukt i Hywind Scotland prosjektet. Den andre og tredje konfigurasjonen benytter seg av polyesterliner i kombinasjoner med klumpvekt og oppdriftsbøye for å tilegne system en geometrisk stivhet, samt redusere risikoen for slakk (null linestrekk). Flere av systemer benytter seg av denne konfigurasjonen for å kunne dokumentere effen av å redusere diameteren og valg av stivhetsmodell for linene. Den siste konfigurasjonen benytter seg av nylontau med linear stivhetsmodell. Det er her kun benyttet oppdriftsbøye for å hindre at tuet kommer i kontakt med havbunnen og for å utnytte de elastiske egenskapene til tauet.

Værsammensettingene baserer seg på værdata fra Bunchan Deep området og inneholder to lasttilfeller der turbinen enda er i operasjonell tilstand, og to ekstremtilfeller hvor turbinen er parkert. Ekstremtilfeller baserer seg på forventet 50 og 10 års returperiode for gjennomsnittlig vind og strømhastighet. Bølgesammensetningen er gitt av konturplottet for Hs og Tp verdien for 50 års returperiode.

Kvaliteten på system vil bli bedømt ut ifra design-linestrekket med hensyn til ULS kravene gitt i *DNVGL-ST-0119 Floating wind turbine structures*. De dynamiske responsene med hovedvekt på strukturbevegele og linestrekk har også blitt vektlagt og analysert. Systemkarakteristikken i jag, samt egenperioden i jag, hiv, stamp og gir er dokumentert.

Resultanten viste at det er mulig å designe et fibersystem for vanndyp på 80meter i henhold til kravene det har blitt testet for. Utfordringene med å redusere diameteren har vist seg å være knyttet til store forflytninger og ikke så mye til linestrekket. Valget av stivhetsmodell har også vist seg å være avgjørende med tanke på maka tillatt forflytning fra utgangsposisjonen.

Nomenclature

Abbreviations

ALS	Accidental limit state
ASL	Above sea level
DAF	Dynamic amplification factor
DP	Dynamic position
FFT	Fast Fourier Transformation
FLS	Fatigue limit state
FWT	Floating wind turbine
LC	Load case
MBS	Minimum breaks strength
MPM	Most probable maximum
Std	Standard deviation
ULS	Ultimate limit state

Variables

ε	Elongation
γ_{dyn}	Dynamic load factor
γ_{mean}	Mean load factor
μ	Mean value
ϕ	Mooring line angle
σ	Standard deviation
A	Cross-section area $[m^2]$
a	Moment arm $[m]$
C_D	Drag coefficient

C_{wind}	quadratic wind coefficient
E	Young's modulus $[N/m^2]$
F_d	Drag force $[N]$
g	Gravitational acceleration=9.81 $\mathrm{m/s^2}$
h	Water depth $[m]$
H_s	Significant wave height [m]
$I_{x,y,z}$	Mass moment of inertia about x, y or z-axis $[kgm^2]$
K_e	Elastic stiffness $[N/m^2]$
K_g	Geometric stiffness $[N/m]$
K_{tot}	Total stiffness $[N/m]$
L	Length $[m]$
M	Moment [Nm]
m	Mass of given component $[kg]$
r	[Distance to parallel axis
s	Length of mooring line between fairing and seabed $[m]$
T	Axial line tension $[N]$
T_d	Design tension $[N]$
T_H	Horizontal line tension $[N]$
T_n	Natural period
T_p	Peak period [s]
T_V	Vertical line tension $[N]$
T_{C-env}	The characteristic environmental tension [N]
T_{dyn}	Dynamic line tension $[N]$
T_{mean}	Mean line tension $[N]$
T_{pret}	The line pretension [N]
U_{10}	Wind speed 10m above sea level [m/s]
w	Mass per unit length of submerged line $[kg/m]$
Ww	weight of submerged line $[N]$

Table of Contents

List of Tables

List of Figures

Chapter 1

Introduction

1.1 Background

With a global focus on reducing greenhouse gas emissions and an increased reliance on electricity, offshore wind development has been developing rapidly over the last 10-15 years. Back in 2013, the global installed capacity for offshore wind was around 6.5GW and exclusively related to bottom fixed turbines. If we look at Europa alone, are the annual offshore wind installations by country and cumulative capacity given in megawatt presented in Figure 1.1, and clearly shows a growing market for offshore wind energy.

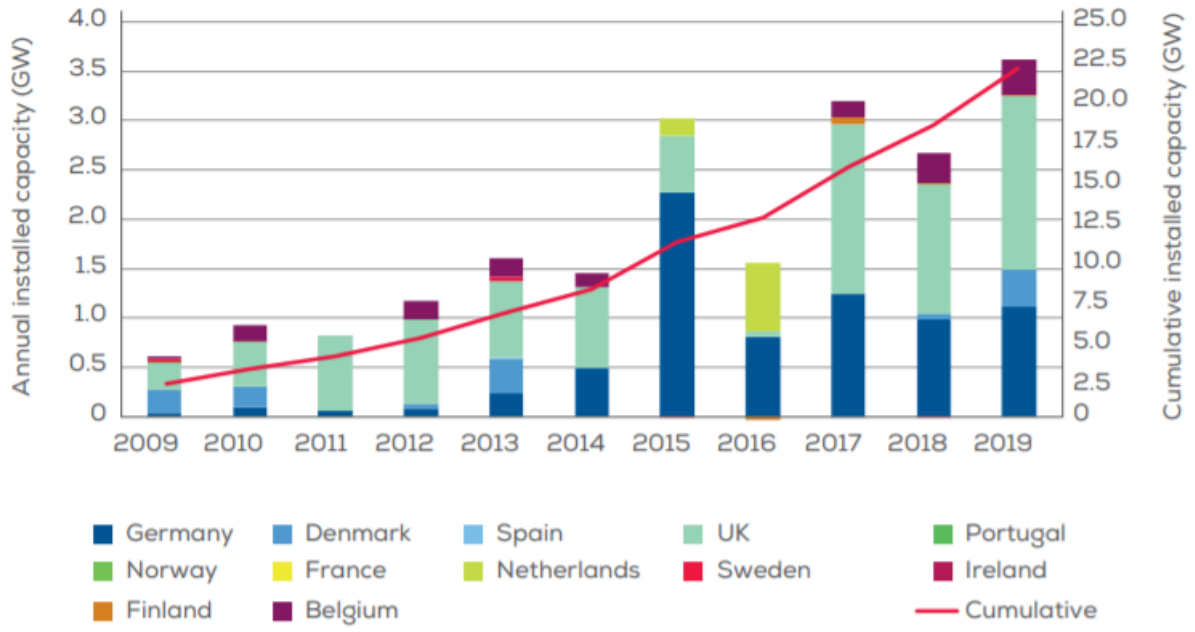

Figure 1.1: Installations and cumulative capacity by country [4]

Offshore wind turbines have offered an opportunity to provide green energy and have many advantages compared to onshore wind energy. Some of them are related to larger available areas to a low cost and visual impact, but also larger wind speeds with lower turbulence and feasible transportation of large components are in favor of offshore wind energy production.

Due to the limited access to feasible production sites for bottom fixed wind production in countries like the US, Japan and Norway, have wind energy production been confined to only a few countries. However, after Equinor opened the first floating wind park outside the coast of Scotland in 2017, many stakeholders have predicted that offshore wind will experience a boom in the development of floating wind parks in the years to come. In the development of floating wind turbines, the companies have utilized technologies from the offshore oil and gas (O&G) industry. Several concepts have been developed and can mainly be characterized by their methods of achieving static stability. Today the dominant types are semi-Submersibles, tension leg platforms (TLPs) and spar, which are all known from the O&G industry and scaled to fit a wind turbine. Most of these are still only concepts, and Hywind Scotland is still the only floating wind park in operation today, with only 9 FWT's grid-connected at the end of 2018 in the EU as a whole, see Figure 1.2. Nevertheless, more and more projects are being proposed, and last year Enova awarded Equinor 2.3 billion NOK to help finance the 88MW floating wind farm, Hywind Tampen. Equinor is also involved in the planning of a deepwater wind park outside the coast of California, and Japan has since 2011 been planning on building a pilot wind park outside Fukushima.

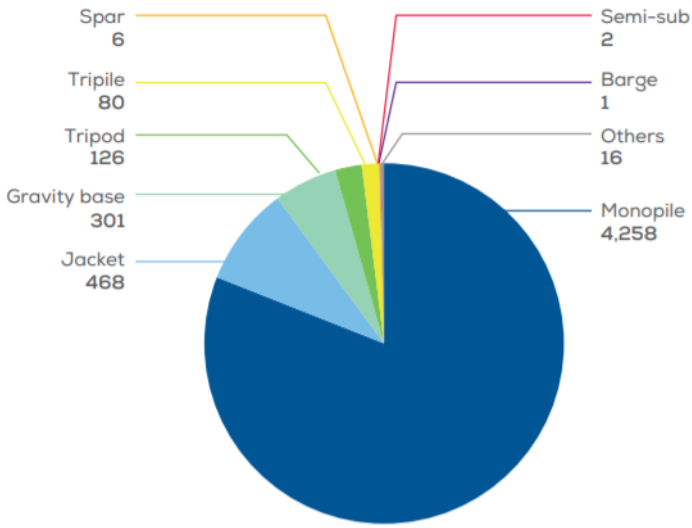

Figure 1.2: Share of substructure types for grid-connected wind turbines at the end of 2018[4]

In addition to the substructure, has also the mooring system been adopted from the O&G industry to keep the floating wind turbine safely at a required position where cable rupture and collisions are common consequences. The cost of the mooring system is also important in making the development of floating wind turbines profitable. The mooring system for floating wind turbines usually consists of a spread catenary system with three mooring lines and has proven to be a challenging task. Hence, by examining the feasibility of low modulus ropes such as synthetic rope, could this help designing a more cost-effective solution for station keeping, which would open up vast areas where fixed turbines of the monopile type become too expensive.

1.2 Scope of work and report outline

The overall objective of this thesis is to gain a greater understanding of the behavior of floating wind turbines and how this is affected by the mooring system, with the aim to optimize such a system for shallow water operations. This involves performing a literature study of different station keeping systems for floating units in general and floating wind turbines in particular. It should also be looked into design limit state from industry standards and especially DNVGL-ST-0119[1] which covers the structural design of floating wind turbine structures. The analysis will be conducted in SIMA Workbench, and it is decided to use an existing SIMO/RIFLEX-model of the CSC10MW FWT which are previously used to perform fully integrated dynamic analysis. In order to reduce the computational effort, simplification of the model should be made. The mooring line tension will mainly be affected by the drag on the line and top end motion at the fairlead. Hence, it is essential that the simplified model is able to recreate the behavior expected from a full-scale FWT.

The mooring line will be attached to the model at fairleads located 15m beneath SWL, resulting in an effective water depth of 65m. The initial mooring design should be based on the present ”Hywind Scotland” system, while alternative systems where synthetic rope, buoys and/or clump weights could be utilized. Each system should then be analyzed to verify the feasibility and compared against each other. The analysis should include a decay test and a pull-out test to determine the characteristics of the system, and numerical simulations for different load cases to document the ULS compliance of the systems.

The project report is structured in the following way:

- Chapter 2-4 provides the theoretical background needed to understand the behaviour of the systems and how these can be be predicted. It will be given a description of the characteristics of the catenary and taut mooring systems where key components like mooring lines and anchors will be further discussed. A description of how short-term statistics can be used to determine he design tension will be given together with the ULS requirement from *DNVGL-ST-0119 Floating wind turbine structures*. The equation of motion will be thoroughly discussed, and a brief description of how SIMA can be used in time domain analysis.

- Chapter 5-7 covers the proposed mooring systems, the load cases which these systems should be tested for, and process of simplifying the exciting SIMO/RIFLEX model. The latter will involve documentation of how the simplification where made with respect to retaining the kinetics of the original model, and how the wind load are implemented. It will also contain description of how the pull-out and decay tests are performed, and how these are used to verify the new model.

- Chapter 8 contains a presentation and discussion of the result obtained from the time domain analysis of each systems for all load cases. It start out with general comparison of the natural period together with extreme and mean statistics, before it is given a more detailed discussion on system characteristics and dynamic behavior.

- Chapter 9 gives some concluding remarks and suggestions for further work.

Chapter 2

Mooring Systems

For floating units will a precise and reliable station keeping system be vital for the planning of safe and effective operations. The station-keeping systems commonly used today are split into three categories; The first category is a mooring system, which uses mooring lines for positioning. We also have dynamic positioning (DP) systems that use thrusters and propellers to achieve the desired position. Lastly, we have the thruster assisted mooring system, which is a hybrid solution of the two. However, it will in this project be emphasized on the mooring system and in the following section, we will be looking at the different aspects of the mooring design concerning; layout, load mechanisms and hardware components.

2.1 Mooring Design

The design of the mooring system will be a trade-off between offset limitations, instability, weight and operational lifetime. Typical arrangement of mooring systems are presented in Figure 2.1, where the number of mooring lines will depend on the floating unit and operational time. To gain a further understanding of the different arrangements' performance characteristics, we must first understand the basic mechanics of a mooring line.

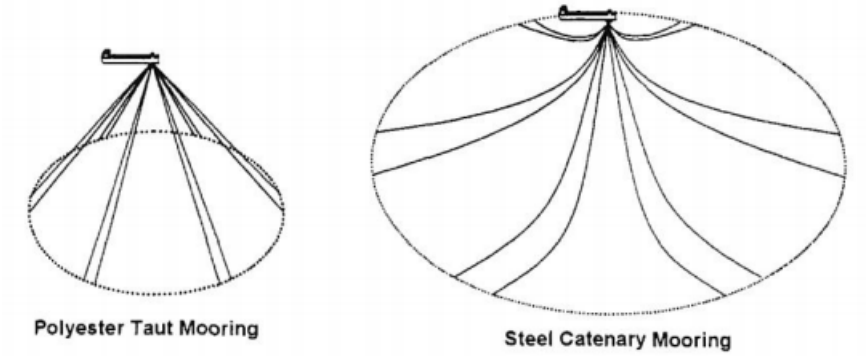

Figure 2.1: Taut and catenary mooring spread[5]

2.1.1 Catenary system

The catenary system has traditionally been the preferred arrangement when it comes to the mooring design of a wide range of floating units. It has its name from the geometrical shape of the mooring line, see Figure 2.2. Several mooring lines are spread and pre-tensioned while it in the bottom end lies along the seabed to get a horizontal pull on the anchor. This is a well-tested system that has proven to be well suited for a broad range of water depths. However, when water depth increases, so does the length of the mooring lines, and the system's weight increases. This results in a reduction of the working payload for the structure, and steel wires and synthetic rope has been preferred used due to its high elasticity and lower weight.

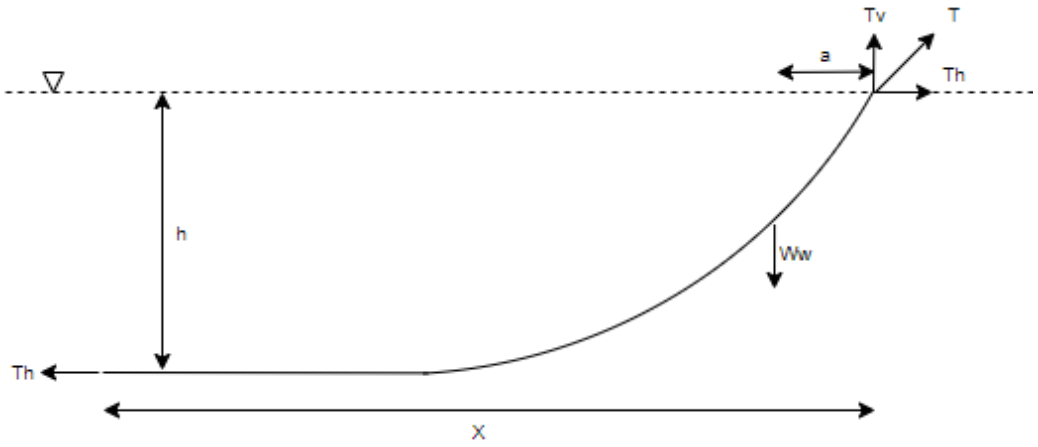

Figure 2.2: Catenary line

The catenary system provides stiffness through the geometric and elastic properties of the mooring lines and controls the mean offset and low-frequency motion of the floating unit. The total stiffness is given by:

$$\frac{1}{K_{tot}} = \frac{1}{K_g} + \frac{1}{K_e} \tag{2.1}$$

Where K_g is the geometric stiffness and K_e is the elastic stiffness. However, for a chain mooring line will the geometric stiffness be dominant, and looking at Figure2.2 it is possible to find the stiffness from the change in the horizontal force:

$$T_H = \frac{W_W a}{h} \tag{2.2}$$

Where W_W is the weight of the submerged line between fairlead and seabed, a is the moment arm for the resulting vertical force (W_W) and h is the water depth. When the floating unit gets a displacement as shown in Figure 2.3, will the change in a and Ww result in a change in T_H and the geometric stiffness is determined by:

$$Kg = \frac{T_H - T_{H0}}{\Delta x} \tag{2.3}$$

Where Δx is a displacement in the horizontal plane.

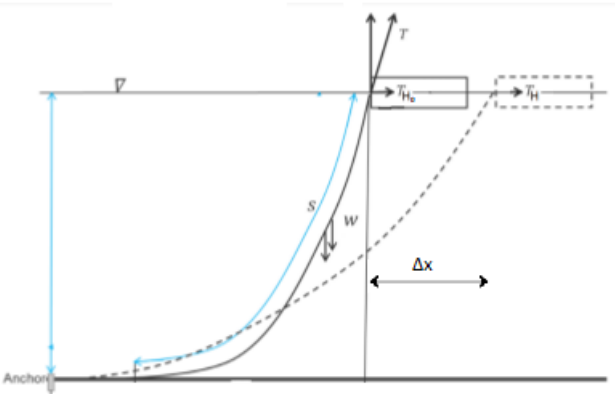

Figure 2.3: Catenary line with different offsets

The mean hydrodynamic forces acting on a unit length of the mooring line are represented by a normal force, D, and a tangential force, F, in Figure 2.4. We can then calculate the static equilibrium in the tangential direction as:

$$dT = \left[w \cdot \sin\varphi - F\left(1 + \frac{T}{EA}\right)\right] \cdot ds \tag{2.4}$$

and in normal direction as:

$$T \cdot d\varphi = \left[w \cdot \cos\varphi + D\left(1 + \frac{T}{EA}\right)\right] \cdot ds \tag{2.5}$$

Here expressed by line tension, T, weight per unit length in water, w, and axial stiffness, EA.

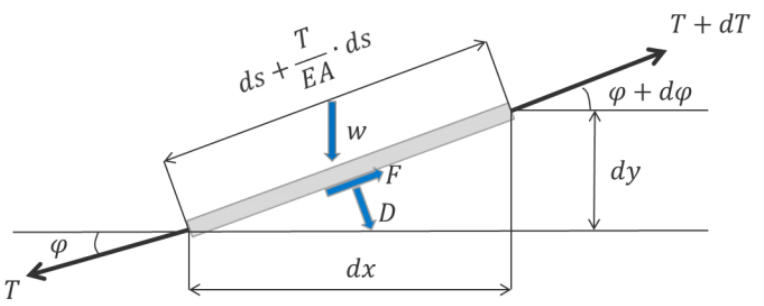

Figure 2.4: Forces acting on mooring line element, [6]

By neglecting current forces, $F = D = 0$, and assuming an inelastic mooring line, $\frac{T}{EA} \approx 0$, Equation 2.4 and 2.5 is reduced to:

$$dT = w \cdot \sin\varphi \cdot ds \tag{2.6}$$

$$T \cdot d\varphi = w \cdot \cos\varphi \cdot ds \tag{2.7}$$

Further references are made to *Sea loads on ship and offshore structures* by Faltinsen [19], but the following relations are obtained for the 2D system in Figure 2.5 (note that T_H and T_V are presented as T_x and T_y in this figure):

$$T_0 = T_H = T\cos\varphi \tag{2.8}$$

$$T_V = w \cdot s \tag{2.9}$$

$$s = \sqrt{h^2 + 2h\frac{T_H}{w}} \tag{2.10}$$

Where h is the water depth. The horizontal distance between the anchor and the mooring line connection point on the floating unit is:

$$X = l + \frac{T_H}{w} \cdot \cosh^{-1}\left(1 + \frac{wh}{T_H}\right) - \sqrt{h \cdot \left(h + \frac{2T_H}{w}\right)} \tag{2.11}$$

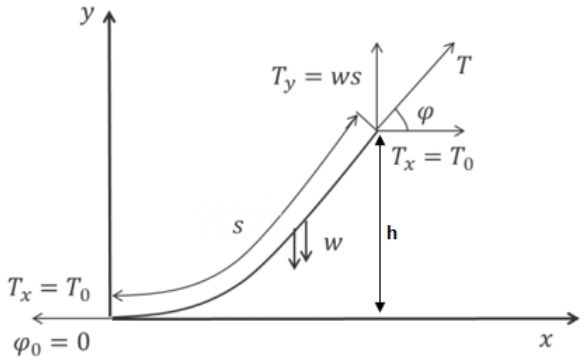

Figure 2.5: 2D mooring line with symbols.

2.1.2 Taut system

The most significant difference between the catenary system and the taut system is the angle in which the mooring line approaches the anchor. As mentioned, will the line tension be pulling the anchor in a horizontal direction, while a taut line will be pulling with both a horizontal and vertical direction. The taut system came as a result of the increasingly deeper oil and gas production, where the heavy chains in a traditionally catenary system became a limiting factor in the design of the floaters. The solution became to use synthetic fiber lines, which have a higher elasticity than traditional chain-lines. Then stiffness will then be generated mainly by the axial stiffness, as seen in Equation 2.12.

$$K = \frac{EA}{L} \tag{2.12}$$

Where E is the Young's modulus, A is the cross-section area and L is the length of the mooring line

2.2 Components

The different components of a mooring system are mainly hardware component such as;

- Mooring line consisting of chains, steel wire and/or synthetic fibre rope.

- Anchors.
- Connection links.
- Buoys or clump weights.

2.2.1 Mooring lines

Chain: The use of chains has historically been the preferred choice when it comes to the mooring of offshore structures in relatively shallow water. This is due to the characteristics concerning good abrasion, strength and the fact that it is easy to handle. There are mainly two types of chain-links in use today and these are presented in Figure 2.6. The first one is the ”Stud-link” and as the name implies has a stud across the chain-ring, providing it with extra stability and strength. The second one in a so-called open link, or stud-less link, which has a lower weight per unit length, but is also less convenient to handle compared to the stud-link. When it comes to chain size, will it be specified by the nominal diameter, seen as the *D* in Figure 2.6.

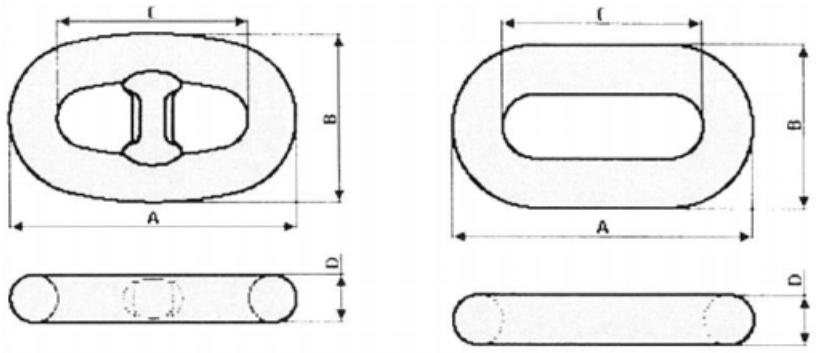

Figure 2.6: Stud-Link (left) and Studless (right) [5].

Steel Wire Rope: These are often combined with chains at the top and along the seabed to avoid fatigue when steel wire ropes are used as a mooring line. Like regular rope, is the wire rope constructed by individual steel wires wound in a helical pattern to form what one calls ”strands,” where the pitch determines the stiffness and flexibility. How the strands are organized varies, but the wire ropes commonly used in mooring are the six-strand (or multi-strand) and spiral strand cables, see Figure 2.7.

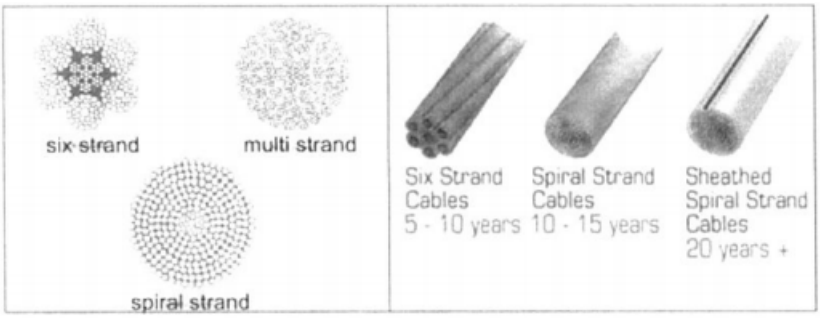

Figure 2.7: Wire rope construction, [5]

The preferred type of cable depends on the planed mooring lifetime. For shorter periods are the six-strand cables favored due to its handling ability during installation. This cable type is commonly subdivided into three classes;

- 6 x 7 Class, 7 wires per strand
- 6 x 19 Class, 16-27 wires per stand
- 6 x 37 Class, 27-49 wires per stand

The spiral strand or single strand cable is more favorable for more permanent offshore structures like production platforms. This cable is built up by helix layers with alternating direction to provide torque balance and prevent twisting. Over time, will corrosion be of increased concern, and zinc filler wire, galvanized wire or plastic sheet are used to reduce this risk.

Synthetic Fibre Rope: Much like steel wire rope, has synthetic fiber rope proven to have many advantages compared to chains when it comes to deepwater mooring systems. The synthetic fiber material in use today is polyesters, aramid, and hmpe with polyester completely dominating the market. Fiber ropes are close to neutrally buoyant, which decreases the vertical pull from the mooring line on the structure. As described previously in this section, polyester ropes are commonly used in pure taut systems where the total stiffness is dominated by the axial stiffness of the mooring lines. One of the challenges has been the modelling of such systems due to limited understanding of the complexity of the material's behaviour. However, in recent researches, manufacturers and organizations like DNV-GL have tried to improve the methods for safe and reliable design of fiber rope mooring systems. The starting point of these studies has typically been the spring-dashpot model seen in Figure 2.8 where the model has been given an elastic and a permanent stretch. The model itself is not well applicable unless all the characteristics of the various components are quantified, but it shows us that the length varies with the rate and duration of loading.

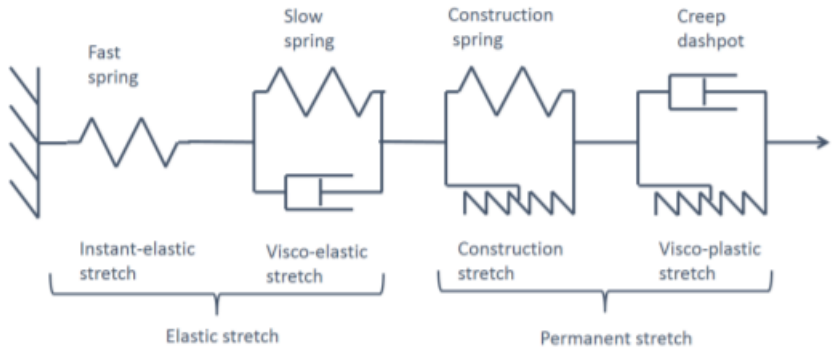

Figure 2.8: Dash-pot model[7]

The conservative method of designing polyester mooring systems has been to use an upper and lower bound axial stiffness to determine mean offset and maximum line tension. However, based on extensive testing on change-in-length behavior in the Syrope JIP project[7] led by DNV GL, do we now have a better understanding of the behavior of synthetic polyester ropes. What they managed to find out was that the length om the rope is mainly determined by the

mean tension, and that the change in length follows the curve in Figure 2.9. On this basis they managed to come up with the Syrope model presented in Figure 2.10 with further references to each line presented in the Syrope JIP project-rapport[7].

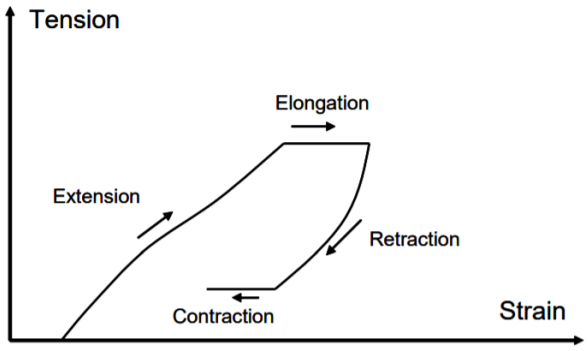

Figure 2.9: Expression of fibre rope change-in-length[7]

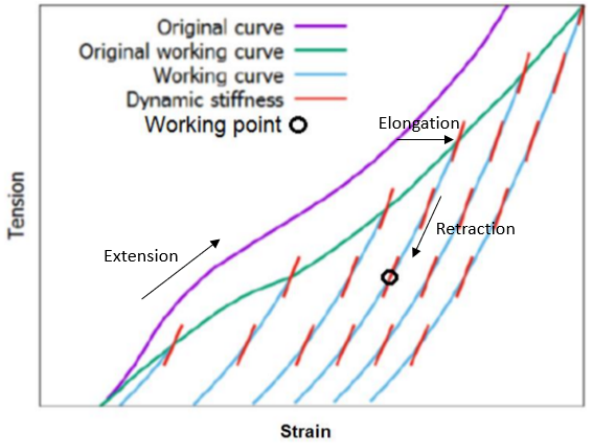

Figure 2.10: Syrope model[8]

The extension and elongation will be affected by the installation process to achieve the correct working curve, and will not be further considered in this thesis. The region of interest in this thesis is the region marked as ”working point” in Figure 2.10. The static stiffness will determine the stiffness in this region following the non-linear working curve and the linear dynamic stiffness curve(red curve). The static stiffness describes the relation between mean tension and mean strain as a result of mean environmental loads, making it possible to estimate a mean offset. The dynamic stiffness on the other hand, is applied for the wave frequency and low-frequency loads, and is therefore frequency-independent and linearly dependent on mean line tension.

In Table 2.1 are the key advantages and disadvantages for the different types of mooring lines commonly used offshore industries summarized.

Table 2.1: Advantages and disadvantages types of mooring lines.

Mooring line type	Advantages	Disadvanteges
Steel chain	- Well testen. - Good resistance to wear and tear.	- Large weight and vertial pull on structure.
Steel wire rope	- Easy to install. - Relatively low weight.	- Reduced resistance against wear and tear. - Prone to material fatigue.
Synthetic fibre rope	- Easy to install. - Near neutrally byouant. - Flexible.	- No resistance to wear and tear from seabed contact. - Complex material beaviour.

2.2.2 Anchors

A mooring design will also involve selecting which anchor is best suited and therefore has to be decided on a case to case basis. This decision will depend on different factors, but the most impotent one is the actual ground conditions on the operation. It will now be given a brief description of the most commonly used anchors for floating unites with reference to Vryhof anchors manual [9].

Drag embedment anchor is the most commonly used anchor for floating offshore units today. The anchor's holding capacity comes from the soil's resistance in front of the anchor as the anchor is either partly or fully penetrating the seabed. This anchor is very well suited for horizontal load, but has weaknesses when it comes to vertical pulling forces and is therefore better suited for catenary system then taut line system.

Figure 2.11: Drag embedment, [9]

Vertical loaded anchor has come up as an alternative to the drag embedded anchor. The installation process is very similar to the embedded one, but it penetrates much deeper into the sea bed. This results in a more considerable holding resistance in the vertical direction in combination with the horizontal direction.

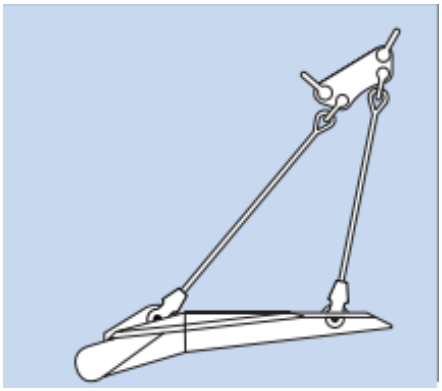

Figure 2.12: vertical loaded, [9]

Pile anchor are hammered or vibrated into the seabed and consists of a hollow steel pile. The holding capacity is generated by the soil resistance, but also by friction between the soil and the pipe. This makes it capable of withstanding both horizontal and vertical loads for sufficiently long piles. The anchor is usually connected to the anchor line with a pad-eye located some distance down the pile to ensure optimum horizontal holding capacity due to soil resistance.

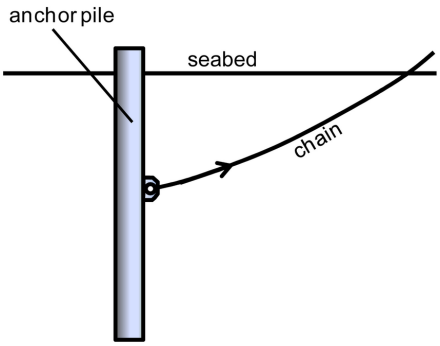

Figure 2.13: Pile anchor, [10]

Suction anchor is in many ways, a pile anchor with a different installation process and holding characteristics. The anchor is forced into the seabed using pumps, which pumps the water inside the hollow pipe out and creates a vacuum. This vacuum then pulls the pile into the seabed, and the holding capacity is a result of the pressure difference, friction and lateral soil resistance.

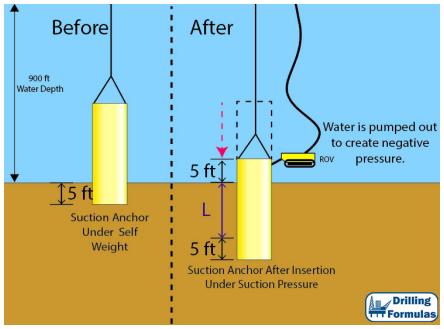

Figure 2.14: Suction anchor, [11]

Anchor summary In Table 2.2 are the key advantages and disadvantages for the anchor categories presented above.

Table 2.2: Advantages and disadvantages for offshore anchor types.

Anchor type	Advantages	Disadvantages
Drag embedded	- Well tested - Suited for horizontal loads - Easily retrievable	- Exact positioning are limited. - Severely restricted vertical holding capacity.
Vertical load	- Well tested. - Resist both horizontal and vertical loads	- Exact positioning are limited.
Pile	- Resist both horizontal and vertical loads. - Exact positioning.	- Requires special anchor handling vessel for installation. - Limited water depth.
Suction	- Resist both horizontal and vertical loads. - Exact positioning. - Large range of water depth.	- High unit cost. - Complex installation process with lower operational limit.

2.2.3 Buoys and clump weights

The buoy and clump weight are components that can be attached to the mooring lines to apply or change the geometric stiffness of a mooring system. Clump weights are generally high-density components that serve two purposes; The first purpose is that a concentrated weight will help increase the pre-tension in combinations with smaller lighter mooring lines. It will also help reduce the angle between the vertical axis and the mooring line, which will be further addressed in the next section. The buoy on the other hand, is a low-density structure with a high net buoyancy. This buoyancy will help lift the mooring line and reducing the vertical pull on the structure. In polyester system can also the buoy be used to keep the polyester off the sea bed in order to avoid wear and tear on the rope.

2.3 Design criteria and challenges

As stated in the beginning of this chapter, is the design of a mooring system very much a play between creating a stiff enough system to avoid large mean offsets, and soft enough not to be stiffness dominated. The meaning of this will be further described in chapter 4, but do in general mean that we want a system that manages to absorb wave- and low-frequency loads and simultaneously be able to prevent severe drift off. Typical limiting factors are the risk of damage on the power cable for large offsets and the risk collision if two or more FWTs are

placed near each other. As this thesis only consider the mooring system of one FWT, will the risk of collision nor safety of the power cable not be prioritized in the analyses. Nevertheless, a maximum allowed top-end offset of 25% of the water depth for the power cable is typically used and will indicate whether or not the system is realistic. The mooring system should also be designed in such a manner that it can resist environmental loads from all angles. For typical three-lined mooring configuration with 120deg angle between each line, must each line have the ability to restrain the least favorable load configuration(typically direction aligned toward one line). This means that the line tension can note exceed the capacity of the line, and a more thorough discussion of this will be given in chapter 3. For chain catenary systems where mainly drag embedded anchors are used, a sufficiently long mooring line required to avoid any vertical pull on the anchor. For systems where synthetic fiber roper is used, it is vital to prevent any contact between the seabed and the rope, and zero tension should not be occurring after installation.

The challenges of designing a catenary mooring system are mainly related to the rapid change in the mooring line geometry as the water depth decreases and the need of heavy chain to achieve adequate pre-tension. According to the equilibrium equation and the assumption that the horizontal tension at the fairlead is equal to the horizontal line tension at the anchor-connection point, do Equation 2.2 and Equation 2.3 provides the following relation:

$$T_{H1} - T_{H0} = \frac{W_{W1} \cdot a_1 - W_{W0} \cdot A_0}{h} \tag{2.13}$$

Where the symbols are given in Figure 2.15 and in the nomenclature.

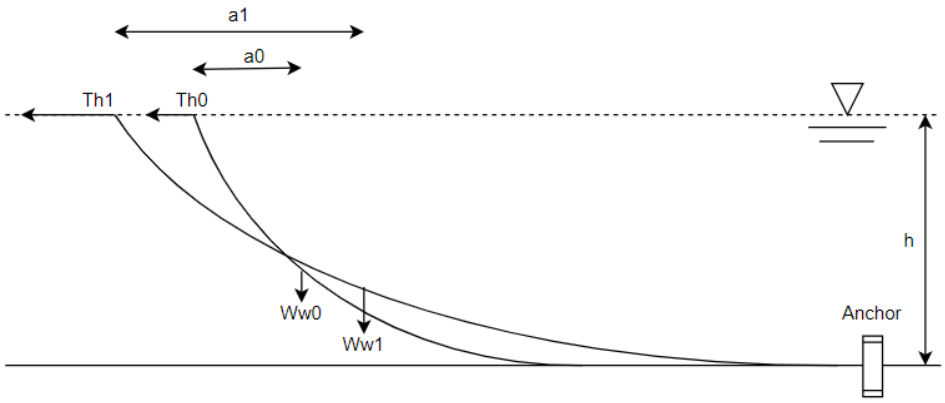

Figure 2.15: Catenary effect.

The change in geometry will rapidly change the weight of the submerged line providing stiffness, which together with the small water depth, leads to large changes in mooring line tension even for small offsets. This is also demonstrated by the horizontal stiffness formulation in Equation 2.14 given by Faltinsen in *Sea loads on ship and offshore structures*[19] for unelstic mooring lines. The reduction in mooring line length provided stiffness in the horizontal plane as water depth increases are depicted in Figure 2.16 under the assumption of constant pre-tension

$$k_G = \frac{\partial T_H}{\partial x} = \omega \left[-\frac{2}{\sqrt{1+2\frac{T_H}{\omega h}}} + \cosh^{-1}\left(1+\frac{\omega h}{T_H}\right) \right]^{-1} \tag{2.14}$$

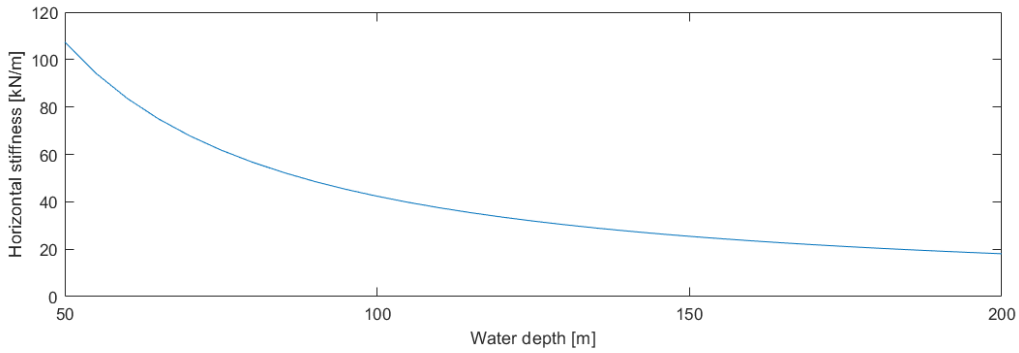

Figure 2.16: Horizontal stiffness as function of water depth for chain catenary systems with constant pre-tension

The top-end angle of the mooring line with respect to the vertical and horizontal axis could also provide challenges in shallow water. How the angle is defined is depicted in Figure 2.17, and demonstrates how the angle between the vertical axis and the mooring line increases for smaller water depth. As the horizontal line tension gives the main restoring force in the horizontal plane, will a large angle result in a large horizontal stiffness. This is especially the case for the taut mooring system, and a solution would be to add a clump weight in order to reduce the angle.

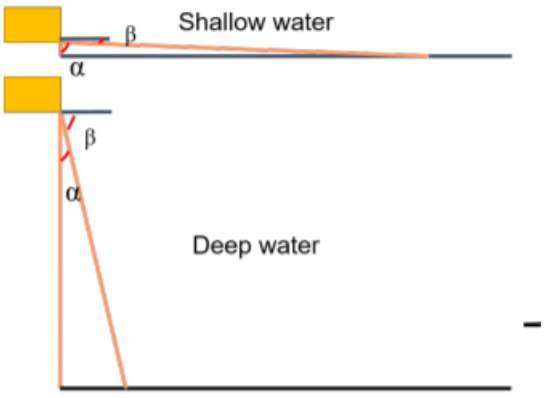

Figure 2.17: Effect from mooring line top angle[12].

Chapter 3

Rules and Regulations

The following section will discuss the different rules and regulations related to station keeping for floating wind turbines. For this project will DNVGL-ST-0119 provide the principles, technical requirements and guidance for the design of the mooring system. This standard covers the catenary and taut mooring system for all three mooring lines discussed in section chapter 2.

3.1 Limit States

A limit state is a condition of a structure beyond which it no longer fulfills the relevant design criteria. The condition may refer to a degree of loading or other actions on the structure, while the criteria refer to structural integrity, fitness for use, durability or other design requirements. According to DNVGL-OS-E301[2], shall all mooring systems be tested against the following three limit state equations:

ULS - Ultimate limit state is categorized as the mooring line's ability to withstand the imposed extreme environmental loads acting on the system.

ALS - Accidental limit state ensures that the mooring system can withstand an unknown failure of one of the mooring lines. In the case of our floating wind turbine, does this means that the two remaining lines must be able to prevent any further drift off.

FLS - Fatigue limit state is related to the possibility of failure due to the effect of cyclic loading. However, since this project will not focus on fatigue, is this limit state not further emphasized in this thesis.

3.2 Mooring Line Design Limits

Either we look at the design of a taut mooring line or a catenary mooring line, one has to design it with respect to extreme line tension. What we mean about this is that the strength capacity has to be higher than the expected line tension. The expected line tension or design tension, T_d, is expressed as:

$$T_d = \gamma_{mean} \cdot T_{c,mean} + \gamma_{dyn} \cdot T_{c,dyn} \tag{3.1}$$

in which $T_{c,mean}$ and $T_{c,dyn}$ are the characteristic mean and dynamic tension respectively, and γ_{dyn} and γ_{dyn} are loads factors. These tensions are defined at the expected line tension for a 50-year condition defined by the significant wave height, H_s, peak period, T_p, and significant wind speed 10m above the sea, U_{10}. The mean tension is caused by both pretension and the mean environmental loads, while low-frequency loads and wave frequency loads cause the dynamic tension. However, it is important to keep in mind that the largest line tension not necessarily occurs at the 50-year value of the sea state. A wind turbine will experience maximum thrust at rated wind speed, which will decrease as the wind speed increases. This might lead to an occurrence of maximum line tension at a much lower mean speed and wave height, and one therefor has to investigate the line tension for the rated wind speed as well. Which load factor to use for ULS- and ALS calculations will depend on whether one is in consequence class 1 or 2, and the given value can be found in Table 3.1. The consequence class is defined by the likelihood of system failure leading to consequences like the loss of life, collision with adjacent units, capsize or sinking. A floating wind turbine is typically within consequence class 1, as they are usually unmanned during operation, and the risk of pollution is significantly small compared to e.g. a FPSO.

Table 3.1: Load factor requirements for design of mooring lines. [1]

Limit State	**Load Factor**	**Consequence Class**	
		1	**2**
ULS	γ_{mean}	1.3	1.5
ULS	γ_{dyn}	1.75	2.2
ALS	γ_{mean}	1.0	1.0
ALS	γ_{dyn}	1.1	1.25

As previously mentioned, must the largest line tension not exceed the characteristic capacity of a mooring line. Whether we evaluate a chain, steel rope or a synthetic rope, it is crucial to consider the line as an assembly of a large number of identical components where the assembled component has a lower capacity than one single component. The characteristic capacity or the characteristic breaking strength of the mooring line is defined as;

$$S_c = \mu_S \cdot [1 - COV_S \cdot (3 - 6COV_S)] \tag{3.2}$$

Where the statistical properties, μ_S and COV_S (< 0.1), are the mean value and the coefficient of variation of the breaking strength of the component respectively.

If such statistical data is not available, a more conservative approach can be used to establish the characteristic breaking strength by using the minimum breaking strength, S_{mbs}

$$S_c = 0.95 \cdot S_{mbs} \tag{3.3}$$

It shall also be mentioned that other components in the mooring system, such as connecting links and terminations shall with a very high confident hold a larger characteristic capacity than the main body of the mooring line.

The mean and dynamic tension can i general, be obtained by either a time domain or frequency domain analysis. However, Due to the method limitations for frequency domain analyses related to inaccuracy in effects like drag loads, variable surface elevation and horizontal restoring forces, this approach will not be further emphasized. The time-domain analysis can be performed in two manners. The first approach is to use one sufficiently long simulation which shall provide adequate statistics, and shall not be taken less than three hours. The duration of the simulation will depend on the response, i.e. the simulation length increases if low-frequency motion is of importance. The extreme value statistic will in this case be based on the maximum response in the mooring lines between two mean-up-crossings. This can be seen as the circled peaks in Figure 3.1 and is is commonly modeled by a 3 parameter Weibull distribution. A Gumbel distribution can then be used to model the extreme value distribution and the dynamic tension is calculated from the most probable maximum, MPM, as $T_{mean} - MPM$.

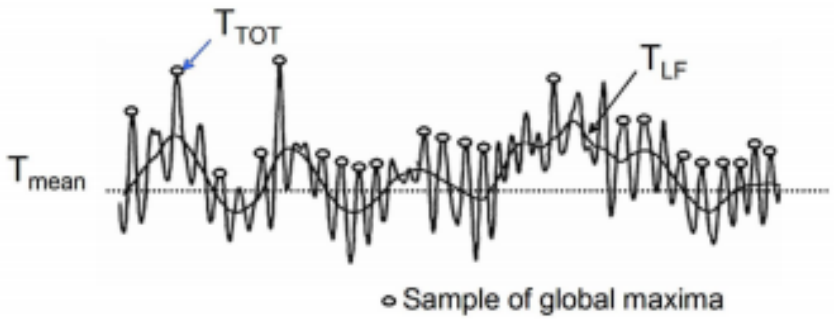

Figure 3.1: Times series with global maxima and LF- and total respons from [2]

An alternative method to establish the extreme value distribution when performing a time-domain analysis is to simulate several 3 hours realizations. We then get an extreme sample consisting of the maximum observed line tension from each simulation, which is modeled by a Gumbel distribution. The dynamic tension is then found in the same manner as above where MPM is given by:

$$MPM = \mu - 0.45 \cdot \sigma \tag{3.4}$$

where μ and σ are mean and standard deviation of the sample.

In DNVGL-OS-E301[2] a second design equation are given for the ULS. The equation is presented in Equation 3.5 and is applicable for both time domain and frequency domain analysis with the partial safety factors, γ_{pret} and γ_{env}, given in Table 3.2. T_{pret} is the mooring line pre-tension while $T_{C-\text{env}}$ is the characteristic environmental tension given as, $T_{C-\text{env}} = MPM - T_{\text{pret}}$.

$$S_C - T_{\text{pret}} \cdot \gamma_{\text{pret}} - T_{C-\text{env}} \cdot \gamma_{env} > 0 \tag{3.5}$$

Table 3.2: Partial safety factors for ULS[2].

		Time domain analysis		**Frequency domain analysis**	
Consequence class	Type of unit	Safety factor on pre-tension, γ_{pret}	Safety factor on env.tension, γ_{env}	Safety factor on pre-tension, γ_{pret}	Safety factor on env.tension, γ_{env}
1	Permanent	1.20	1.45	1.20	1.80
1	Mobile	1.20	1.35	1.20	1.50
2	Permanent & mobile	1.20	1.90	1.20	2.30

This expression can be rewritten to give a better understanding of the utilization of the mooring line material and its limit by formulating a utilization factor, UF. This utilization factor is given as:

$$UF = \frac{T_{\text{pret}} \cdot \gamma_{\text{pret}} + T_{C-\text{env}} \cdot \gamma_{\text{env}}}{s_C} < 1 \tag{3.6}$$

Chapter 4

Time Domain Analysis

4.1 Equation of Motion

The equation of motion is an equation describing the physical behavior of a system with respect to time and/or frequency. For a floating system with 6 degrees of freedom, the equation be expressed as shown in Equation 4.1

$$\big(M+A(\omega)\big)\ddot{r}+C(\omega)\cdot\dot{r}+D_l\cdot\dot{r}+D_q\cdot\mid\dot{r}\mid\dot{r}+K(r)\cdot r=Q(t,r,\dot{r}) \tag{4.1}$$

Where;

M Mass matrix

$A(\omega)$ Frequency-dependent added mass matrix

r**,**$\dot{r}$**,** $\ddot{r}$ Position, velocity and acceleration vector respectively

$C(\omega)$ Frequency-dependent potential damping

D_l Linear damping matrix

D_q Quadratic damping matrix

$K(r)$ Stiffness matrix (non-linear)

$Q(t,r,\dot{r})$ Excitation force vector which consist of;

- q^1_{wave} First order wave force
- q^2_{wave} Second order wave force
- q_{wind} Wind force
- $q_{current}$ Current force

A way to simplify this equation to bette explain the physics, is by looking at it as a single degree of freedom system, where the position vector, r, can be simplified to a position function, x. Equation 4.1 can therefor be rewritten as:

$$\big(M+A\big)\ddot{x}+C\dot{x}+Kx = F_0 cos(\omega t) = \Re(F_0 e^{i\omega t}) \tag{4.2}$$

And the position function can be expressed by;

$$x = x_0 cos(\omega t+\varepsilon) = \Re(\mid x_0 \mid e^{i\omega t+\varepsilon}) \tag{4.3}$$

ω Angular velocity=$\frac{2\pi}{T}$ and T is the wave period.

ε Phase angel between excitation and response.

x_0 Displacement amplitude.

The responses due to the dynamic loads will depend on the ratio between the static and dynamic response, called the dynamic amplification factor, DAF, and is defined by:

$$DAF = \mid \frac{x_{max}}{x_{static}} \mid = \frac{1}{\sqrt{(1-\beta)^2+(2\beta\xi)^2}} \tag{4.4}$$

where,

β Frequency ratio between incoming load and natural frequency of the system, $\frac{\omega}{\omega_0}$.

ξ Damping ratio = $\frac{C}{C_{cr}} = \frac{C}{2(M+A)\omega_0}$.

The value of the DLF will depend on the frequency ratio, β, and can be both larger and less than 1.0 which means that we can have either an amplification or a reduction of the dynamic response[20]. In Figure 4.1 are the DAF and the phase angle, ε, given as functions of β for given values of damping ratio, ξ.

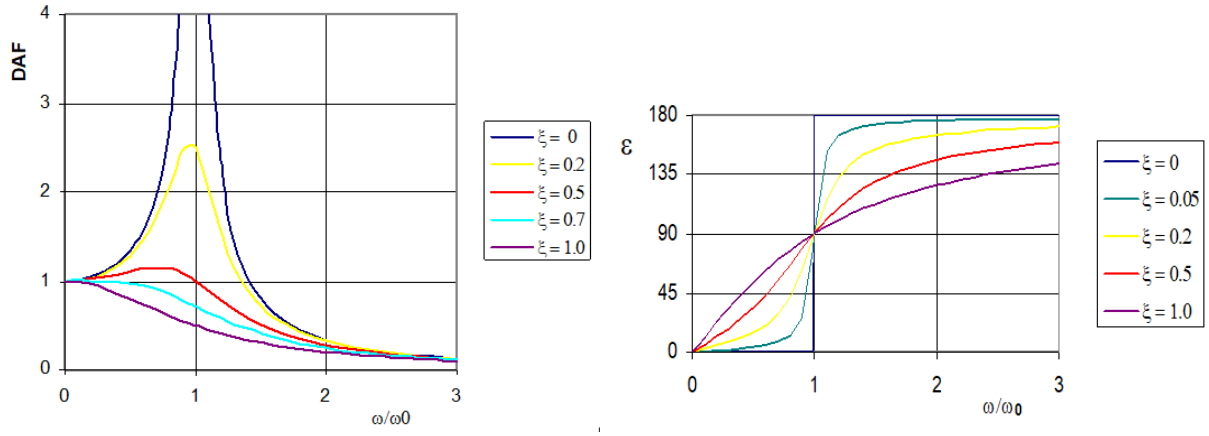

Figure 4.1: Dynamic Amplification Factor and Phase Angle [6]

The dynamic response is characterized as three different regions determining the force balance in the time instant with maximum external load[21]. These regions will be depending on the frequency ratio, and are defined as:

Stiffness dominated $\beta < 1$

Resonance $\beta \approx 1$

Inertia dominated $\beta > 1$

For stiffness-dominated system will the load variation experienced by the system be slow and no significant inertia forces will be mobilized, and the structure will therefore behave quasi-statically. The phase angle will in these cases be approaching zero and for $\omega t = 0$ give $x = \mid x_0 \mid$, $\dot{x} = 0$ and $\ddot{x} = -\omega^2 \mid x_0 \mid$. Equation 4.2 then becomes;

$$-\omega^2 |x_0| (M+A) + K |x_0| = F_0 \Rightarrow K |x_0| = F_0 + \omega^2 |x_0| (M+A) \tag{4.5}$$

As ω becomes small, Equation 4.5 will in general be an equilibrium relation between the external force and the restoring force. Since the inertia term acts in the same direction as the excitation force, which leads to a higher response than the static system.

From Figure 4.1 it is seen that the phase angle, ε, is $-\frac{\pi}{2}$ for the resonance region and the displacement, velocity and acceleration are found to be $x = 0$, $\dot{x} = i\omega \mid x_0 \mid$ and $\ddot{x} = 0$ respectively. This results in a force balance between the damping force and the external force, as shown in Equation 4.6.

$$iC\omega \mid \dot{x} \mid = F_0 \tag{4.6}$$

The third regime occurs when the inertia of the system becomes too large for the displacement mobilize a restoring force, and the phase angle is then $-\pi$. Hence, $x = -\mid x_0 \mid$, $\dot{x} = 0$ and $\ddot{x} = \omega^2 \mid x_0 \mid$, creating a equilibrium between the external force, restoring force and the inertia force. From Equation 4.7, it is seen that the inertia force balances the external force, and that the restoring force in fact will increase the response. With respect to this project will the mooring system create a larger dynamic surge motion compared to if the structure was freely floating without the mooring system.

$$\omega^2 |x_0| (M+A) - K |x_0| = F_0 \Rightarrow \omega^2 |x_0| (M+A) = F_0 + K |x_0| \tag{4.7}$$

As the regions depends on the ratio between the load frequency and the natural frequency of the system, it is essential to know the expected natural period for each degree of freedom. The natural periods are determined by the inertia and stiffness of the system as shown in Equation 4.8:

$$T_0 = 2\pi \sqrt{\frac{M+A}{K}} \tag{4.8}$$

and the ”preferred” periods of motion response for a semi submersible are presented in Table 4.1.

Table 4.1: Natural oscillation periods for a semi-sub

Response	Surge	Sway	Heave	Roll	Pitch	Yaw
Natural period, T_0	$\approx 100s$	$\approx 100s$	$20-25s$	$45-60s$	$45-60s$	$>> 100s$

By further investigation of the right-hand side of the equation, one sees that both waves, wind and current forces should be divided into their acting frequency, see Figure Table 4.2 for elaboration. The loads that will be considered for our structure are the three mean forces; the 1. order wave frequency force, and the low-frequency forces.

Table 4.2: Time scales of excitation loads

	Mean	**Impulse (<1s)**	**High frequency (1-5s)**	**Wave frequency (5-30s)**	**Low frequency (>30s)**
Waves	Mean drift forces (2.order)	Extreme wave slam on column	"Springing" forces	Wave forces (1.order)	Wave drift forces (2.order)
Wind	Mean wind speed				Wind gust (2.order)
Current	Mean current speed				

4.1.1 Excitation forces

Wave

The excitation forces due to waves in linear wave theory are the sum of the Froude-Kriloff forces and diffraction forces. The FK-forces corresponds to the forces acting on the wetted surface due to the undisturbed pressure field, while the diffraction forces are due to disturbance of the wave kinematics caused by the presence of the structure. For second-order wave theory, we keep all terms in the velocity potential, fluid pressure and wave loads that are either linear with respect to the wave amplitude or proportional to the wave amplitude squared. This theory then gives us a mean wave drift and the low-frequency wave forces which are of importance for a moored semi-submersible. The drift force in potential theory is due to the structure's ability to generate wave which will decrease as the structure becomes smaller. From second-order wave theory it is possible to calculate the non-linear wave effects by considering the quadratic term in the Bernoulli's equation. From *Sea loads on ship and offshore structures* by Faltinsen[19], this term is derived as:

$$\frac{1}{2}|\phi|^2 = \frac{1}{2}\left[V_1^2 + V_2^2 + V_3^2\right] \tag{4.9}$$

where V_1^2, V_2^2 and V_3^2 are the particle x-, y- and z-component of velocity respectively. For a sea state consisting of N different wave components of different frequency, ω_i, an approximate of the velocity in the x-direction is found by:

$$V_1 = \sum_{i=1}^{N} A_i \cos\left(\omega_i t + \varepsilon_i\right) \tag{4.10}$$

where A_i is the velocity amplitude. From Equation 4.9 and 4.10 one can derive a constant term represented by $-\frac{1}{2}\rho\sum_{i=1}^{N}\frac{A_i}{2}$, but also pressure terms oscillating with the sum frequency, $(\omega_j + \omega_k)$, and the difference frequency, $(\omega_j - \omega_k)$. The magnitude of the second-order effect will in general be small compared to the first-order effects, but could in fact be of great interest since the slowly varying drift forces might induce resonance in surge sway and yaw.

So far, we have only considered the inviscid effect derived from potential theory. However, wave drift forces will also be caused by viscous effects. As mentioned, will the structure's ability to generate waves decrease as the structure becomes smaller. For sufficiently large wave amplitude compared to the cross section dimension, the viscous effect will contribute to the drift forces. While the potential drift force on a vertical cylinder is proportional to the wave amplitude squared, conducted S.K Chakrabarti a study where he concluded that the viscous drift force is at least a third-order term[22]. This will be applicable for the CSC semi-submersible which consists of slender elements with low capability of generating waves. Figure 4.2 are based on known analytical results for a vertical cylinder in regular waves, and can be used to determine the dominant forces.

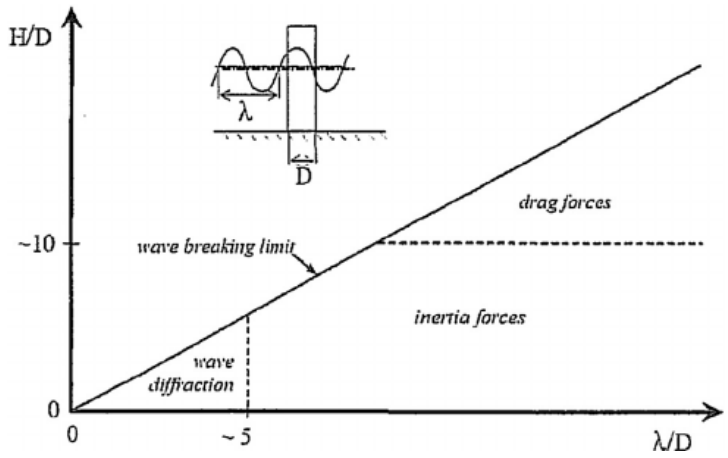

Figure 4.2: Relative importance of inertia, drag and diffraction wave forces

For slender systems like the CSC, will inertia and drag forces be the dominant force and Morison's equation can then be used. Morison's equation will in general be giving the horizontal force, dF, on a strip, dz, of a vertical rigid circular cylinder. However, the equation can be modified for cases with moving slender elements and expressed as:

$$dF = \frac{1}{2}\rho C_D D(u-\dot{x})|u-\dot{x}|dz + \rho C_M A a dz - \rho(C_M - 1)A\ddot{x}dz \tag{4.11}$$

Where ρ is the density of the fluid, D is the diameter of the cylinder, A is the cross-section area, u and a are the undisturbed fluid velocity and acceleration respectively acting normal on the cylinder and $\dot{x}$ and $\ddot{x}$ are the motion velocity and acceleration. C_M and C_D are the inertia- and drag coefficient and have to be found empirically and will depend on the characteristic of the flow. *DNV-RP-C205 Environmental Conditions and Environmental Loads[13]* gives the 2D drag coefficient as function of Reynolds number for various surface roughness presented in Figure 4.3. The inertia coefficient is given from the same standard and presented as function of KC-number in Figure 4.4. The first term on the right hand side of the equation will then be the drag forces, the second term will be the Froude-Kriloff forces and the last term is the hydrodynamic mass force due to added mass.

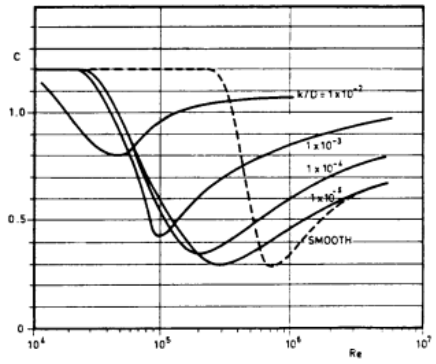

Figure 4.3: Drag coefficient for circular cylinder for various roughness[13]

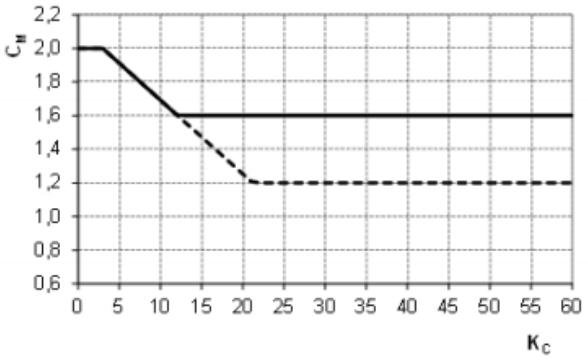

Figure 4.4: Mass coefficient for smooth (solid) and rough (dotted) cylinder[13]

Wind

The induced wind forces acting on the structure from the incoming wind field are the drag force on the tower and the thrust force from the rotating blades. The forces on the tower can be determined by using Morison's equation, and can be considered relatively small compared to the forces from the blades. The thrust force is derived from momentum theory as:

$$dT = 4\pi r\rho U_\infty a(1-a)dr = 4\pi r\rho U_\infty C_T dr \tag{4.12}$$

Where ρ is the density of the fluid, U_∞ is the velocity of the undisturbed wind field, C_T is the thrust coefficient given by the axial induction factor, a. The rotation of the blades will also create a torque on the shaft which will induce a roll motion. This torque is expressed by;

$$dQ = 4\pi r^3\rho U_\infty \Omega(1-a)a'dr \tag{4.13}$$

where a' is the rotational induction factor and Ω is the rotational velocity.

Since the turbine blades have the shape of an airfoil, can the local forces be obtained by simple airfoil theory. A cross-section of a blade is presented in Figure 4.5 and shows how an incoming wind with velocity W induces a drag, D, and lift force, L, on the foil.

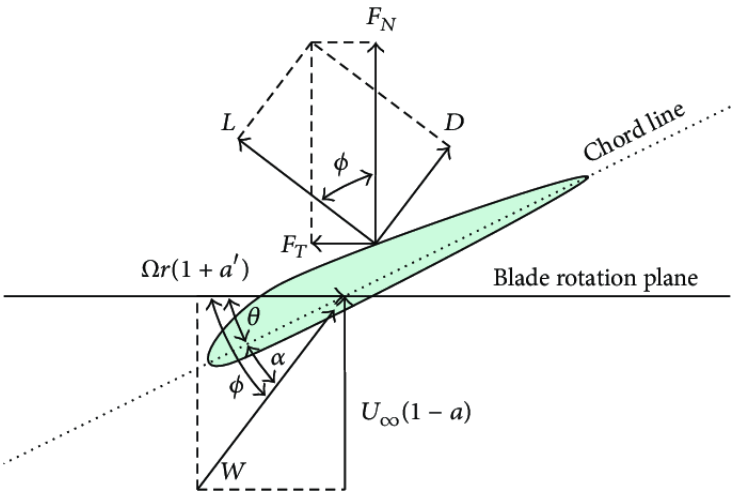

Figure 4.5: Local forces on an airfoil [14]

Here W is a resulting wind velocity between the axial fluid velocity through the blade rotation plane, $U_\infty(1-a)$, and the velocity the airfoil experience as is rotates, $\Omega r(1+a')$. U_∞ is the undisturbed flow velocity for the incoming wind field, while Ωr is the rotational speed at a given point on the blade. ϕ in the flow angle of W relative to the rotor plane, α is the angle of attack, and θ is a local initial pitch angle.

The lift and drag can then be found by Equation 4.14 and Equation 4.15 respectively.

$$L = \frac{1}{2}\rho c W^2 C_L \tag{4.14}$$

$$D = \frac{1}{2}\rho c W^2 C_D \tag{4.15}$$

Where c is the chord-length, C_L and C_D are lift and drag coefficient given by the characteristics of the foil. Figure 4.6 shows how these coefficients can change with respect to the angle of attack for a DU21 airfoil.

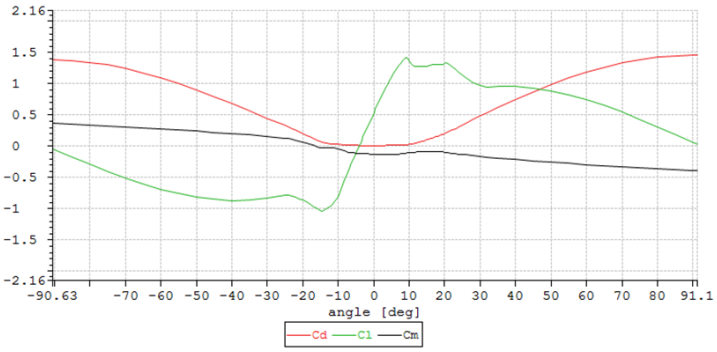

Figure 4.6: Airfoil characteristics of the DU21 airfoil [15]

By decomposing L and D with respect to the rotor plane, will the parallel force, F_T, make the blades rotate while the perpendicular force, F_N, be a thrust force acting in the same direction as the incoming wind. The global thrust and torque load are then given as:

$$dT = BF_N dr = B(L\cos\phi + D\sin\phi)dr \tag{4.16}$$

$$dQ = BrF_T dr = Br(L\sin\phi - D\cos\phi)dr \tag{4.17}$$

Where B is the number of blades. We can then introduce the normal coefficient C_N, tangential coefficient C_T and the solidity ratio σ;

$$C_N = C_L\cos\phi + C_D\sin\phi \tag{4.18}$$

$$C_T = C_L\sin\phi - C_D\cos\phi \tag{4.19}$$

$$\sigma = \frac{Bc}{2\pi r} \tag{4.20}$$

By combining Equation 4.12 and 4.13 obtained from momentum theory with Equation 4.16 and 4.17 from foil theory, the following expression for a and a' can be derived:

$$a' = \frac{1}{\frac{4\sin\cos\phi}{\sigma C_T} - 1} \tag{4.21}$$

$$a = \frac{1}{\frac{4\sin^2\phi}{\sigma C_N} + 1} \tag{4.22}$$

By assuming no radial dependency and an infinite number of blades, the classical blade element method, BEM, is used to compute the local loads on each cross-section of the blades. BEM is a convergence algorithm which can be divided into four steps:

1. Initialize a and a'.
2. Calculate ϕ and consequently α, C_L and C_D.
3. Update a and a' from Equation 4.21 and 4.22.
4. Check for convergence within given tolerance, if not, repeat from step 3, else continue to calculate local loads.

To correct for the assumption of infinite number of blades, one has to include the Prandtl's tip loss factor,F, for Equation 4.12 and 4.13. The factor is computed as:

$$F = \frac{2}{\pi}\cos^{-1}\left[\exp\left(-\frac{B(R-r)}{2r\sin(\phi)}\right)\right] \tag{4.23}$$

R is the total radius while r is the local radius. By including this factor, Equation 4.21 and 4.22 yields:

$$a' = \frac{1}{\frac{4F\sin\cos\phi}{\sigma C_T} - 1} \tag{4.24}$$

$$a = \frac{1}{\frac{4F\sin^2\phi}{\sigma C_N} + 1} \tag{4.25}$$

As the BEM method uses the momentum theory, one also has to account for the fact that this theory breaks down for a-values larger than 0.4 due to negative wake. Different empirical relations between a and the thrust coefficient can be found to fit with the measurements, i.e;[23]

$$C_T = \begin{cases} 4a(1-a)F, \text{ for } a \leq a_c \\ 4\left[a_c^2 + (1-2a_c)a\right]F, \text{ for } a > a_c \end{cases} \tag{4.26}$$

Where a_c is approximately 0.2. We can the again use the results obtained from local aerodynamics to derive the expression for a as;

$$a = \frac{1}{2}\left\{2 + K(1-2a_c) - \sqrt{\left[K(1-2a_c)+2\right]^2 + 4\left(Ka_c^2 - 1\right)}\right\} \tag{4.27}$$

Where,

$$K = \frac{4F\sin^2\phi}{\sigma C_N} \tag{4.28}$$

The result of this is exemplified in Figure 4.7 where the total wind force is given by the sum of rotor thrust and wind drag on the tower. The decrease in thrust after the thrust has reached its peak at rated wind speed is due to pitching of the blades which changes the angle of attack and gives a constant power production.

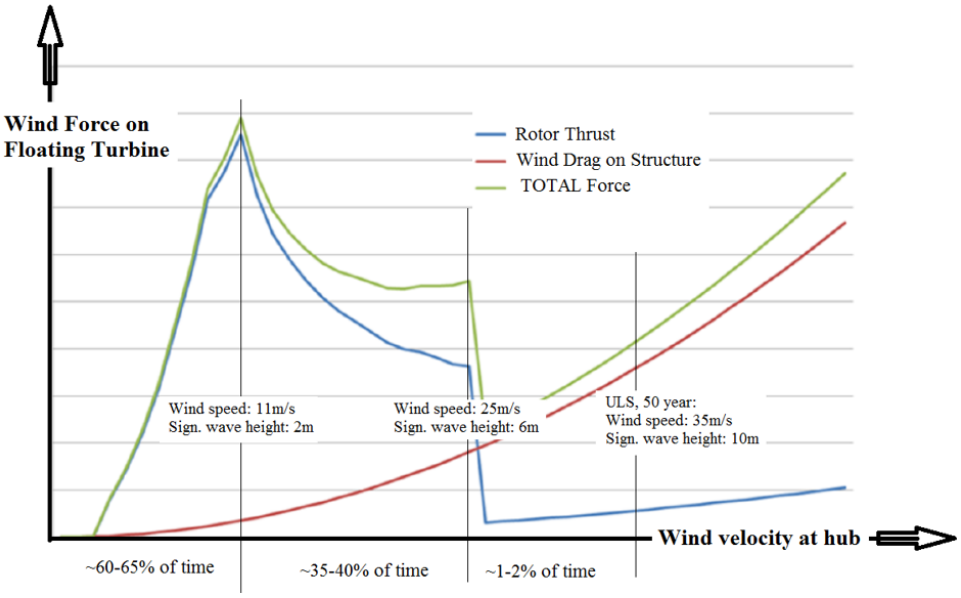

Figure 4.7: Total wind loads for different wind speeds[6].

Current

Current forces might cause large steady excursions and slow drift motions of moored structures, as well as generate lift and drag which can give rise to vortex induces motion[13]. The statistical distribution of currents is generally scarce for most areas, and it should therefore be considered to do current measurements for the requested site. The governing causes for currents are:

- Wind - friction and atmospheric pressure gradient.
- Waves - density gradients
- Tidal - motion of the planet.
- Circular - Ocean circulation, i.e Gulf stream.

When the velocity field is found, Morison's equation, Equation 4.11, can be used to obtain the current forces.

4.1.2 Mass, added mass, damping and stiffness

The left side of Equation 4.1 consists of an inertia term, a damping term and a stiffness term. The inertia term is proportional to the acceleration of the structure and is given by the mass-matrix, M, and the added mass-matrix, A. The mass-matrix consist of the structure mass for the translation acceleration and the mass moment of inertia for the rotational acceleration. This

matrix can relatively quickly be constructed from the geometry and material composition of the structure. The added mass- matrix is a result of the acceleration of the water particles around the body as the body is forced to oscillate. The added mass will be frequency-dependent, and since it is a result of the body's ability to generate waves, it can be found from the velocity potential for the radiating waves, ϕ_R. The integration of ϕ_R and the hydrostatic pressure will also give the potential damping and stiffness. Different methods can be used to solve the velocity potential. For the model used in this project, the boundary integral equation method, also known as panel method has been used through the computer program, WAMIT[24], with the model seen in Figure 4.8.

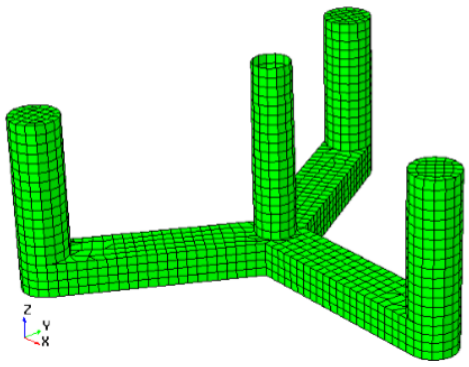

Figure 4.8: Panel model of the semi-submersible floating wind turbine[3]

The structure will also be exposed to other types of damping acting on the structural components. Since the potential damping is generally low for slender structures, will the impotence of the viscous damping for the wave and low frequency responses increase in resonance. The primary sources of low-frequency damping are viscous hull damping and mooring system damping in form of drag on the mooring lines. It is stated in a study by Larsen et al.[25] that pretension, water depth and mooring line material are important parameters when damping from mooring systems shall be quantified.

The restoring force in surge sway and heave are determined by the horizontal force from the mooring line, described in chapter 2. For roll, pitch and heave, will the restoring force be given by the hydrostatic forces given by the structural characteristics. For heave will the restoring force be determined by the submerged volume and changes in the vertical position will change the buoyancy force. The stiffness coefficient in heave can then be expressed as:

$$K_{33} = \rho g A_w \tag{4.29}$$

Where g is the gravitational acceleration and A_w is the waterplane area. For roll and pitch will the tangential and longitudinal metacentric height give a restoring moment and the stiffness coefficients are given as:

$$K_{44} = \rho g G M_t \nabla \tag{4.30}$$

$$K_{55} = \rho g G M_l \nabla \tag{4.31}$$

Where ∇ is displaced volume.

4.1.3 Solving the equation of motions in time domain

When all the terms in Equation 4.1 are found, it is time to solve it. The equation can be solved in either the frequency domain or in the time domain. Due to the complexity of the environmental loads and responses, do we typically use time-domain analysis for floating structures. Because Equation 4.1 contains both time-dependent terms and frequency-dependent terms will a retardation function be used to solve the analysis exclusively in the time domain. The retardation function is depicted in surge direction for the original CSC10MW model by Wang in Figure 4.9. The function is either calculated from the frequency-dependent added mass, $A(\omega)$, or the frequency-dependent potential damping, $C(\omega)$ as shown in Equation 4.32

$$h(\tau) = \frac{2}{\pi}\int_0^\infty C(\omega)\cos(\omega\tau)d\omega = -\frac{2}{\pi}\int_0^\infty \omega A(\omega)\sin(\omega\tau)d\omega \tag{4.32}$$

We also have the following relation:

$$\begin{aligned} A(\omega) &= A_\infty + a(\omega), \quad A_\infty = A(\omega=\infty) \\ C(\omega) &= C_\infty + c(\omega), \quad C_\infty = C(\omega=\infty) = 0 \end{aligned} \tag{4.33}$$

By combining Equation 4.32 with the relation presented in Equation 4.33, the convolution integral can be used to account for the added mass and potential damping. The equation of motion, Equation 4.1, is then solved in the time domain as:

$$(M+A_\infty)\ddot{r}(t) + \int_{-\infty}^{\infty} h(t-\tau)\dot{r}(\tau)d\tau + d\tau D_l\cdot\dot{r} + D_q\cdot\dot{r}|\dot{r}| + K(r)\cdot r = Q_{exc}(t,r,\dot{r}) \tag{4.34}$$

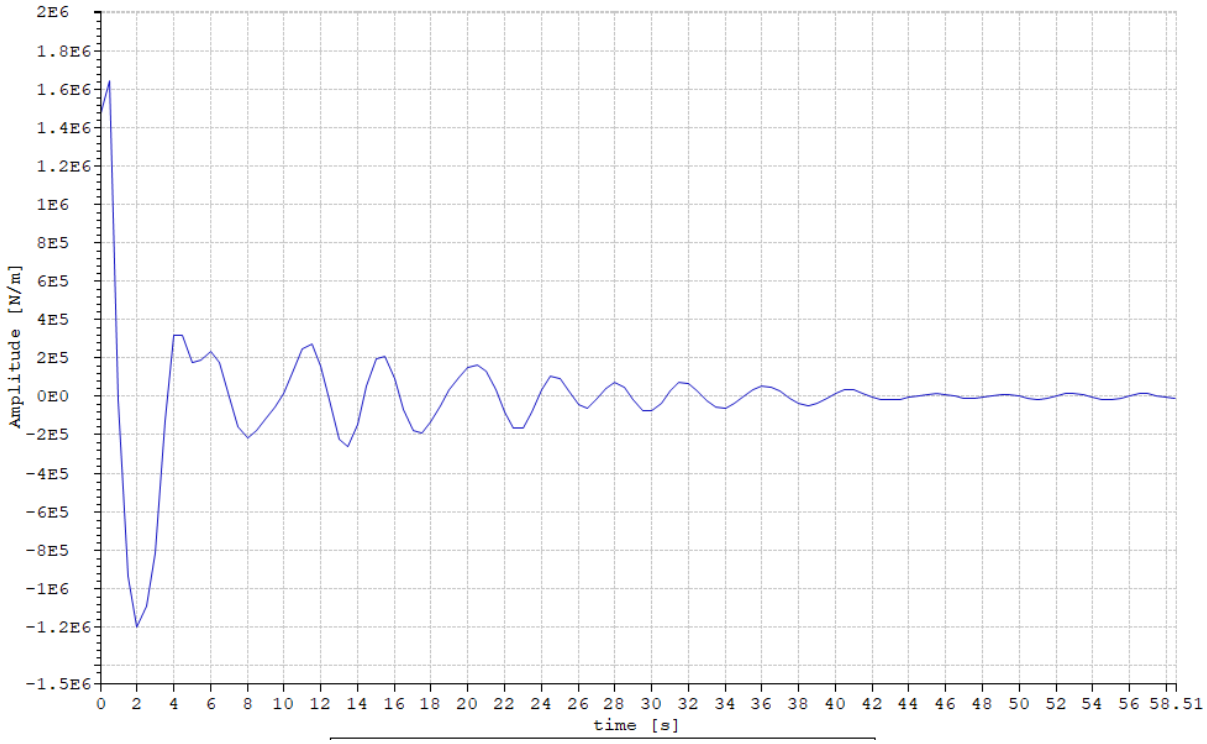

Figure 4.9: Retardation function in surge from Wang's original SIMO/RIFLEX model[3]

4.2 SIMA Workbench

SIMA workbench is a computer simulation and analysis program for marine operations and floating systems[26]. Sima also supports several physics engines, included SIMO and RIFLEX which will now be further described.

SIMO is a simulation tool used for simulation of motions and station-keeping behavior. This simulation tool features i.e., environmental forces due to wind, waves and current, flexible modeling of multi-body systems and non-linear time-domain simulation of wave frequency as well as low-frequency forces[16]. RIFLEX was initially developed to analyze risers, but has proven to be well suited for a wide range of slender structure elements included mooring lines. The program is based on a non-linear finite element formulation, and further references are made to [27].

When performing a time-domain analysis of a moored floating wind turbine, SIMA utilizes both SIMO and RIFLEX in either a separated or coupled analysis method. We will now look further into the two methods and try to evaluate their strengths and weaknesses.

4.2.1 Separated analysis

The separated analysis starts by finding the total motion of the SIMO body. For simplicity will we only consider surge motion, x, and two approaches can then estimate the total surge motion. The body of consideration is presented in Figure 4.10 where we have the excitation forces and damping terms presented in chapter 4, while the stiffness, $K(x)$, are given by the catenary equation in chapter 2.

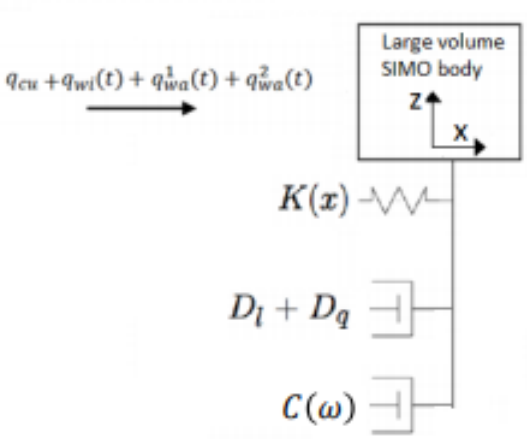

Figure 4.10: SIMO body

The first approach uses the superposition principle where the total motion is the sum of the wave frequency motion, x_{WF}, and low frequency, x_{LF}. The equation of motion concerning first-order wave loads is then written as:

$$(M + A(\omega)) \cdot \ddot{x}_{WF} + (C(\omega) + D_l) \cdot \dot{x}_{WF} + K \cdot x_{WF} = q^1_{wa}(\omega) \tag{4.35}$$

The wave frequency response will then be solved in the frequency domain which requires the

motion to be a linear response to waves. This means that the quadratic damping term, D_q, is set to zero and the following relation can be used:

$$\begin{aligned} \ddot{x}_{wF} &= -\omega^2 x_{WF} \\ \dot{x}_{WF} &= i\omega x_{WF} \\ q^1_{wa}(\omega) &= H^1(\omega) \cdot \bar{\zeta}_a(\omega) \end{aligned} \tag{4.36}$$

From this, x_{WF} can be expressed as:

$$x_{WF} = \frac{H^1(\omega) \cdot \bar{\zeta}_a(\omega)}{(-\omega^2(m + A(\omega)) + i\omega\,(C(\omega) + D_l) + K)} \tag{4.37}$$

The low frequency motion will be solved in the time domain where the potential damping is approximately equal to zero, and the equilibrium equation is written as:

$$(m + A(\omega = 0)) \cdot \ddot{x}_{LF} + D_l \cdot \dot{x}_{LF} + D_q \cdot \dot{x}_{LF}\,|\dot{x}_{LF}| + K\,(x_{LF}) \cdot x_{LF} = q_{WI} + q^{(2)}_{WA} + q_{CU} \tag{4.38}$$

The total total motion then becomes:

$$x_{tot} = x_{WF} + x_{LF} \tag{4.39}$$

The second approach for finding the total motion is to calculate the total motion directly by use of the retardation function described in 4.1.3.

When the total motion has been calculated, these motions can be applied as top-end displacement in the finite element model in RIFLEX. RIFLEX will then be able to calculate the total dynamic line tension of one mooring line for the expected dislocations. The argument for using this separated method is connected to computational time since SIMO only solve the equilibrium equation for the 6dof large volume body. On the other hand, will the excitation and damping forces from the mooring lines not be encountered for, and the results might not be as accurate.

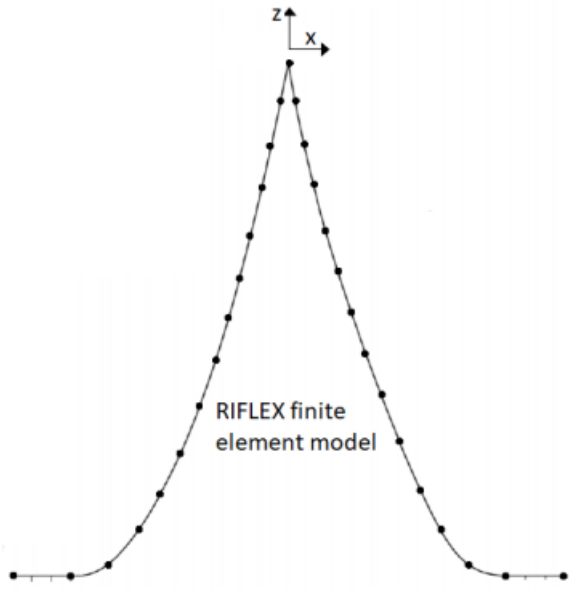

Figure 4.11: RIFLEX model

4.2.2 Coupled analysis

A coupled analysis method account for the coupled effect between the floating structure and the mooring lines and uses a coupled SIMO-RIFLEX model seen in Figure 4.12. This means that two simulations will be done simultaneously and the two simulation tools communicated with each other. The coupled method calculates the total motion for each node in the finite element model and large volume SIMO-body by direct numerical integration in the time domain by use of the retardation function in Equation 4.32. The stiffness from the mooring lines found in the finite element analysis is applied to the floating structure for each time step. The simulation will therefore account for all environmental forces acting on the floating structure and the mooring lines. It is then possible to create a time series of line tension and total motion in 6 degrees of freedom.

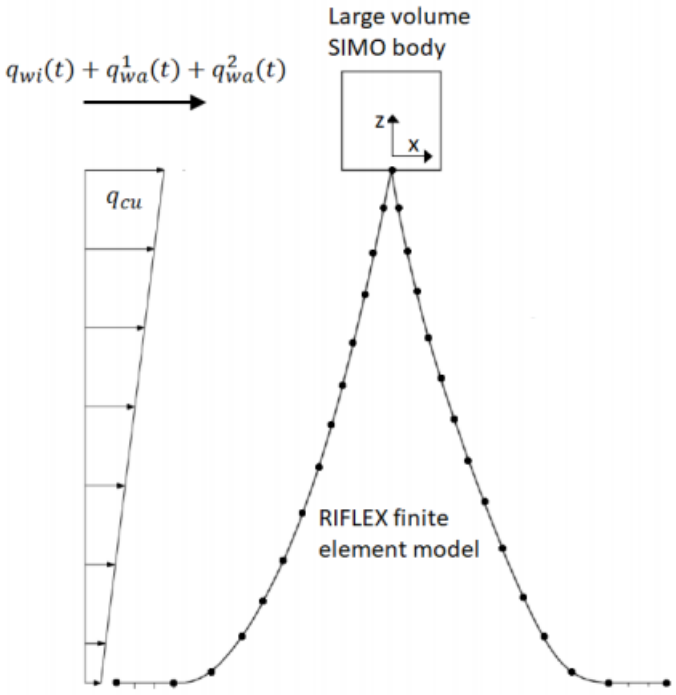

Figure 4.12: SIMO-RIFLEX body

4.2.3 SIMO/RIFLEX-modelling

Out of the two methods of analysis described above, the second method will be used for the simulation of the different system in this thesis. A simple flowchart of the simulation outline is given in Figure 4.13 to better understand the process, and we will now give a brief description of how a SIMO/RIFLEX model is modeled. Prior to the analysis of i.e a floating wind turbine must the hydrodynamic coefficient of the hull be determined. This could as mentioned in chapter 4 be done by using WAMIT where the results are applied to the SIMO body.

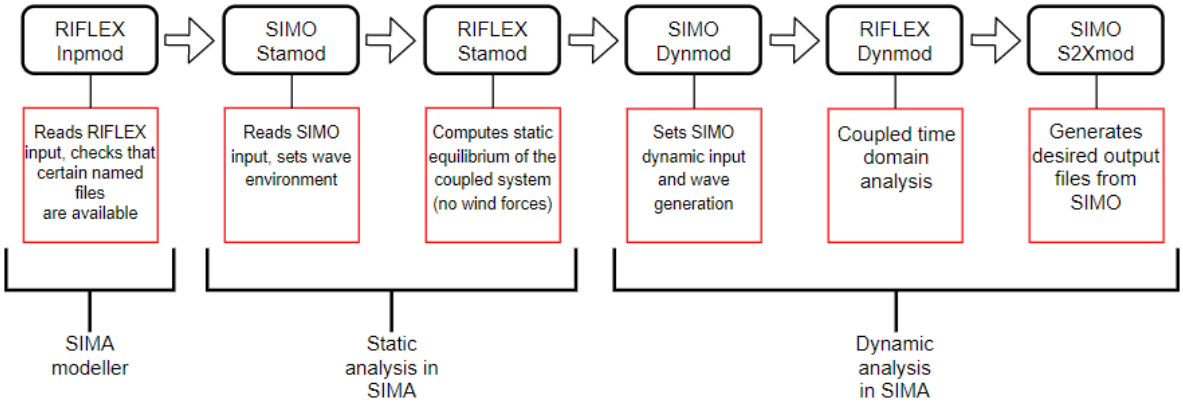

Figure 4.13: Simulation flow chart[15]

The SIMO body will typically for a FWT consist of the hubmass, nacelle and the hull which will consist of one or more rigid components. The body consist of all the relevant data, which includes the quantity and location of the mass as well as the mass moment of inertia determined by the hydrostatic stiffness. The body will also contain data about the first and second order wave force transfer function, and retardation functions that are used to solve the equation of motion in the time domain. The RIFLEX model will be built up by bar and beam elements as the the program uses finite element method to determine the displacement and stresses inside the body. This body is defined by supernodes at each end of the body, and lines characterized by line types and cross-section properties. The line type is a definition of the different parts of each line/body which could be divided into different segments consisting of different cross-sections and number of elements. The cross-section determines the physical properties of each segment.

The static analysis initialise the starting position for the dynamic analysis. During this analysis will the volume, body and specified forces be applied to the body, but also apply the specified displacement and boundary changes. The initial position of the of the RIFLEX model defined by the supernodes needs to define a stressfree configuration of the lines. The specified displacement will hence apply the correct pre-tension to the mooring lines during this analysis.

In the dynamic analysis, will the wave time series be generated from the pre-defined wave spectrum. Excitation forces from waves will, as previously mentioned, be divided into first- and second-order wave excitation forces. The magnitude of the first order force is proportional to the wave amplitude and acts with the same frequency as the incident wave from linear potential wave theory. The first-order wave force is as seen in Equation 4.40 expressed in the frequency domain by the first-order wave force transfer functions, exemplified in Figure 4.14, and wave elevations.

$$q_{wa}^{1}(\omega) = H^{1}(\omega) \cdot \bar{\zeta}_{a}(\omega) \tag{4.40}$$

Where $H^{1}(\omega)$ is the complex first-order transfer function and $\bar{\zeta}_{a}(\omega)$ is the complex harmonic wave component[26]. It is seen from Figure 4.14 that the larges 1. order wave forces will occur for waves with a period between 6 and 15 seconds in surge direction.

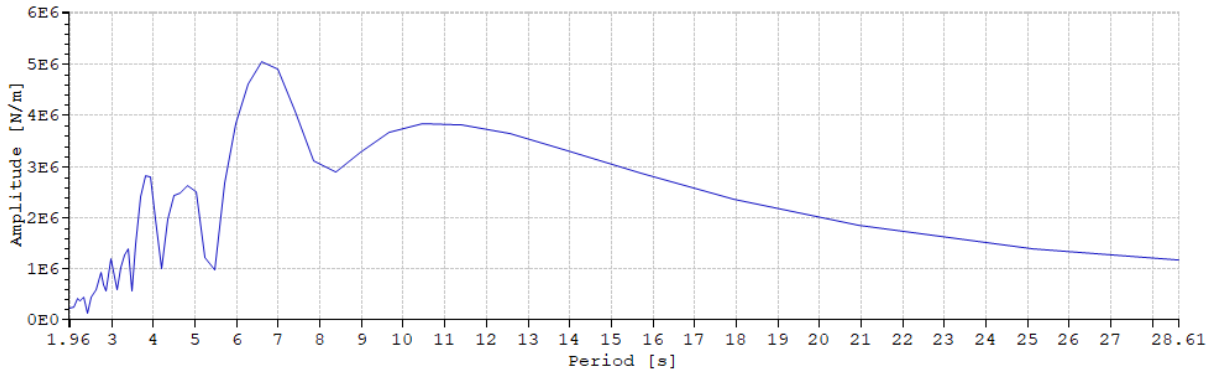

Figure 4.14: First order wave force transfer function in surge[3]

The wave loads from second-order theory could be implemented to the model i a similar method. From the SIMO user guide[16] it is stated that Newman's method can be used to calculate the second-order force and expressed in the form:

$$q(t) = \mathrm{Re}\left\{\sum_m \sum_n \tilde{\zeta}_m \tilde{\zeta}_n H_{mn}^{(2+)} e^{i(\omega_m+\omega_m)t}\right\} + \mathrm{Re}\left\{\sum_m \sum_n \tilde{\zeta}_m \tilde{\zeta}_n^* H_{mn}^{(2-)} e^{i(\omega_m-\omega_n)t}\right\} \tag{4.41}$$

Where;

ζ_m	Complex Fourier component of sea surface elevation with frequency ω_m.
$H_{mn}^{(2+)} \equiv H^{(2+)}(\omega_m, \omega_n)$	Second-order transfer function for the sum-frequency force.
$H_{mn}^{(2-)} \equiv H^{(2-)}(\omega_m, \omega_n)$	Second-order transfer function for the difference-frequency force.

However, as stated earlier, an FWTs ability to generate waves will be relatively small, and the viscous second order forces will play a more significant part. SIMO here offers the possibility to model the structure by slender elements where the loads can be computed by Morison's equation. The slender elements can be given hydrodynamical and aerodynamical properties, thus being applicable for the current and aerodynamic drag forces as well. Taking the aerodynamic drag on the tower of a FWT as an example, is the force on a strip, dz, defined by the relative velocity between the acting wind speed and structure motion, $(U(t) - \dot{x})$, and expressed by Equation 4.42;

$$dF_{D,tower} = \frac{1}{2} \cdot \rho_{air} \cdot D \cdot C_D \cdot (U - \dot{x})^2 = Q_{D,tower} \cdot (U - \dot{x})^2 \tag{4.42}$$

where

ρ_{air} Density of air.

D Diameter of the tower.

C_D Drag coefficient defined by structure shape.

$\dot{x}$ Motion velocity of the tower.

$Q_{D,tower}$ Quadratic drag coefficient given as aerodynamical input for tower slender element.

The wind velocity, U. will be the sum of the mean wind velocity, $\bar{U}$, and wind gust, $u(t)$. Thus, $(U(t)-\dot{x})^2 \Rightarrow ((\bar{U}+u(t))-\dot{x})$ where $\bar{U} > u(t) > \dot{x}$ and Equation 4.42 can be rewritten as:

$$q_{wind} = \underbrace{Q_{D,tower} \cdot \bar{U}^2}_{\text{Constant force}} + \underbrace{2Q_{D,tower} \cdot \bar{U} \cdot u(t)}_{\text{LF excitation force}} - \underbrace{2Q_{D,tower} \cdot \bar{U} \cdot \dot{x}}_{\text{LF damping force}} \tag{4.43}$$

For waves and currents will the only difffent be defined by the hydrodynamical and aerodynamical input, and the particle velocity a formulation. The LF damping force is a result of the relative motion between the mean pricle velocity and the system motion. It is automatically implemented in the time domain analysis as part of $D_l \cdot \dot{r}$ term in Equation 4.1.

As one of the objectives of the project is to create an simplified model where the complexity of the wind turbine is removed, will there not be described how the blades and nacelle are modelled to apply the thrust force from the theory described in Figure 4.1.1. However, a full documentation of how widn coefficient are used as a simplified method will be given in chapter 6.

Chapter 5

Load Cases

The site conditions that will be used in the time domain analysis is based on the Hywind Scotland wind power site north-east of Aberdeen. As the focus in this thesis has been to compare and analyze the compatibility of different mooring line configuration, are the environmental loads from waves, wind and current assumed to be directional aligned. It is also assumed that significant wave height H_s, and peak period, T_p, are statistically dependent on wind speed. The environmental data will be taken from *Hywind Bunchan Deep Metocean Design Basis*[17]. The wind speed will be given at 10m above sea level and selected at rated wind speed, shutdown wind speed and 50-year extreme wind speed at the given site. The turbulence model we will be using the ISO 19901-1, previously known as NPD wind spectrum, to generate the wind field. This spectrum can be seen exemplified in Figure 5.1 for a mean wind speed of 20m/s and demonstrates how the majority of energy is located at frequencies below 0.005Hz. This is interesting concerning how much LF response one should expect due to wind gust which could excite resonance in surge, sway and yaw.

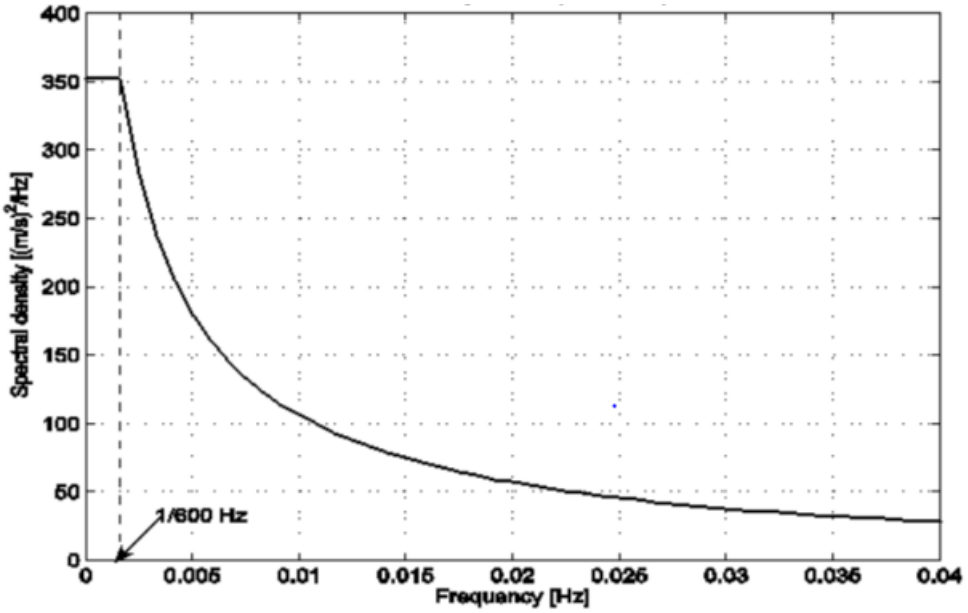

Figure 5.1: NPD spectrum for 1 hour mean wind speed of 20m/s[16]

The wind profile that will be used in the wind spectra is given by the mean wind velocity at 10m, $\bar{U}_{10}$, and formulated as:

$$\bar{U}(z) = \bar{U}_{10}\left[\frac{z}{10}\right]^{\alpha} \tag{5.1}$$

Where z is the location above water plane and α is the height coefficient which according to the SIMO user manual is always set to 0.11 for the NPD spectrum. From a study by Bak et al.[18] of the DTU 10MW reference wind turbine, will the rated wind speed be approximately at 11m/s while shutdown will occur for wind speeds above 25m/s. This wind speed is given at hub height and according to Equation 5.1 corresponds this to a wind speed of 8.4m/s and 19m/s at 10m above sea level when the hub is located 119 m above sea level. The extreme value is taken directly from the 1-hour average wind speed 10m above sea level with a return period of 50 years in *Hywind Bunchan Deep Metocean Design Basis*[17].

The irregular sea state will be generated by a JONSWAP wave spectrum determined by the significant wave height and peak period. The wave parameters will, as mentioned, be assumed statistically dependent on the wind speed for rated and shutdown condition. This implies that the probability of not exceeding the wind speed is equal to the probability of not exceeding the significant wave height in a given environmental condition. Hence, the significant wave height is determined by the fitted distribution at probabilities corresponding to the wind speeds mention above with the procedure demonstrated the arrows in Figure 5.2.

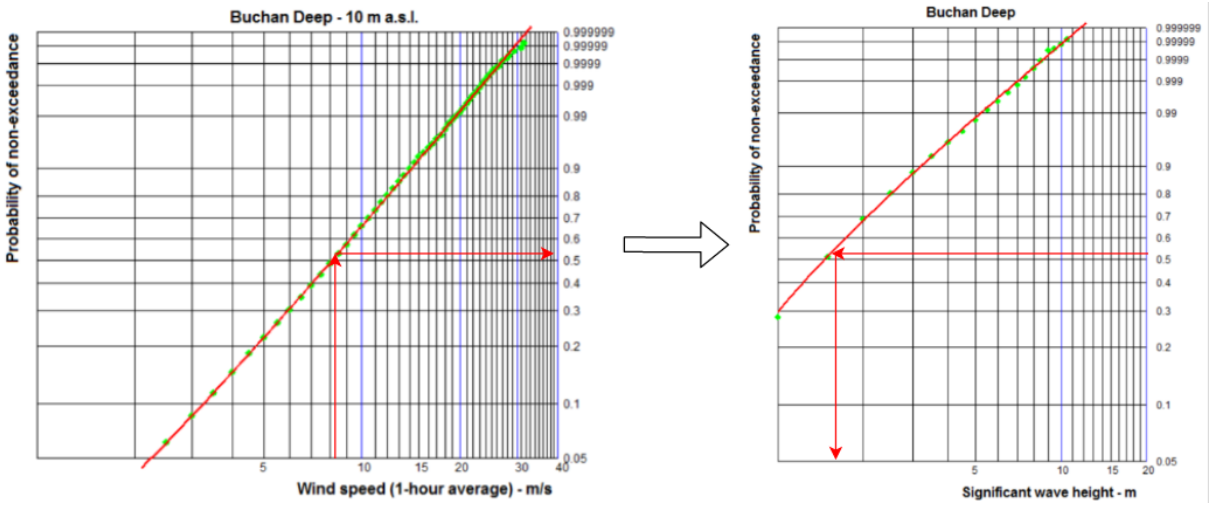

Figure 5.2: Statistically dependency between U_{10} and H_s for mean wind speed of 8.4m/s

The extreme value of H_s and T_p are based, but not extracted directly due to the difference in water depth, on the contour plot for different H_s and T_p combinations in **??**.

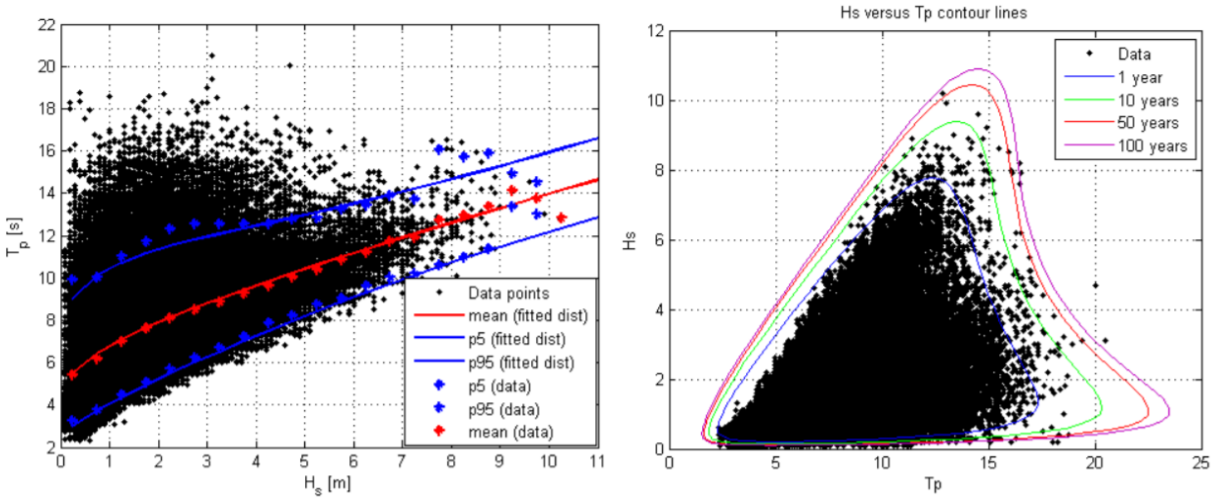

(a) Spectral peak period.

(b) Probability contour lines

Figure 5.3: Spectral peak period for given significant wave height and Probability contour lines for return periods of 1, 10, 50 and 100 years[17]

A summary of all load cases with respect to wind and waves are given in Table 5.1. It should be mentioned that load case 3 is not taken directly from the plots in Figure 5.3b, and correlate more with sea state along the 100-year contour line. The reason it is included is that the expected wave period for a water depth of 80m versus 110m are lower and it is considered interesting to analyze the system i such aggressive sea state.

Table 5.1: Load cases

	Mean wind speed 10m ASL [m/s]	**Significant wave height [m]**	**Peak period [s]**	**Turbine state**
Load case 1	8.4	1.8	7	Operational. (Max rotor thrust)
Load case 2	19	5	10	Operational. (Immediately before shutdown)
Load case 3	31	10.5	12	Parked.
Load case 4	31	10	14	Parked.

Due to limited knowledge and the complexity of the governing causes for current, are the same current profile used for all load cases. The profile is based on a 10 year return period for current speed data from Bunchan Deep[17]. The profile uses data from the current speed at sea surface as well as 25m, 40 and 60 depth and can be seen in Figure 5.4. The current speed is given by 10 minutes average speeds, and due to SIMA limitations with respect to turbulence current model, the current profile will be assumed constant for the entire simulation.

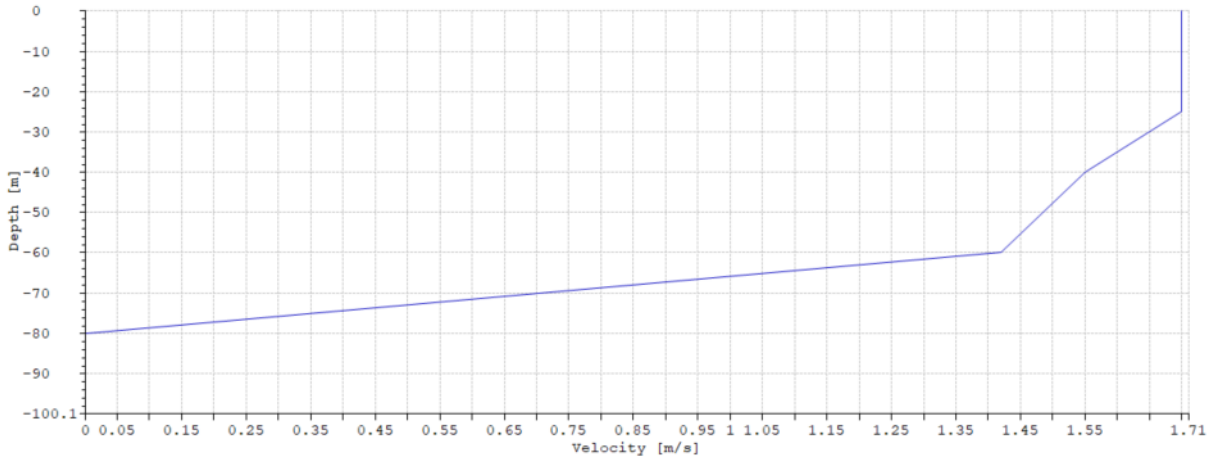

Figure 5.4: Current profile

Chapter 6

Simplified Model and initial mooring system

The initial model used for the time domain analysis is a concept design by Wang[3], which is a semi-submersible supporting the 10MW DTU reference turbine. However, to reduce the computational effort needed for each simulation, has the aim been to create a simplified model where the wind turbine's complexity is removed. It will now be given a detailed description of the modification made to the initial model in order to recreate the kinematics and behavior of the original model.

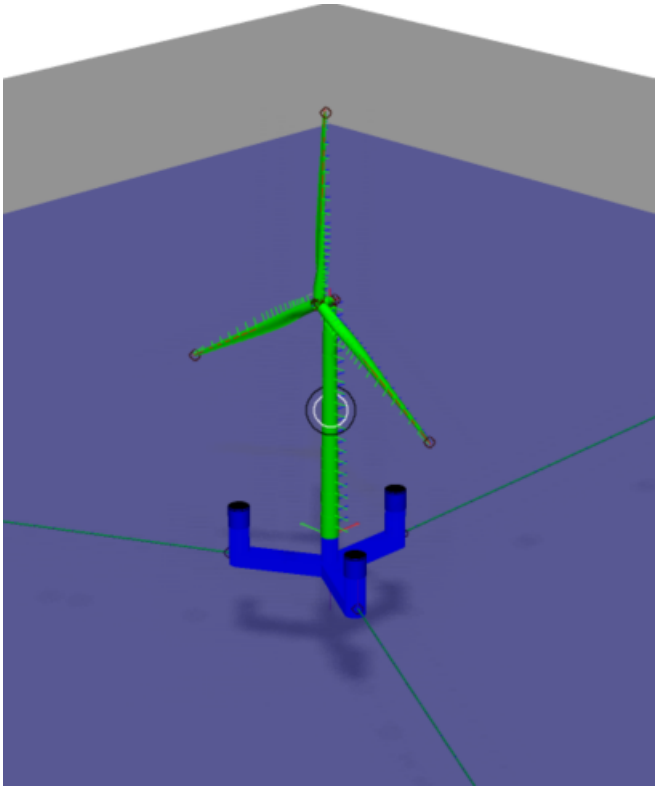

Figure 6.1: SIMA model of the CSC10MW used in full integrated dynamic analysis.

6.1 Geometry

The original model is built up by a combination of slender elements, beam elements and bar elements. The bar elements are used to model the mooring line while beam elements are used for the tower and the rotor blades. These are used in a finite element analysis to calculate the forces and stresses in these components and will in many cases be a costly process with respect to time and computational effort. It has therefore been decided to remove the tower together with the hub, nacelle and blades in an effort to reduce this cost. The Semi-submersible is modelled as a SIMO-body with slender elements for Morison's calculations.

The geometry of the floating wind turbine is presented in Figure 6.3 and all dimensions are given in meters, while angles are given in degrees. The coordinate system is defined with the origin at sea level and the x-axis in the same direction as the wind velocity in Figure 6.2. z-axis will be pointing upwards along the center of the turbine tower, and the degrees of freedom are:

Surge - Translation along x-axis

Sway - Translation along y-axis

Heave - Translation along z-axis

Roll - Rotation about x-axis

Pitch - Rotation about y-axis

Yaw - Rotation about z-axis

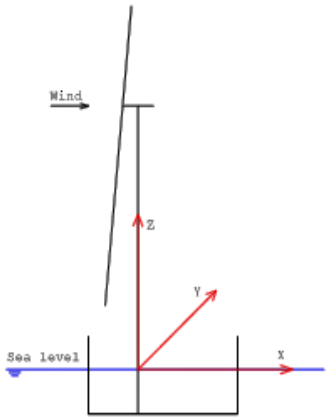

Figure 6.2: Coordinate system, Wang[3].

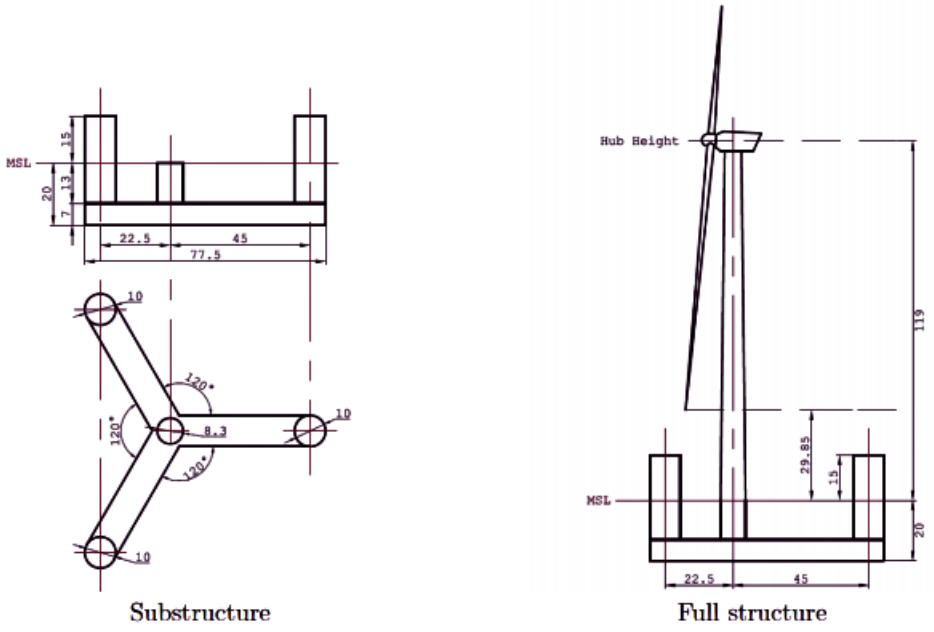

Figure 6.3: Geometry and dimensions of CSC10MW proposed by Wang[3].

6.2 Kinetics

In order to obtain the proper responses, it is important to retain the same kinetics as the original model. This involves retaining the same excitation loads, hydrostatic stiffness and inertia about origin as if the tower and rotor are still there. The new kinetics will be applied to the center of flotation which is the geometric center of the waterplane of a floating unit and is the point the unit will rotate about when exposed to an external force.

Inertia calculations

The total mass is found by superposition with calculations carried out by Wang for each component, and presented in Table 6.1

Table 6.1: Total mass calculation of CSC10MW, [3]

	Components	**Mass[tonn]**	**x[m]**	**y[m]**	**z[m]**
	Rotor	230	-7.1	0	119
	Nacelle	446	2.7	0	121.5
	Tower	628	0	0	47.6
WT	Overall	1305	-0.3	0	85.5
	Columns	1005	0	0	1.2
	Pontoons	1583	0	0	-16.5
Semi	Overall	2588	0	0	-9.6
	Ballast	10188	0	0	-16.5
Total	**Total**	14080	0	0	-5.7

The global mass moment of inertia is a measurement of an objects resists to rotational acceleration about an axis which in our case is defined by the the Cartesian system located at center of flotation. The general formulation of the mass moment of inertia is given as:

$$I_i = \int r^2 dm \tag{6.1}$$

Where r is normal distance between the axis and the the mass element, dm. However, according to *Physics for scientists & engineers* by Serway [28], is the moment of inertia of homogeneous rigid bodies with symmetry relatively easy calculated in a closed-form expression. By dividing the structure components into nacelle, rotor, tower, pontoons and side columns, it is possible to use the simplified inertia calculation for each rigid body by applying the parallel-axis theorem. Serway defines the parallel-axis theorem as; *The parallel-axis theorem states that the moment of inertia about any axis that is parallel to and a distance r away from the axis that passes through the center of mass is given by:*

$$I_i = I_{i,local} + \underbrace{M_{comp} \cdot s^2}_{\text{Steiners contribution}} \tag{6.2}$$

where $I_{i,loc}$ is the local moment of inertia of the local axis passing through the center of mass and M_{comp} is the component's mass. The Steiners contribution can then be derived from the values given in Table 6.1.

As a result of the structure's symmetry, will the remaining mass moments of inertia about x and y-axis be assumed equal. Due to the complexity of the nacelle and the rotor, will these component be considered as point loads and the inertia contribution is found by:

$$I_x \approx I_y = m \cdot r^2 \tag{6.3}$$

By considering the tower to be a rod with length, $L = 119m$, and mass, m, from Table 6.1, will the local mass moment of inertia be determined as:

$$I_{x,local} = I_{y,local} = \frac{mL^2}{12} \tag{6.4}$$

When considering the semi-submersible, will the orientation of the pontoons have different contribution to the inertia and each pontoon has to be calculated individually. However, as previously stated will $I_x = I_y$ and one therefor only have to calculate the inertia about one of the two horizontal axis. The mass of each rigid pontoon will be the sum of the pontoon itself and the ballast, $\frac{m_{pontoon}+m_{ballast}}{3} = 3924tonn$, and assumed homogeneously distributed. Each pontoon has the shape of a rectangular cuboid where two of the cuboids are tilted with and angle, $\beta = 60deg$, in the xy-plane (see Figure 6.4 for further elaboration).

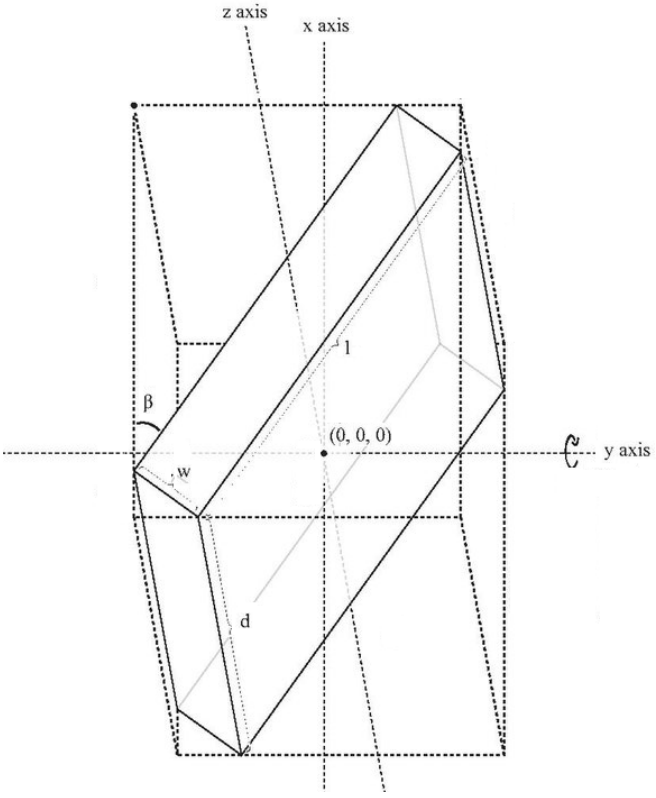

Figure 6.4: Tilted rectangular cuboid

For such case will the local moment of inertia about the y-axis be given by:

$$I_{y,local} = \frac{m}{12}(l^2 \cos^2\beta + w^2 \sin^2\beta + d^2) \tag{6.5}$$

Where l, w, and d is the pontoons length, width and height respectively. For the non-tilted cuboid with mass center along the x-axis, is the inertia determined by:

$$I_{y,local} = \frac{m}{12}(l^2 + d^2) \tag{6.6}$$

The local moment of inertia about the vertical axis will be the same for all three pontoons and formulated as:

$$I_{z,local} = \frac{m}{12}(l^2 + w^2) \tag{6.7}$$

By making the same assumption for the side columns as we did for the pontoon where we assumed a rigid homogeneous body. Will the local moment of inertia for a solid cylinder with a constant outer radius, r, and height , h, be given by:

$$I_{x,local} = I_{y,local} = \frac{m}{12}(3r^3 + h^3) \tag{6.8}$$

$$I_{z,local} = \frac{mr^2}{2} \tag{6.9}$$

It is here evident that the largest contribution will come as a result of the steiners contribution from the parallel-axis theorem.

The final results can be seen in Table 6.2, where the local moment of inertia and the Steiners contribution for all components are added together to find the global mass moment of inertia about origin. These result corresponds well with the ones from the original model and will be used for further simulations.

Table 6.2: Global moment of inertia

Components	**Global I_x**	**Global I_y**	**Global I_z**
Columns	1.11E+09	1.11E+09	2.09E+09
Pontoons (incl. ballast)	7.61E09	7.61E+09	1.61E+10
Tower	2.16E+09	2.16E+09	2.16E+07
Nacelle	6.58E+09	6.58E+09	3.25E+06
Rotor	3.26E+09	3.26E+09	1.16E+07
Total	2.07E+10	2.07E+10	1.02E+10

6.2.1 Quadratic wind coefficients

Initially, slender elements were utilized to implement the rotor thrust with large quadratic drag coefficients to imitate the rotor thrust. However, due to a bug in SIMO that was supposedly fixed in SIMO v4.8, but seems to be occurring again, a new method had to be used in order to include the aerodynamic wind forces.

The new method involves adding a quadratic wind coefficient to the SIMO-body's kinetics, and it has many similarities to the quadratic drag force. Nonetheless, instead of creating a force on a strip, will the quadratic wind coefficient creates a force an moment in/about origin, and be a function of the wind speed squared at a given reference height, see Equation 6.10 and 6.11.

$$F_{wind,i} = C_{wind,i} \cdot U_{10}^2, \quad \text{for } i = 1,2 \tag{6.10}$$

$$M_{wind,i} = C_{wind,i} \cdot U_{10}^2, \quad \text{for } i = 4,5 \tag{6.11}$$

Here $F_{wind,i}$ and $M_{wind,i}$ is the wind force and moment acting in the center of flotation. $C_{wind,i}$ is the product of the drag loads on the tower and the thrust force from the rotor. As mentioned in chapter 5 will there be used a wind profile coefficient which encounters for changes in wind speed. Hence, should this wind profile be implemented in the quadratic wind coefficient as the coefficient only uses the wind speed at 10m above SWL.

The drag on the tower is given by the standard drag force formulation:

$$F_d = \int_0^{Zhub} \frac{1}{2} \rho_{air} C_D D(z) U(z)^2 dz \tag{6.12}$$

Where ρ_{air} is the air density and C_D is the drag coefficient. The air density is assumed constant and set to $1.225\,\mathrm{kg/m^3}$, which is the ISA standard for air density at sea level and 15 degrees Celsius. The drag coefficient is found using DNV-RP-C205[13] for different Reynolds numbers and surface roughness. The surface roughness is assumed to be $5 \cdot 10^{-10}$, which is equivalent to a painted steel surface, while the Reynolds number is approximated greater than 10^6. The drag coefficient is then assumed constant and equal to 0.7. $D(z)$ is the diameter of the tower which has a conical shape given by:

$$D(z) = 8.16 - 0.022z \tag{6.13}$$

The total drag on the tower with reference wind speed at 10m is given by:

$$F_{tower,i} = \int_0^{119} \frac{1}{2} \rho_{air} C_D (8.16 - 0.022z) \left(\frac{z}{10}\right)^{0.22} dz \cdot U_{10}^2 = C_{i,tower} \cdot U_{10}^2 \quad \text{for } i = 1,2 \tag{6.14}$$

This force will naturally create a moment acting around the center of flotation and is expressed as:

$$M_{tower,i} = \int_0^{119} \frac{1}{2} \rho_{air} C_D (8.16 - 0.022z) \left(\frac{z}{10}\right)^{0.22} z dz \cdot U_{10}^2 = C_{i,tower} \cdot U_{10}^2 \quad \text{for } i = 4,5 \tag{6.15}$$

The rotor thrust will depend very much on the blade's operational state and can be seen in Figure 6.5. Hence, it is natural to estimate a thrust coefficient for each of the following regimes; below rated (0-11.4m/s), operational (11.4-25m/s) and shutdown (above 25m/s).

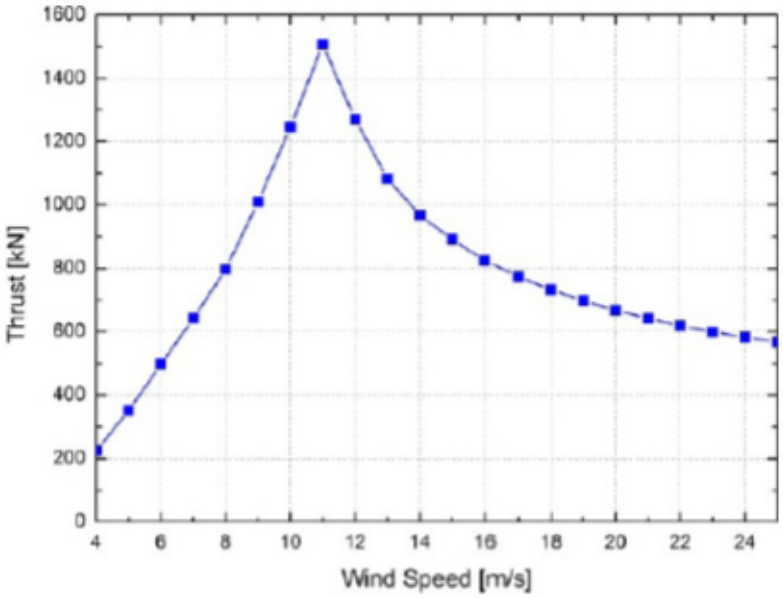

Figure 6.5: Thrust curve as function of wind speed at hub height, [18]

A quadratic coefficient for below rated is obtained by using a regression tool and approximated to 12 500 $\mathrm{Nm^2/s^2}$. The quadratic wind coefficient for below rated rotor thrust is then given by:

$$F_{i,thrust} = C_{i,thrust} * U_{hub}^2 = 12500 \cdot \left(\frac{119}{10}\right)^{0.22} \cdot U_{10}^2 = C_{i,wind} \cdot U_{10}^2 \quad \text{for } i = 1,2 \tag{6.16}$$

Where U_{hub} is the wind velocity at hub height (119 m). The resulting moment can then be found by:

$$M_{i,thrust} = F_{i-3,thrust} \cdot z_{hub} = C_{i,wind} \cdot U_{10}^2 \quad \text{for } i = 4,5 \tag{6.17}$$

Where z_{hub} is the hub height above still water level.

When the wind speed enters the second regime, the thrust force starts to decrease, and modelling this force with quadratic wind coefficients becomes more difficult. However, as stated in chapter 5 will the region of interest for this operational regime be immediately before shutdown.. For simplicity reasons, is the thrust assumed constant for wind speed aroudn 25 $\mathrm{m/s}$. The magnitude is approximated by the thrust curve at 25 $\mathrm{m/s}$ and applied to the model by a specified force of 580 kN located at z_{hub} which again will create a moment about center of flotation.

When the wind speed exceeds 25 $\mathrm{m/s}$, the blades are feathered which results in a drop in the aerodynamic forces and the turbine is said to be ”parked”. The force acting on the rotor shaft be more or less equal to the drag on the blades and significantly smaller than in region 1 and 2. In order to quantify the loads on the parked model for wind speeds above 25 $\mathrm{m/s}$, is an example model in SIMA used to create the thrust/shaft-load curve in Figure 6.6. The model is of a land-based 10MW turbine based on the DTU reference turbine by Bak et al[18]. This was done by pitching the blades -90 degrees and switch off the induction which avoids the use of BEM. The turbine is then fixed by creating a master-slave connection between the shaft and the tower top.

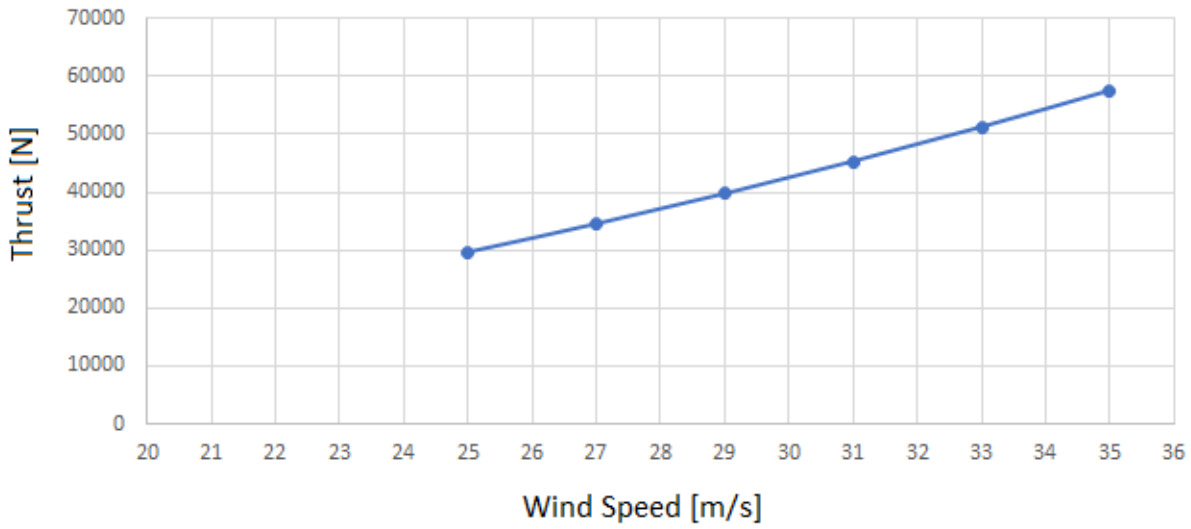

Figure 6.6: Thrust curve for parked turbine as function of wind speed at hub height

Like for the first region, is a regression tool used to approximate a quadratic load coefficient of $49\,\mathrm{Nm}^2/\mathrm{s}^2$. By implementing the wind speed relation, will the thrust contribution be given as:

$$F_{i,thrust} = C_{i,thrust} * U_{hub}^2 = 49 \cdot \left(\frac{119}{10}\right)^{0.22} \cdot U_{10}^2 = C_{i,wind} \cdot U_{10}^2 \quad \text{for } i = 1,2 \tag{6.18}$$

$$M_{i,thrust} = F_{i-3,thrust} \cdot z_{hub} = C_{i,wind} \cdot U_{10}^2 \quad \text{for } i = 4,5 \tag{6.19}$$

The resulting quadratic wind coefficient is found by adding the contributions together with the drag loads by superposition principle. It should again be mentioned that the thrust force in region 2 is not included in the quadratic wind coefficient but added as a specified force directly at the model. The coefficients for surge and pitch direction (i=1 and 5) are presented in Table 6.3.

Table 6.3: Quadratic wind coefficients, C_i, for i = 1 and 5 from tower drag and rotor thrust

	C_1 $[Nm^2/s^2]$			C_5 $[Nm/s^2]$		
	4-11m/s	11-25m/s	Above 25m/s	4-11m/s	11-25m/s	Above 25m/s
$C_{i,tower}$	495	495	495	30630	30630	30630
$C_{i,thrust}$	22649	-	85	2.695e+06	-	10115
$C_{i,tot}$	23144	495	580	2.725e+06	30630	40745

6.3 Initial mooring line configuration

The initial mooring design is based on the spread catenary design used for Hywind Scotland. The mooring lines consist exclusively of chains and will be modeled in RIFLEX using bar elements with one degree of freedom in axial direction. The system has been modeled by following the conversion of SIMO catenary system to RIFLEX slender system description in the SIMA User Manual[16] which goes through the procedure of create mooring lines out of bar and beam elements. The mooring lines will be defined between one supernode located at the semi, and one at the anchor position. The line length is assumed to be of the same length as

Hywind Scotland, and the anchors' location in Table 6.4 are calculated based on the catenary equations from chapter 2 in order to achieve an adequate pre-tension.

Table 6.4: Anchor position for initial design

	X-position	Y-position	Z-position
Anchor 1	671.44	0	-80
Anchor 2	-335.72	581.49	-80
Anchor 3	-335.72	-581.49	-80

The lines are then given several cross-section properties found from the hardware catalogues by Ramnas[29], containing information about breaking strength and unit mass in air for different diameters. It also suggests an estimate of unit mass in air to water ratio of $\frac{Ww_{water}}{Ww_{water}} = 0.87$, which account for the buoyancy of the chain. This mass-ratio is then used to estimate the external cross-section area from Equation 6.20 and used as RIFLEX input.

$$Ext\_Area = \frac{W_{air}}{\rho_{water}} \left(1 - \frac{W_{water}}{W_{air}}\right) \tag{6.20}$$

As a bar element has no bending stiffness, will only the axial stiffness be added to the cross section. This stiffness is given in *kN* by Equation 6.21 where d_{chain} is chain diameter in meter.

$$EA = 0.854 \cdot 10^8 \cdot d_{chain}^2 \tag{6.21}$$

A way to improve numerical stability is to create an elongation-force relationship for the axial stiffness. This makes it possible to use one stiffness in tension and another one in compression. Hence, the stiffness from Equation 6.21 is used in tension, while the system will be given a much lower stiffness in compressed which will be more realistic considering the chain characteristics.

The preliminary mooring line properties are presented in Table 6.5 with drag coefficient for studless chain taken from DNV-GL-OS-E301[2] and added mass presented in the SIMO manual[16].

Table 6.5: Preliminary mooring system properties

Mooring line Properties		
Chain type	Studless	R5
Diameter	0.147	m
Break load	22.3	kN
Length	640.0	m
Unit mass in air	432.0	kg/m
External cross-section area	0.055	mˆ2
Axial stiffness, EA	1.85E+06	kN
Drag coefficient in normal dir.	2.4	[-]
Drag coefficient in tangential dir.	1.15	[-]
Added mass coefficient in normal dir.	1.0	[-]
Added mass coefficient in tangential dir.	0.0	[-]

6.4 Model verification

6.4.1 Decay test

In order to document the system's natural periods will a decay test be performed. The decay test will be performed by applying a specified force/moment in order to achieve an initial displacement. The specified force will consist of a ramp force acting over 100 s, followed by a constant force for the next 200 s. The load set up can be seen in i Table 6.6. The time series of surge, heave, pitch and yaw are presented in Figure 6.7 - 6.10 with natural period calculations taken from results between 350-1000s to avoid coupling effect at the ends.

Table 6.6: Simulation parameters for the decay tests

Motion	Force/Moment	Ramp duration (s)	Constant duration
Surge/Sway	1000 kN	100	150
Heave	10000 kN	100	150
Roll/Pitch	180000 kNm	100	150
Yaw	17000 kNm	100	150

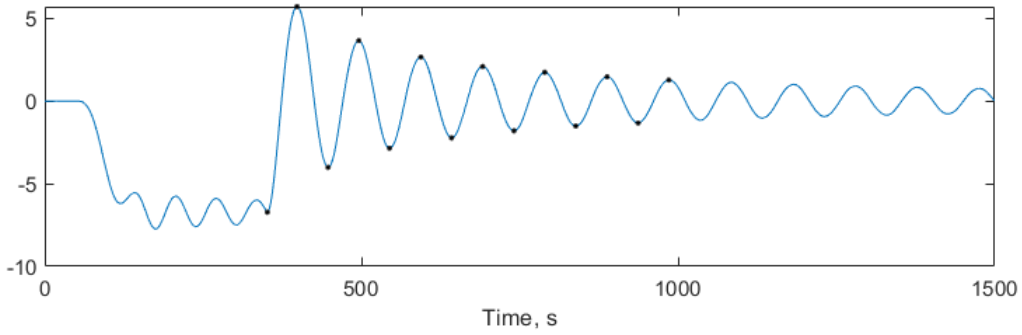

Figure 6.7: Decay test in surge, initial design

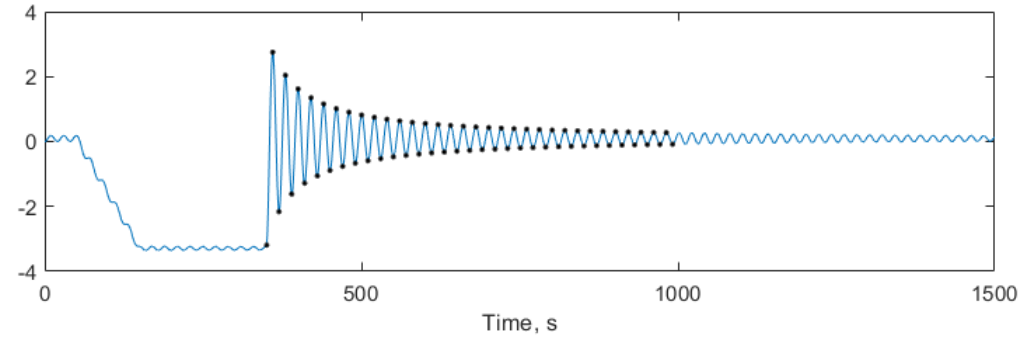

Figure 6.8: Decay test in heave, initial design

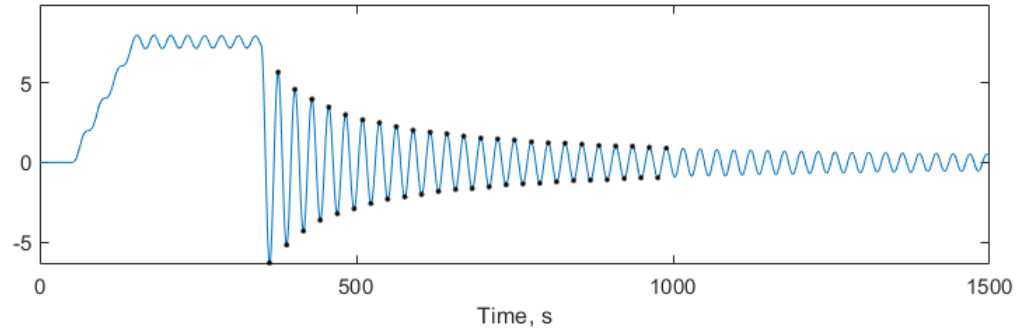

Figure 6.9: Decay test in pitch, initial design

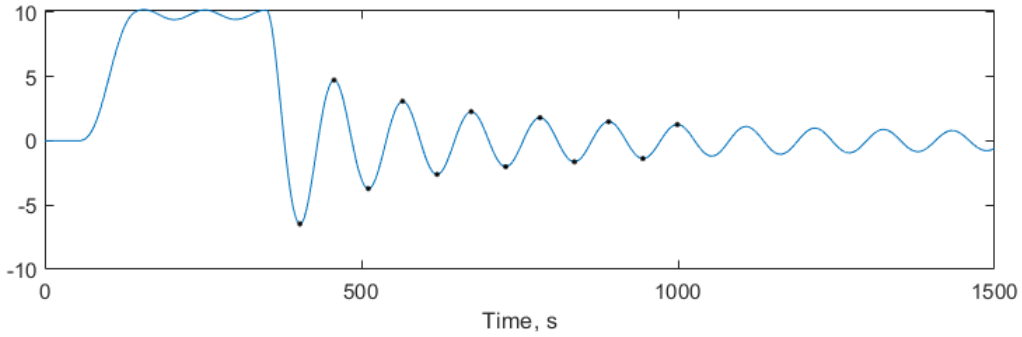

Figure 6.10: Decay test in yaw, initial design

The result from the decay test are summarized in Table 6.7 together with the natural period presented by Wang and the expected periods based on simple hand calculations for heave and pitch. These calculations are based on the hydrostatic stiffness described in chapter 4 and determined by Equation 6.22 and 6.23.

$$T_{n,heave} = 2\pi \cdot \sqrt{\frac{M + A_{33}}{K_{33}}} \tag{6.22}$$

$$T_{n,pitch} = 2\pi \cdot \sqrt{\frac{I_y + A_{55}}{K_{55}}} \tag{6.23}$$

Where M and I_y are the total mass and global moment of inertia about the y-axis presented previously in this section. A_{33} and A_{55} are the added mass in heave and pitch motion and are taken from the radiation data from the original model at the expected oscillation period.

Table 6.7: Natural period of initial design

Degree of freedom	Decay test	Original Model	Hand calculations
Surge	97.5s	-	-
Sway	97.4s	-	-
Heave	20.0s	20.5s	20.1s
Roll	27.1s	-	-
Pitch	26.5s	26.3s	28.5s
Yaw	107.2s	-	-

The results gives an good indication that the model represents a realistic FWT with natural periods within the expected range. The test also shows that the simplification made is within what we might call an acceptable aberration from the original model with respect to heave and pitch motion. The slight difference in pitch is probably mainly due to the difference in the moment of inertia as a result of the simplifications made when calculating these, which as seen in Equation 6.23 has a direct effect on the natural period. The reason we do not get the same result in heave is assumed to be due to some extra stiffness from the weight of the mooring lines which is not included in the hand calculations.

6.4.2 System characteristics

A load-displacement test, or a pull-out test is performed to establish a restoring curve in surge direction. Due to the arrangement of the mooring lines, is the test performed in both positive and negative x-direction, as the system is expected to be softer when exposed to an external force in-between two mooring lines versus when aligned. The result of the test can be seen in Figure 6.11 and the difference between in-line($180deg$) and in-between($0deg$) is well visualized (see Figure 6.2 for def. of coordinate system). The test is conducted in the same manner as the decay test, but it do not let the structure go after a certain time and apply numerous different values of the specified forces.

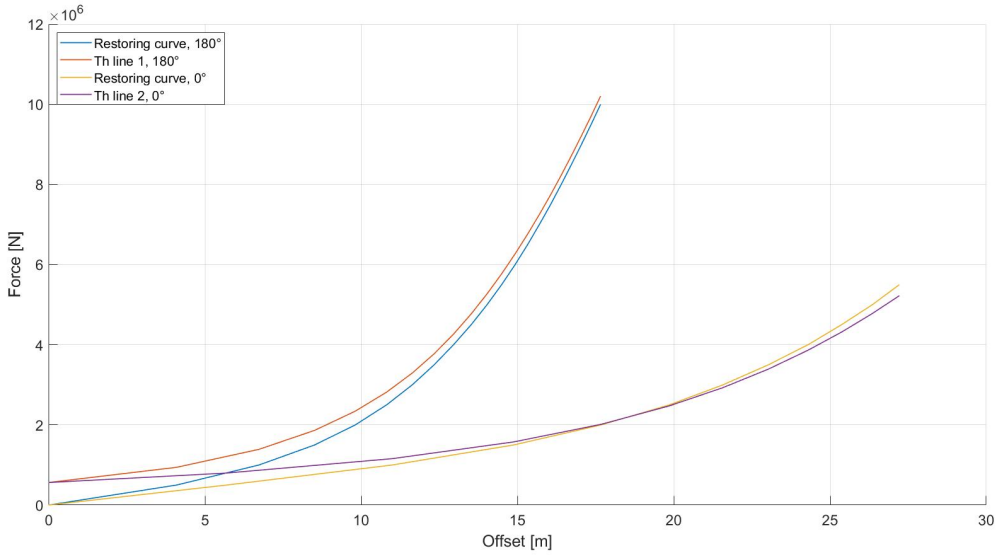

Figure 6.11: Pull out test in surge

From these results, it is possible to determine an expected surge offset from the complete restoring curve in x-direction, as seen in Figure 6.12. By assuming positive excitation force in positive x-direction and vice versa, it is possible to determine whether or not the force components are modeled correctly for the simplified model. In other words, it will be possible to test how well the quadratic wind coefficient and the slender element on the semi-submersible are working based on hand calculation.

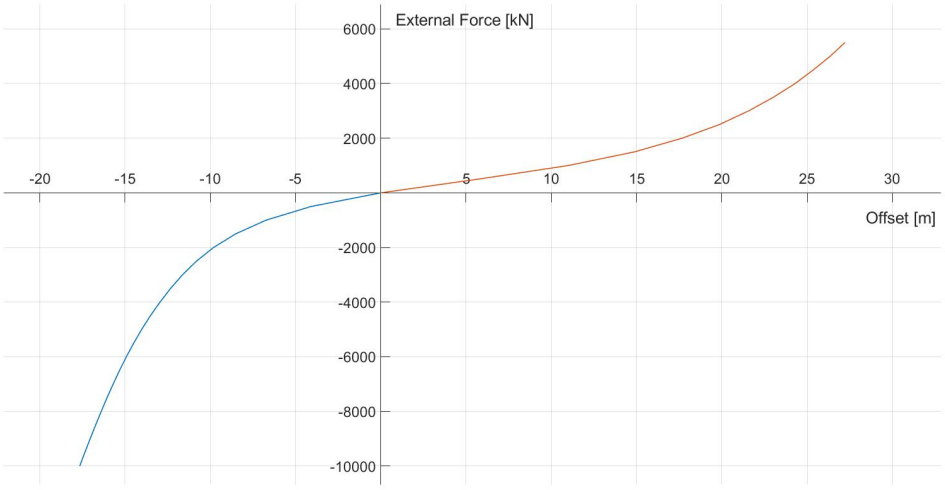

Figure 6.12: Restoring curve in surge

It is decided to run one 3-hour simulation from each operation state, meaning we will run one condition for the rated wind speed, one immediately before shutdown and one extreme condition for wind, waves and current. This test will also give a good indication on which condition will give the largest design tension, T_d, for the ULS test. However, the main goal is to verify the quadratic wind and drag coefficients by doing an estimate based on the restoring curve and the hydrostatic stiffness. This is done by calculating the current force and the wind force from the given wind and current velocity. The expected surge motion is then read directly from Figure 6.12, while the expected pitch motion, r_5, is given by:

$$r_5 = M_{tot}/K_{55} \tag{6.24}$$

Where M_{tot} is the total moment about the center of flotation as the sum of the contribution from wind and current force. The calculated mean loads and expected motion is presented in Table 6.8, while the results from the simulations are summarized Table 6.9.

Table 6.8: Expected motion from hand calculations

Load/motion	Rated wind speed	Shutdown windspeed	50-year return period
F_{tot} [N]	-3.6E+06	-2.8E+06	-2.5E+06
M_{tot} [Nm]	-1.6E+08	-8.7E+07	-1E+07
Surge [m]	-12.2	-11.3	-11.2
Pitch [deg]	-7.2	-2.27	-0.46

Table 6.9: Motion and line tension statistics from 3 hour simulations

Statistics	Data	rated wind speed	Shutdown wind speed	50-year return period
	Surge [m]	-12.9	-11.7	-11.5
	Pitch [deg]	-6.4	-1.9	-0.1
	Line 1 [kN]	4106	3392	3549
Mean	Line 2 [kN]	482	520	534
	Surge [m]	-14.3	-13.4	-16.0
	Pitch [deg]	-11.9	-3.4	-4.1
	Line 1 [kN]	6231	5675	11531
Extreme	Line 2 [kN]	781	806	808
	Surge [m]	0.4	0.4	1.3
	Pitch [deg]	1.5	0.4	0.9
	Line 1 [kN]	341	444	1692
Std	Line 2 [kN]	13	18	49

The result in the tables above provides good verification that at least the current loads and the aerodynamic loads are been implemented correctly. From the standard deviations in extreme weather condition, one could expect large dynamic responses which will provide a significant large design tension in the mooring line.

6.4.3 Seed convergence test

The results above are only represented by one realization for each load condition. From chapter 3 it is stated that a total of 10-20 3-hour realization is needed to establish the extreme value distribution for the largest line tension. It is also stated that the Gumbel distribution is a good statistical model for the largest line tension, which also is demonstrated by the probability plot in Figure 6.13.

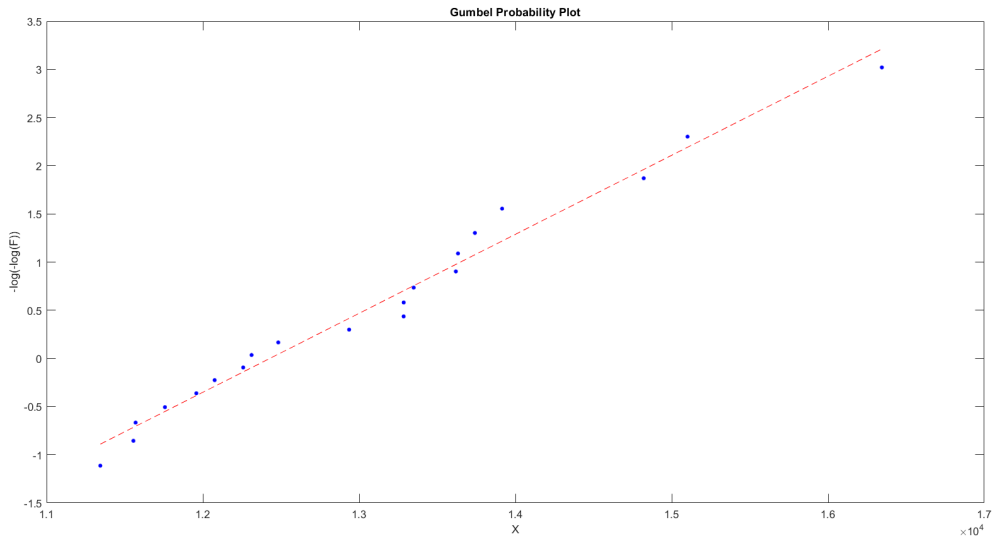

Figure 6.13: Gumbel probability plot where the blue dots are measured extreme values and the red line is a linearization of the Gumbel distribution

In order to establish the number of realizations needed to account for stochastic variability, a convergence test is performed to determine when the value of the MPM no longer changes with respect to the number of realizations. This is demonstrated by plotting both the probability density function, PDF, for different sample sizes, and by a convergence plot. Figure 6.14 shows how the pdf moves towards a larger line tension as the number of seeds increases from 3 to 11 seed and then stabilize around one value. In Figure 6.15 it is clear that the MPM-value converges after approximately 10 realizations, and it is therefore decided that 12 realizations will be used to determine the most probable largest line tension used to estimate T_{dyn}.

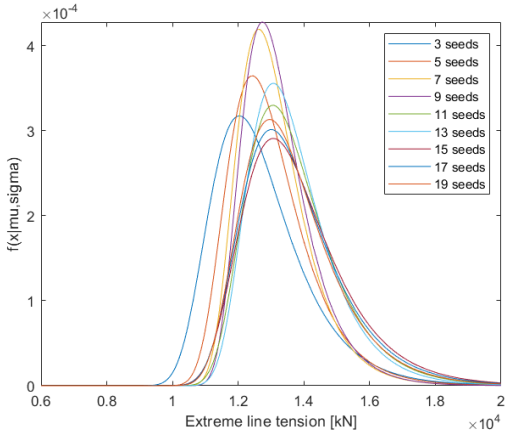

Figure 6.14: Probability density function of different extreme value samples

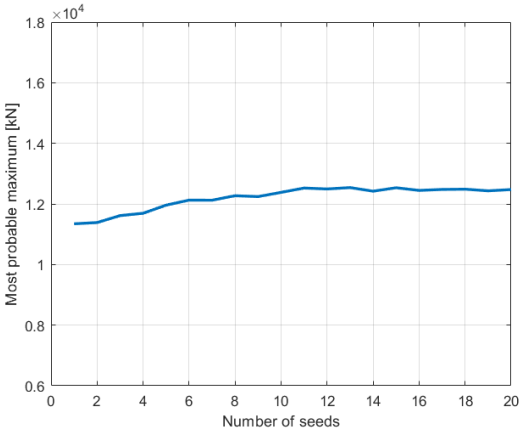

Figure 6.15: MPM convergence plot

Chapter 7

Proposed mooring line configurations

In addition to the initial catenary mooring system, which consists of chain lines, an additional three configurations will be proposed where there will be two polyester configurations and one nylon configuration. The design of these are based on theory of taut mooring systems in order to determine the required mooring line length and anchor position for adequate pre-tension and horizontal stiffness. The systems are then interpolated in SIMA to account for the use of buoy and/or clump weights.

The first polyester configuration will be divided into three different sub systems with different diameters. These will be tested with the objective to compare and verify the feasibility of thinner ropes as a solution to reduce cost. For the second polyester configuration, a comparison analysis will be performed where a linear and non-linear stiffness models will be used for the same configuration. The base case of the linear polyester systems assumes $EA = 20 \cdot MBS$, while the non-linear model uses a tension-elongation relationship based on Equation 7.1 proposed by Larsen[8]. In addition to the base case, $EA = 20MBS$, will a $EA = 15MBS$ be tested in the stiffness model comparison analysis.

$$\frac{T}{MBS} = 0.11 \cdot [exp(50 \cdot \varepsilon) - 1] \tag{7.1}$$

All line properties for the synthetic ropes are taken from Bridon hardware catalogue[30] where Superline Polyester and Superline Nylon OCIMF 2000 line will be used. Due to the limited line dimension for the nylon rope, will these properties be approximated by interpolation. The base case for nylon axial stiffness is $EA = 5 \cdot MBS$ and is based on a study by Huntley[31].

All systems will be tested for the water depth of 80m and the synthetic rope systems will all be attached to a 30m chain at the upper and lower ends with the same properties as the one used for the catenary system. The polyester systems will also be equipped with a buoy and clump weight attached to the mooring lines as seen in Figure 7.1. This will help keeping the polyester off the seabed at the lower end, and reduce the angle between the vertical axis and mooring line, hence reduce the stiffness in the horizontal plane. For the nylon system it has been decided only to use the buoy, see Figure 7.2, to keep the rope off the seabed and take full advantage of the elastic stiffness and reduce the mooring line length.

A detailed description of each system's properties are given Table 7.1 atthe end of this section.

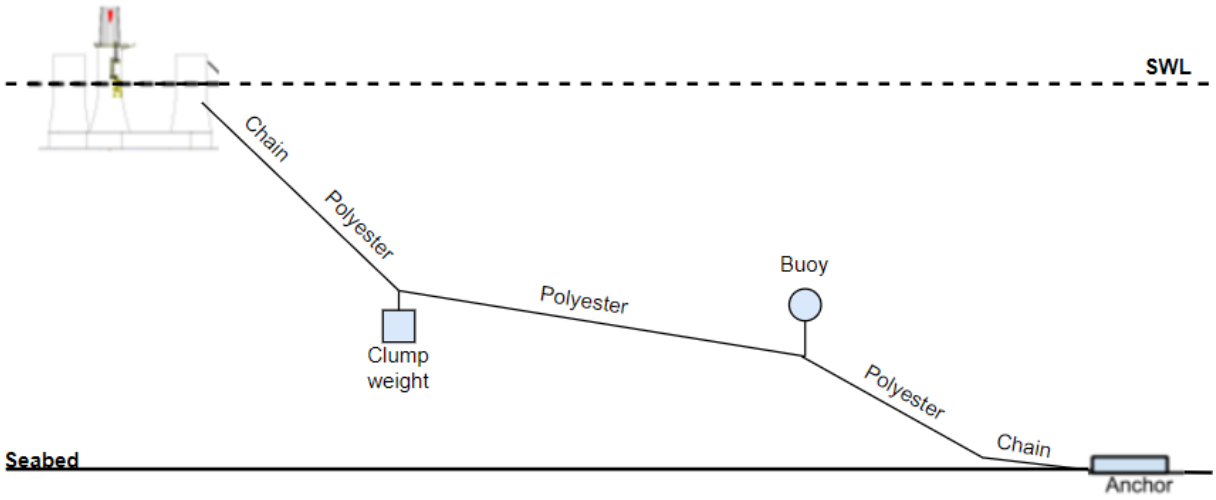

Figure 7.1: Polyester mooring line configuration.

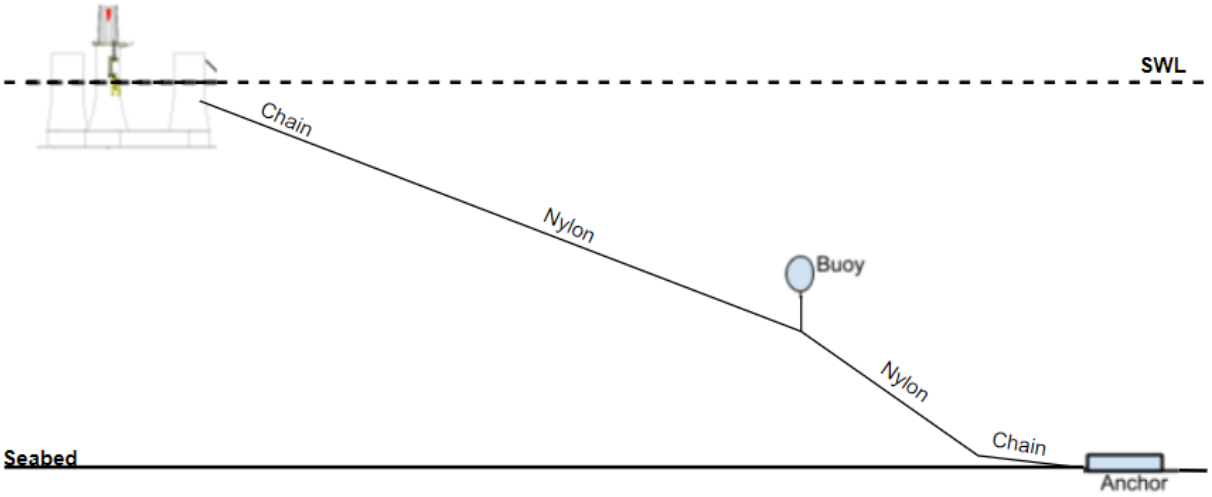

Figure 7.2: Nylon mooring line configuration.

Table 7.1: Proposed mooring line properties

	System #	Diameter [m]	Mass air [kg/m]	Mass water [kg/m]	MBS [kN]	Length [m]	Anchor radius [m]	Clump [tonn]	Buoy [tonn]	Stiffness model
Chain	I	0,147	432	375	22294	640	671	[-]	[-]	Equation 6.21
Polyester	II	0.286	52.5	13.2	22563	1100	1150	25	10	20MBS
	III	0.257	42.2	10.6	17858	1100	1150	25	10	20MBS
	IV	0.223	31.9	8.0	13734	1100	1150	25	10	20MBS
	V	0.286	52.5	13.2	22563	997	1050	25	10	20MBS
	VI	0.286	52.5	13.2	22563	997	1050	25	10	15MBS
	VII	0.286	52.5	13.2	22563	997	1050	25	10	Equation 7.1
Nylon	VIII	0.305	66.9	9.1	15000	600	660	25	10	5MBS

Chapter 8

Results and Discussion

In the following section will the results obtained from the time domain analysis of all the proposed systems be presented and further discussed. It will start with a presentation of the main statistics concerning the feasibility of a mooring system. The subsections that then follow will give a more comprehensive comparison between some of the systems with a focus on frequency responses and system characteristics.

The results from the decay tests are summarized in Figure 8.1 for surge, heave, pitch and yaw motion. The sway and roll motions are documented for the chain catenary system in subsection 6.4.1 approximately identical as the surge and pitch motion respectively, hence have only surge, heave, pitch and yaw motion been considered for the other systems. By comparing the natural period in heave and pitch, it is clear that the mooring system will have very little effect on the motion response. The natural period in surge is significantly larger for System I compared to the rest of the systems, and we will therefore expect more resonance response due to the energy density of the NPD spectrum in Figure 5.1 for load cases with large quadratic wind coefficients.

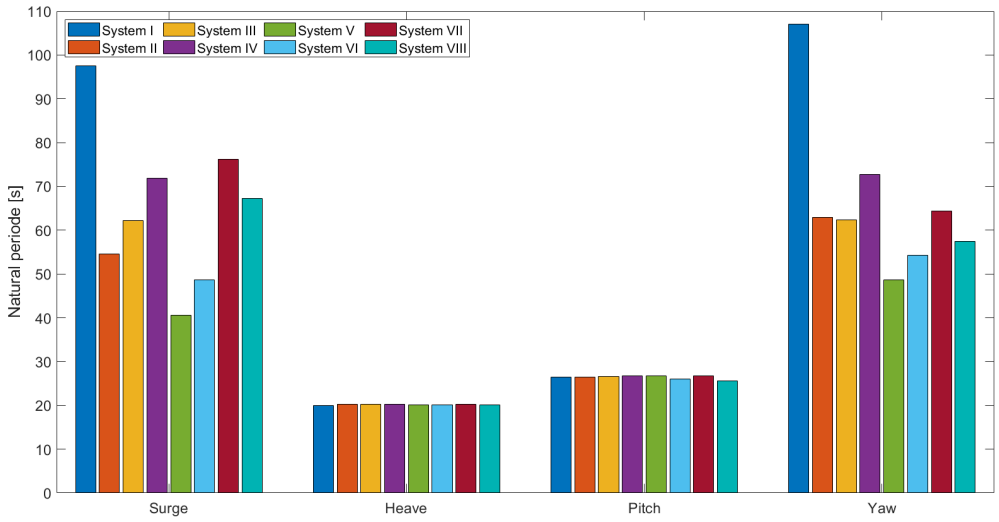

Figure 8.1: Extreme and mean surge response

In Figure 8.2 to 8.4 are the absolute value of the motion responses for each loads case presented by bar graphs. The extreme value is color-coded for each system while the mean value i represented by the dark bar located at the center of each extreme value bar. The extreme values are taken as the most probable maximum, MPM, from the ULS test where the number of seed are determined i the same manner as in subsection 6.4.3 for each system. The surge graph also includes a conservative power cable offset limitation on 25% of the water depth. However, this has not been largely emphasized in this thesis and used more as an indication of whether or not the systems are within a reasonable extreme. The statistical values are given by the ULS-test, and a complete summary of each realization is given in Appendix B

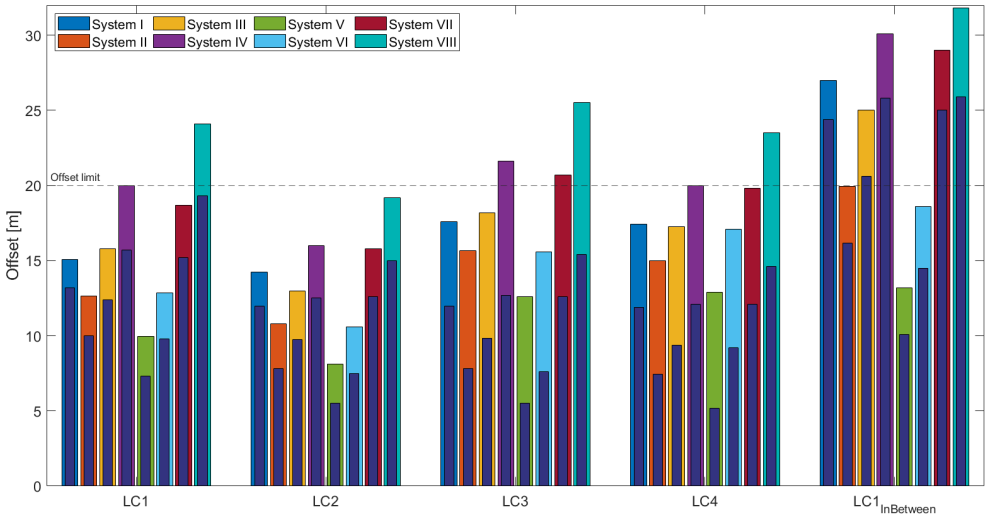

Figure 8.2: Extreme and mean surge response

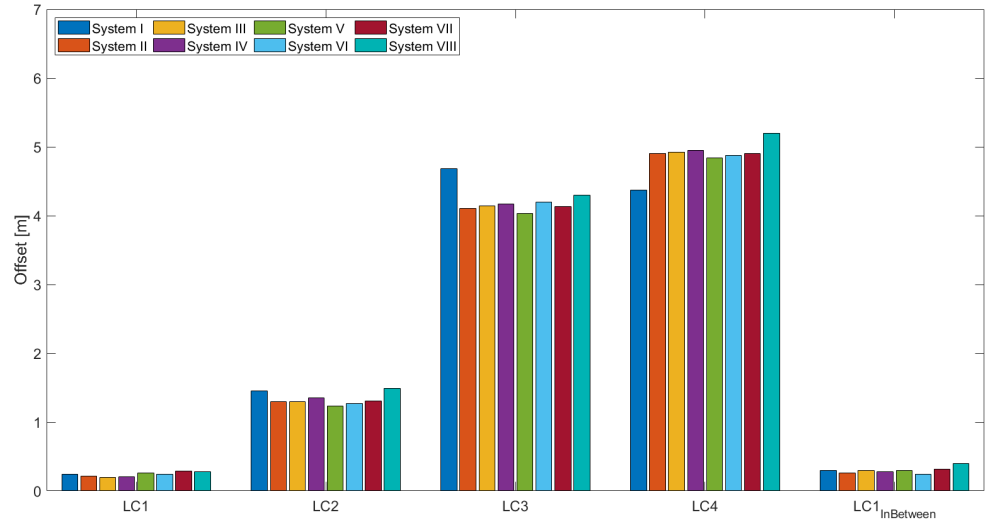

Figure 8.3: Extreme and mean heave response

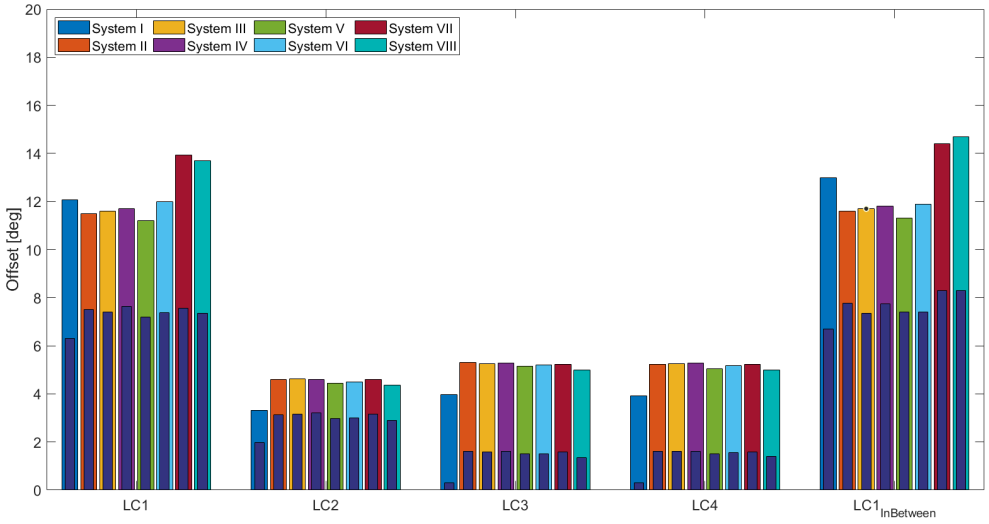

Figure 8.4: Extreme and mean pitch response

By study the result, it becomes clear that the largest offset in surge will be occurring when the environmental loads are aligned between two mooring lines. It is also interesting to see how little difference there is in the largest offset for load case 1 and load case 3 even though the environmental conditions are very different. This substantiates what was stated in chapter 3 about the importance of evaluating the responses at not only the extreme weather condition.

The heave motion barely differs between the different systems and only increases when the significant wave height increases. The slight exception is the chain catenary, system I, which is assumed to be a result of some extra excitation load from the movement of the heavy mooring lines, but is not further examined.

It has already been stated in Table 6.8 that the wind loads will dominate the mean offset in pitch. Hence, a reduction in thrust will result in a smaller mean offset which is also observed when comparing the mean offset for load case 1 and 2 with load case 3 and 4 where the turbine is parked. It is observed that the catenary system will have a slightly smaller mean offset which is a result of the moment created by the heavy mooring lines when the windward line is stretched and applies more vertical pull. The dynamic response in pitch will be caused by wind gusts and surface elevation due to waves.

The mooring line tension is summarized in a similar manner as the motion response, with the extreme value color-coded with the mean value inside it. The extreme values in Figure 8.5 will also here be representing the MPM value for the most loaded mooring line given for all systems and load cases. The extreme value in Figure 8.6 on the other hand, represents the most probable minimum line tension for the leeward mooring line.

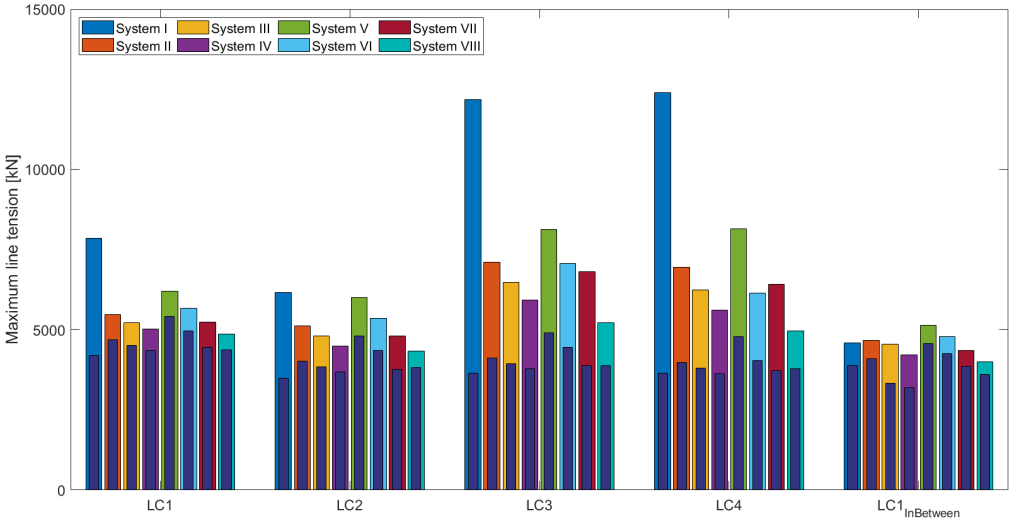

Figure 8.5: Extreme and mean windward line tension response

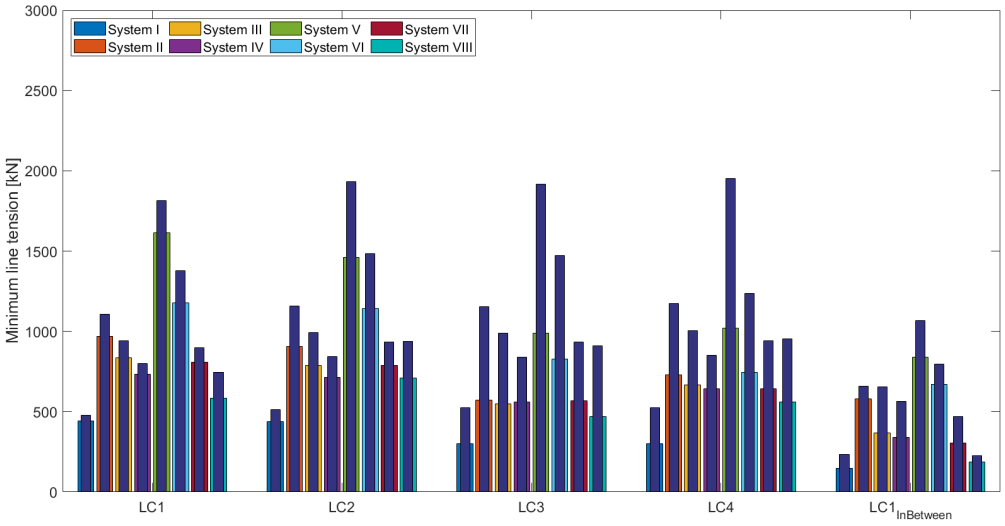

Figure 8.6: Extreme and mean leeward line tension response

For the largest loaded mooring line is the mean tension found to be quite similar both between the different load cases, but also to some extent between the systems. The largest difference is therefor given by the dynamic response and demonstrated by the extreme value. This is particularly noticeable for the System I for LC3 and LC4 compared to LC1 and LC2. This proves the difference in mooring line behavior between a chain catenary system and a synthetic fiber robe system, as a smaller offset in the horizontal plane for the catenary system leads to larger line tension compared to e.g system III and VII. This is also observed between the polyester systems where a large axis stiffness results in larger top end line tension.

The lowest line tension for the leeward mooring line is found to be very much dependent on the pre-tension given in Table 8.1. The most noticeable is how little dynamic response there is in system I, especially for LC1 and LC2. Table 8.1 also provides a summary of the largest extreme response and its respective mean value for each system. These values will provide an indication of the utilized capacity related to each mooring line material limit and the ULS requirement presented in chapter 3. As a recap is the requirement of the design tension, T_d, and utilization factor, UF, defined respectively for consequence class 1 as:

$$T_d = 1.3 \cdot T_{c,mean} + 1.75 \cdot [MPM - T_{c,mean}] < S_c \tag{8.1}$$

$$UF = \frac{T_{\text{pret}} \cdot 1.2 + \left[T_{\text{pret}} - MPM\right] \cdot 1.45}{S_c} < 1 \tag{8.2}$$

The largest design tension is found at LC3 for all eight systems, and judging by the requirements from DNV GL do all the systems pass the ULS-test with $T_d < S_c$ and $UF < 1$. A utilization factor of 88% tells us that the chain catenary system is the closest to experiencing a line tension above the mooring line capacity. For the polyester systems the utilization factors are found to be between 45 to 64 percent, indicating a relatively high redundancy within the mooring line material.

Table 8.1: Summary of the valued for the ULS requirements provided by DNV GL.

System #	S_c [kN]	Pre Tension [kN]	MPM (minimum for leeward)			Mean Value			T_d [kN]	UF
			Surge Motion [m]	Windward Line Tension [kN]	Leeward Line Tension [kN]	Surge Motion [m]	Windward Line Tension [kN]	Leeward Line Tension [kN]		
I	21179	785	27.77	12930	82	21.62	3660	290	20981	0.88
II	21435	1665	19.95	7105	574	16.15	4119	1155	10580	0.58
III	16965	1460	22.82	6481	369	15.0	3939	653	9574	0.54
IV	13047	1270	28.10	5923	342	19.90	3778	566	8665	0.64
V	20981	2710	13.17	8157	838	10.10	4787	1066	12121	0.53
VI	20981	2200	18.60	7064	670	14.51	4452	796	10359	0.46
VII	20981	1360	28.91	6809	306	25.00	3857	471	10180	0.45
VIII	14250	1864	35.2	7285	1828	23.7	6363	2218	9885	0.72

8.1 Dynamic analysis of chain catenary system

As the static analysis result are presented in chapter 6, will the results of the dynamic analysis now be presented. It has previously been stated that the expected largest design tension will be occurring at the extreme load case. This is further verified by looking at Figure 8.7 where the line tension responses for the windward mooring line are compared between the rated load case, LC1, and extreme load case, LC3. Its also given a plot showing the energy density of the line tension for the same load cases in Figure 8.8. The energy spectrum has been verified by calculating the area under the graph which according to energy density theory should be equal to the variance of the time series it represents. The square root of the area should hence be equal to the standard deviation of the time series which is given in Figure 8.9 as; $dev = 1.636 \times 10^6$ N. The area in Figure 8.8b is calculated to be 1.661×10^6 N. The small difference is assumed to be related to the first 200 second called the transient phase which is not included in the energy spectrum.

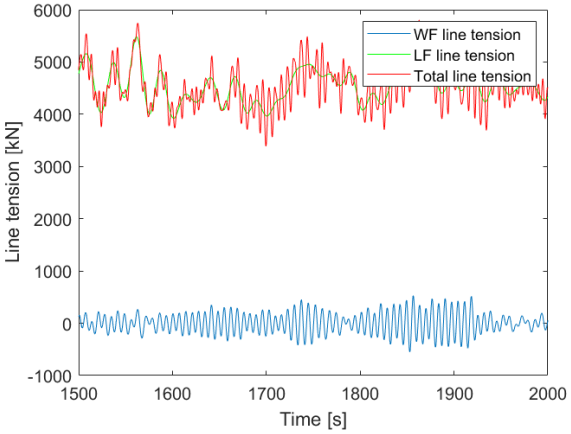

(a) Windward mooring line tension for load case 1.

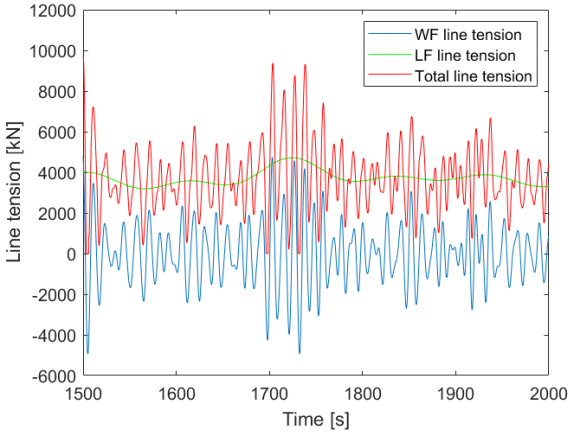

(b) Windward mooring line tension for load case 3.

Figure 8.7: Time series comparesions of WF, LF and totalt top end line tension for LC1 and LC3

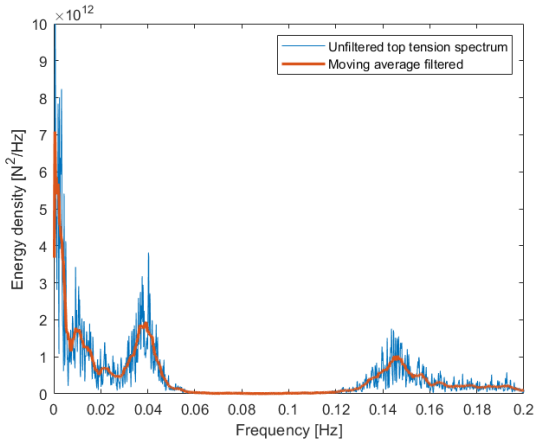

(a) Load case 1

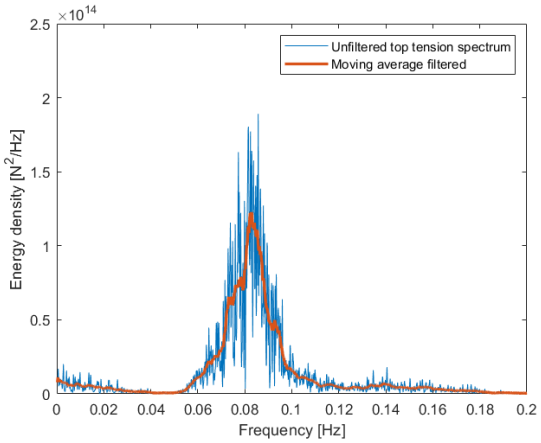

(b) Load case 3

Figure 8.8: Energy density comparison of windward top end line tension for LC1 and LC3

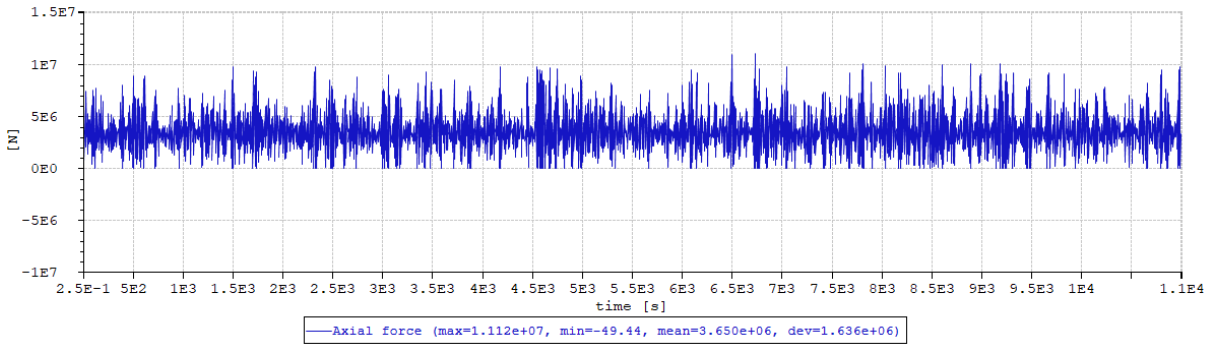

Figure 8.9: Full time series of windward top end mooring line tension for load case 3.

From the comparison in Figure 8.7 it becomes clearer that even if the mean line tension is larger for the rated condition, will the WF dynamic responses for the extreme condition be generating severely larger maximum line tension. The comparison also demonstrates the difference in LF

response which is probably due to the wind gust and the fact that the rated model has a larger quadratic wind coefficient due to rotor thrust. This also emerge from the comparison of the energy spectrum where for load case 3 is located primarily around the wave frequency. For load case 1 is most of the energy located around a very low frequency which is where the NPD spectrum has most of its energy. The two peaks at around 0.01 and 0.38 are related to resonance motion in surge and pitch respectively.

In Table 8.2 are the statistics of the windward and leeward mooring line summarized. The extreme value for line 1 represents the maximum line tension for each realization, while it represents the minimum line tension for line 2 and verifies that the zero tension, "slack", do not occur during the 3-hour simulation. It also shows the design tension calculated by Equation 3.1 presented in chapter 3.

Table 8.2: Line tension statistics and design tension, T_d,

	Line 1 (Windward)			**Line 2 (Leeward)**		
Seed number (wind and wave)	**Extreme value**	**Mean**	**Std**	**Extreme value**	**Mean**	**Std**
1	11637	3662.2	1748.5	301.94	524.28	43.713
2	11938	3653.9	1730.1	324	524.21	43.015
3	14083	3660.6	1759.3	312.69	524.33	43.913
4	12553	3659.1	1754.2	334.97	524.38	43.527
5	14211	3663.3	1764.4	322.24	524.31	43.844
6	13742	3671.8	1802.8	317.08	524.12	44.076
7	12814	3654.8	1769.4	342.43	524.32	43.251
8	14320	3659.3	1754.8	296.4	524.17	43.31
9	12764	3654.3	1757	319.1	524.12	43.281
10	15378	3667.2	1786.6	300.62	524.29	44.269
11	15737	3653.6	1756.1	242.24	524.35	44.249
12	12936	3663	1781.6	346.7	524.4	44.392
Mean	13509.4	3660.3				
Std	1287.9					
MPM	12929.9					
Tdyn	9269.6					
Td	20980.2					

According to DNVGL-ST-0119[1] shall the design tension be less than the characterized breaking strength, S_c, given by Equation 3.3. From Table 6.5 we see that the chain has a break load of 22.3 kN, which equalizes a characterized breaking strength of 21.2 kN and the system is within the requirement of the ULS-test.

In Figure 8.10 to 8.12 are the motion responses in surge, heave and pitch presented by separating the wave- and low-frequency motion from the total motion. The low-frequency motion also includes the static response, and will therefore oscillate around the mean offset. There is also here a presentation of the energy spectrum, showing the distribution of energy over different frequencies. The energy spectrum of the heave motion also includes the JOSNWAP spectrum used in load case 3, and it should be mentioned that this wave spectrum is presented according to the y-axis on the right-hand side.

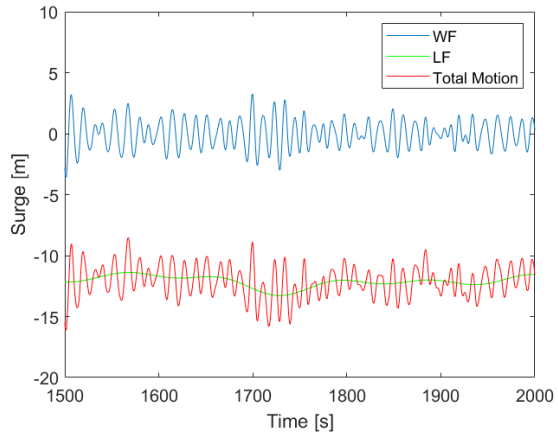

(a) Response in surge.

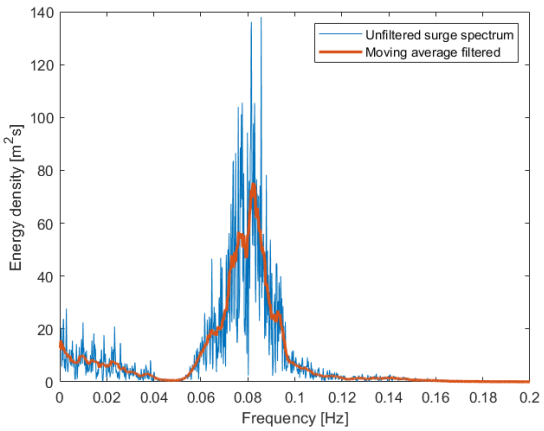

(b) Energy spectrum in surge.

Figure 8.10: Surge response and energy spectrum of dynamic surge for LC3.

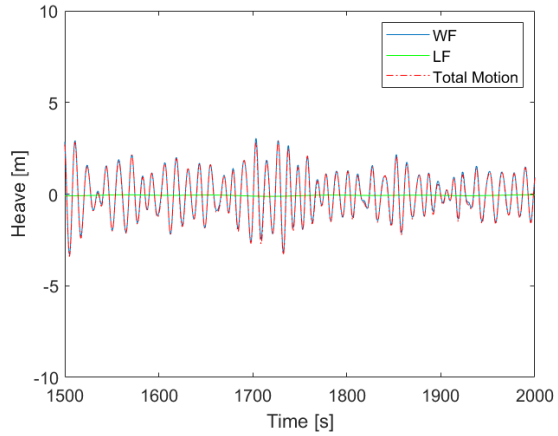

(a) Response in heave.

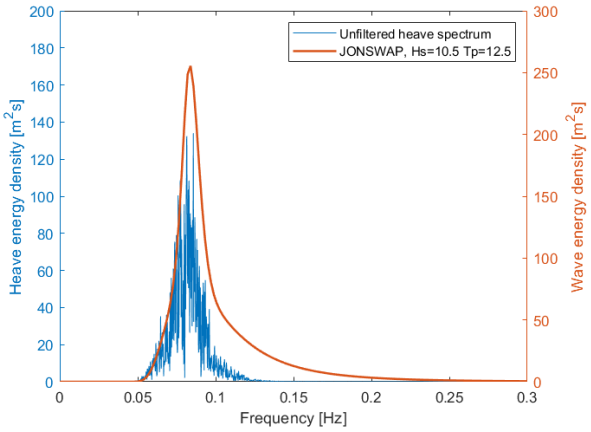

(b) Energy spectrum in heave and JONSWAP spectrum.

Figure 8.11: Heave response and energy spectrum of dynamic heave for LC3.

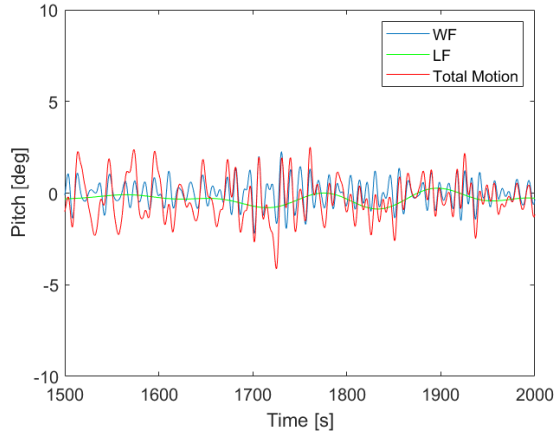

(a) Response in pitch.

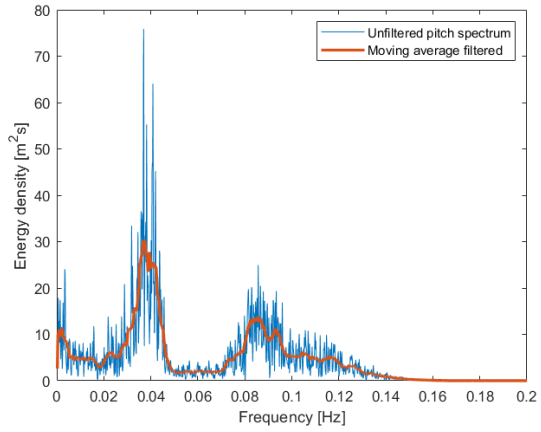

(b) Energy spectrum in pitch.

Figure 8.12: Pitch response and energy spectrum of dynamic pitch for LC3.

By first looking at the result for the surge motion, is it clear that there is a non zero mean drift off around 12 m. On top of that, there is a large WF motion which is about 1/3 of the mean offset. There is also some LF motion, which is mainly due to the wind gust acting on the tower and the feathered rotor blades. From the power spectrum, it is seen that the energy from the dynamic response is dominated by WF responses between 0.075-0.09 Hz which is around the peak of the JONSWAP spectrum used for the extreme load condition. The energy of the LF response is located around the natural period in surge, hence due to resonance motion.

In heave, there is as expected a zero mean offset with a motion totally dominated by the WF responses as there are no low-frequency loads. This is also shown by the power spectrum, where all the energy is located within the JONSWAP spectrum. Hence to the relatively small offset, will it not be affecting the line tension to the same extent as the surge motion.

No significant mean offset in pitch is observed for load case 3. The dynamic response is dominated by a resonance response which is within what's defined as the wave frequency region. there is also some energy located around the T_p value of the wave spectrum, and also some LF energy from the tower drag and the parked wind turbine

8.2 Diameter comparison, system II, III and IV

In the following section we will have a more detailed look at system II, III and IV, which all apply the same base case stiffness model of $E = 20MBS$ and line configuration, but differ in mooring line diameter. Like for System I, will the decay and pull out test be used to compared the characteristics of each system. It will also be looked at how the dynamic response varies for load case 1 to 3.

8.2.1 Decay test

From Figure 8.13 and 8.16 it is documented how much the mooring system influences the motion in the horizontal plane. This is here represented by a significant difference in both offset and oscillation period for each of the three mooring line thicknesses. As previously mentioned will the heave and pitch motion be largely influenced by the hydrostatic stiffness, and this is also the case in Figure 8.14 and 8.15. The slight difference at the end of the timer series for the pitch motion is due to the coupling effect between pitch and surge, and this region should not be included for natural period calculations. The result of the natural period calculations are presented in Table 8.3.

Table 8.3: Natural period for linear system II, III and IV.

System #	Surge	Heave	Pitch	Yaw
System II	54.6	20.2	26.5	62.9
System III	62.2	20.2	26.6	62.4
System IV	71.9	20.2	26.8	72.7

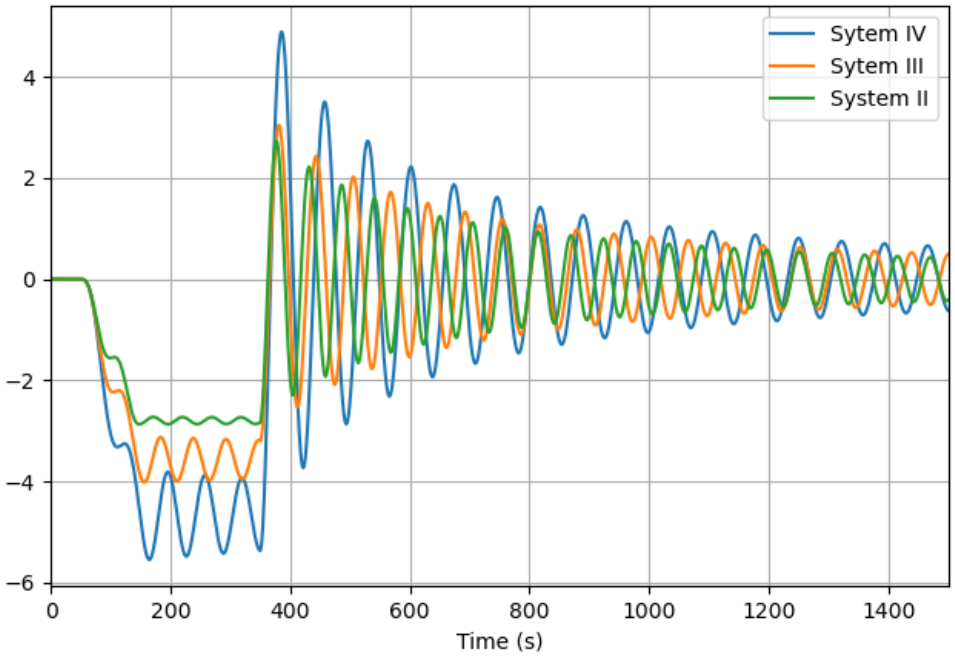

Figure 8.13: Decay in surge, linear polyester system

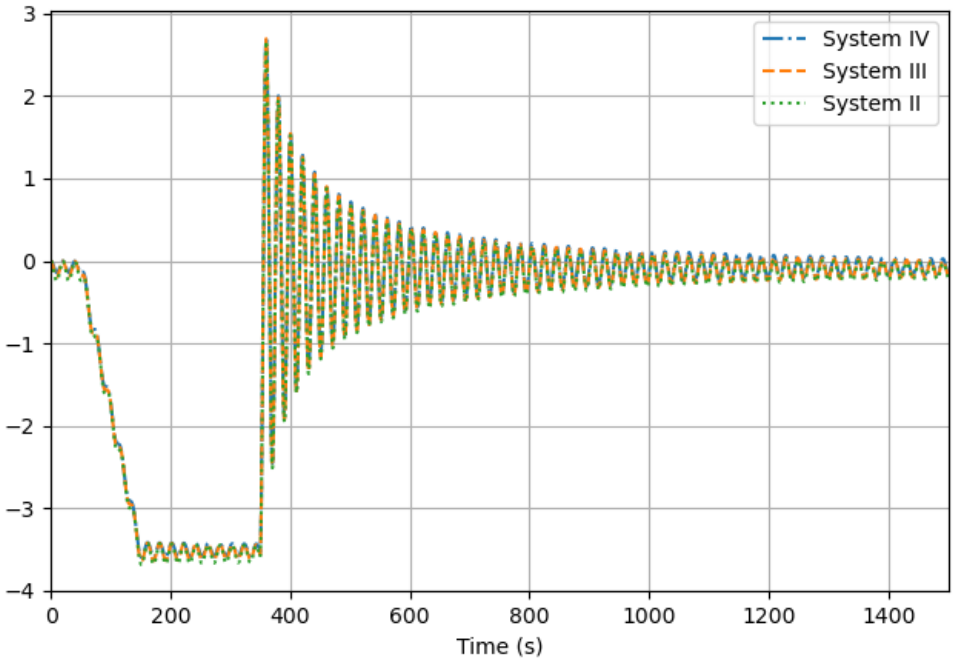

Figure 8.14: Decay in heave, linear polyester system

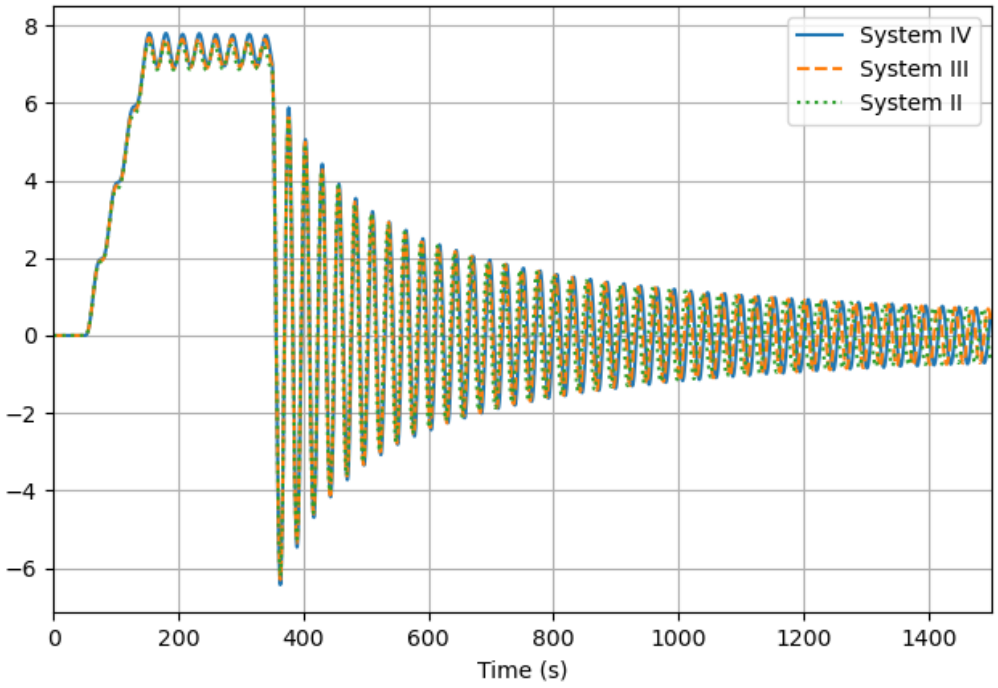

Figure 8.15: Decay in pitch, linear polyester system

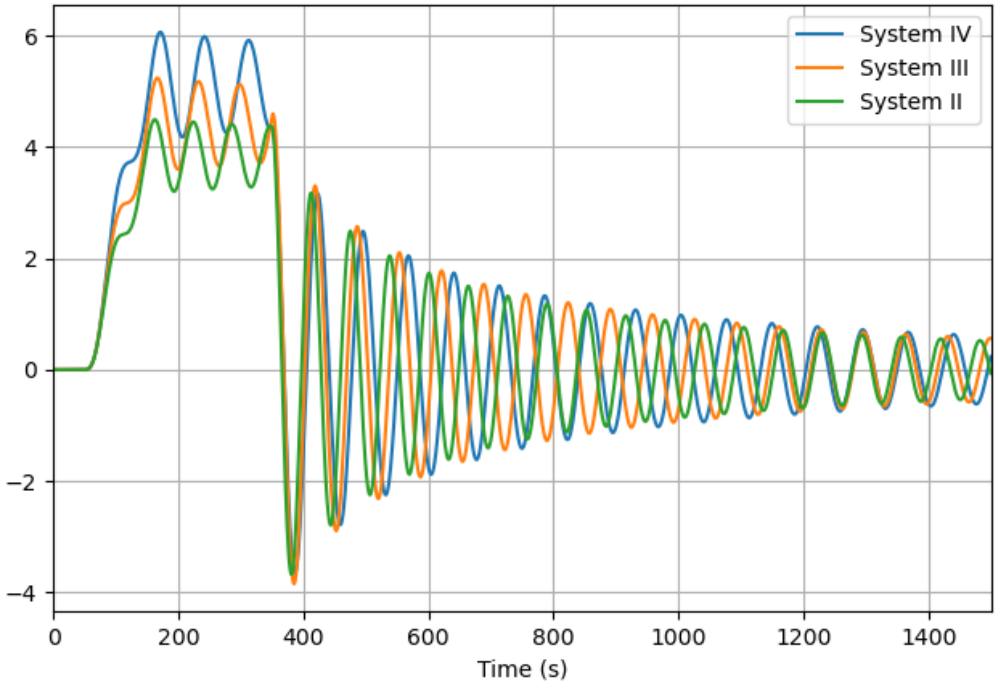

Figure 8.16: Decay in yaw, linear polyester system

8.2.2 Static analysis

The results from the pull-out test are given in Figure 8.17 for system II, III and IV and as for the chain system given presented by a restoring curve for displacement in both positive and negative x-displacement.

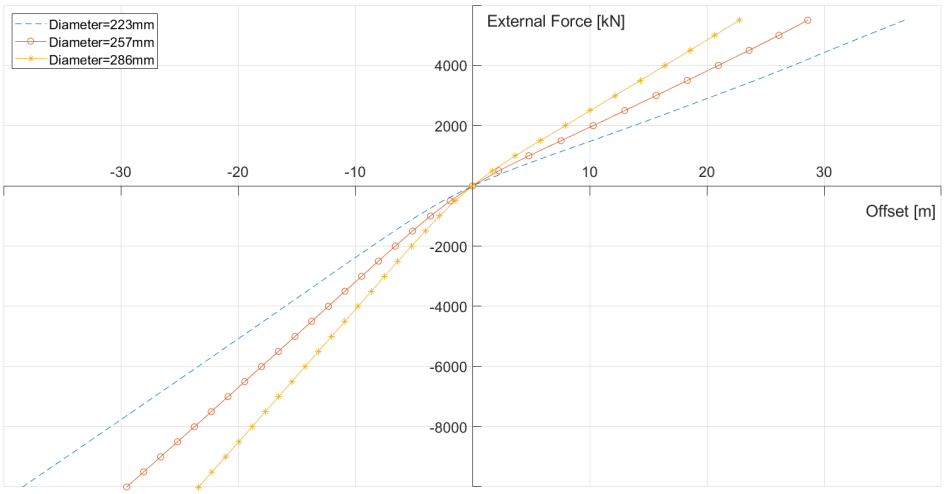

Figure 8.17: Restoring curve comparison for linear axial stiffness model

The restoring curves demonstrate that even with the buoy and clump weight, will the stiffness of the system very much be determined by the elastic stiffness of the mooring lines, thus the linear shape of the curves. The small curve at lower offsets are a result of the the rapid change in the leeward mooring line which stops provident much horizontal stiffness when the offsets becomes larger. Thus, some differences in positive versus negative x-direction is observed and is due to the orientation of the mooring lines relative to the offset direction. As commented at the start of this chapter, could this ”softness” in positive x-direction cause problems in the design of the power cable.

8.2.3 Dynamic analysis

In the first section, only the dynamic response of the platform motion and top end line tension of load case 3 were presented. We should now have a look at how the top end windward mooring line tension is affected for load case 1 to 3 to better understand where the energy in located. Hence, System II is used as an example and a partition of the windward line tension times series from each of the three load cases are given in Figure 8.18 while the energy spectrum are shown in Figure 8.19.

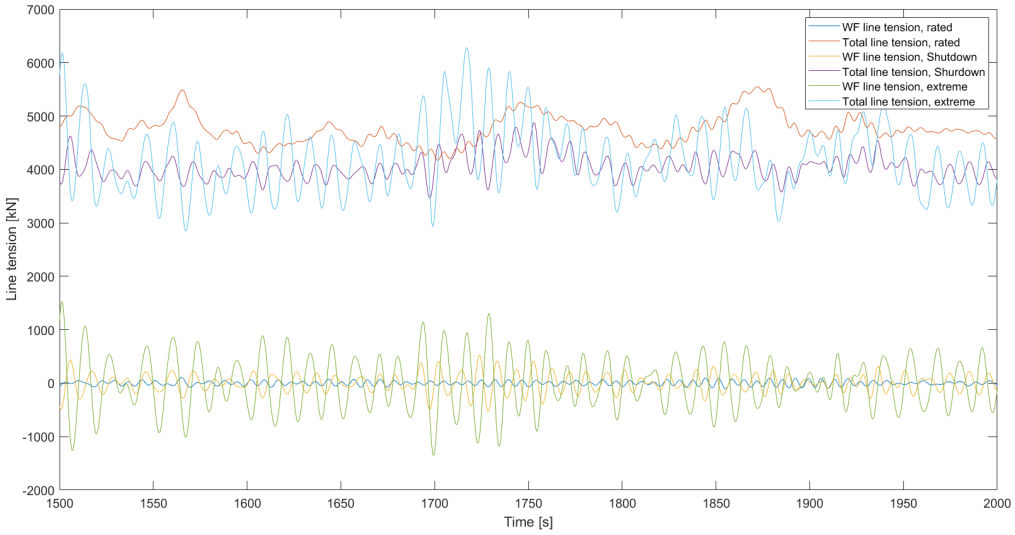

Figure 8.18: Line tension for all three condition cases for system II

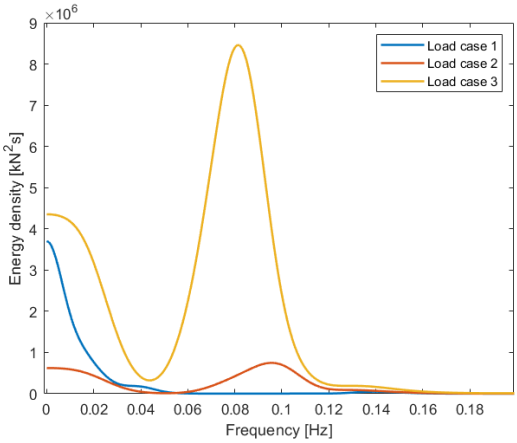

Figure 8.19: Energy spectrum with large smoothing factor of top end windward line tension for load condition comparison.

The first observation we make is the very small LF response in both time series and the energy spectrum for load case 2 compared to load case 1, even though both load cases are for an operational turbine. The reason for this is due to the way the thrust force is modeled for load case 2. By using a specified force instead of a wind coefficient to model the thrust force, will wind gust only be implemented through tower drag. This could be seen as a weakness in the simplified model, as it implies a near perfect pitch control of the turbine blades. For load case 1 are all the energy located in the low-frequency region while the largest peak for load case 3 is at the wave frequency, but there is also here some energy in the low-frequencu region due to the large wind speeds.

Another interesting observation is the significant difference in dynamic response compared to the chain system where the largest tension was easily observed for the LC3. For System II, is not the largest tension as easily connected to one specific load case. Nor is it intuitively which

load case will result in the largest design tension where both static and dynamic tension are included.

Nevertheless, by comparing the result of the 10 realizations for LC1 and LC3 given in Table 8.4, it becomes clear that the largest design tension will also here be occurring along the 50 year contour. This is because even if the larges line tension could occur for rated wind speed, will the contribution from the dynamic tension in Equation 3.1 be the dominating factor in the calculation of design tension. As presented previously in this chapter, is the characteristic breaking strength from Equation 3.3 equal to 21 434 kN, 16 965 kN and 13 047 kN for system II, III and IV respectively. This makes it clear that the design tension won't be the problem in the design of such a polyester system, and the focus should be on reducing the mean offset.

Table 8.4: ULS-test for system II, III and IV.

Seed#	**System II**				**System III**				**System IV**			
	LC1		**LC3**		**LC1**		**LC3**		**LC1**		**LC3**	
	Extreme	Mean	Extreme	Mean	Extreme	Mean	Extreme	Mean	Extreme	Mean	Extreme	Mean
1	5594.72	4685.91	6741.43	4120.62	5345.347	4513.210	6078.69	3940.88	5134.48	4358.98	5650.41	3778.96
2	5574.09	4685.47	7065.30	4114.76	5303.213	4512.763	6480.38	3935.15	5083.02	4358.48	5871.08	3773.53
3	5631.32	4667.92	7324.72	4119.79	5432.634	4495.196	6621.91	3939.97	5212.13	4340.89	6113.51	3778.14
4	5393.85	4671.56	6935.57	4118.19	5167.127	4498.916	6437.81	3938.73	4972.85	4344.69	5940.07	3776.94
5	5456.17	4677.37	7617.94	4121.97	5181.845	4504.590	6860.81	3942.32	4959.76	4350.28	6153.34	3780.40
6	5499.28	4666.65	7536.87	4128.57	5256.144	4493.890	6963.68	3948.93	5079.35	4339.54	6370.82	3787.17
7	5417.02	4682.06	6946.63	4113.56	5156.602	4509.415	6418.29	3933.82	4981.51	4355.21	5891.23	3772.04
8	5502.47	4692.68	7672.52	4119.54	5285.580	4520.037	6975.11	3939.90	5084.24	4365.84	6313.58	3778.29
9	5544.57	4687.44	7055.10	4114.44	5322.530	4514.849	6375.95	3934.86	5093.32	4360.69	5742.85	3773.36
10	5472.00	4675.38	7617.18	4123.95	5238.772	4502.670	6857.80	3944.23	5019.25	4348.43	6130.43	3782.50
Mean	5508.55	4679.25	7251.32	4119.54	5268.98	4506.55	6607.04	3939.88	5061.99	4352.30	6017.73	3778.13
Std.	77.34		342.90		87.31		298.71		79.39		237.23	
MPM	5473.75		7097.02		5229.69		6472.62		5026.27		5910.98	
Tdyn	798.48		2979.57		727.13		2534.83		677.97		2134.91	
Td	7480.36		10569.65		7131.00		9557.80		6844.45		8647.66	

8.3 Linear VS non-linear stiffness model

While the previous system configuration assumed the same stiffness model for all three systems, will system V, VI, and VII be using different stiffness model for the second polyester configuration. This is done to verify the effect of using a less stiff fiber rope and compare the results with the model using the previously described non-linear tension-elongation relationship.

8.3.1 Decay test and static analysis

It has already been established how the mooring system will to a limited extent affect the natural period in heave and pitch, and due to the load case configuration will only surge motion be presented. The results of the decay test of the second polyester configuration in surge are presented in Table 8.5 with its respective stiffness models.

Table 8.5

Stiffness model	Natural period in surge
20MBS	40.6
15MBS	48.6
Non-linear	76.2

The results show how this configuration has a significantly lower natural period than the first polyester configuration and chain system, mainly due to the larger stiffness as a result of shorter lines. We also notice that the natural period of the non-linear system is larger than the two linear systems. This can be explained by the restoring curve in Figure 8.20 where the tangent of the lines crossing origin is much steeper for the linear models compared to the non-linear. The plot also demonstrates how the non-linear model creates a much softer system at small excitation forces, but becomes stiffer when the offset surpassing 10m. Like for the first polyester system, can this complicate the design of the power cable.

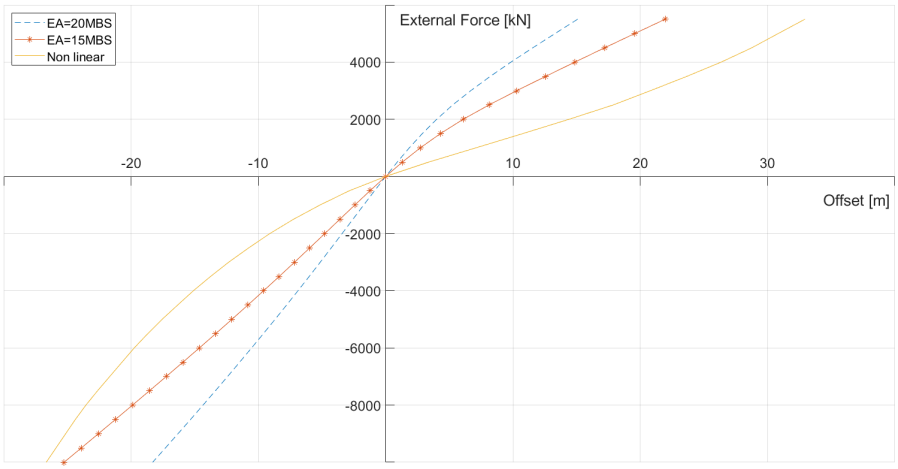

Figure 8.20: Restoring curve comparison between system V, VI and VII

An interesting observation of the linear systems is the small change in the restoring curve which is especially noticeable at 5m offset in positive x-direction for $EA = 20MBS$. The explanation is probably due to the loss of horizontal restoring force from the leeward mooring line as the angle between the vertical axis and the mooring line approaches zero. The simplified line characteristic in Figure 8.21 exemplifies this for a linear system where T_h windward is the result of line 2 and line 3 in the x-direction. From this figure, the small drop in restoring force increment occurs when the leeward stops provide horizontal stiffness.

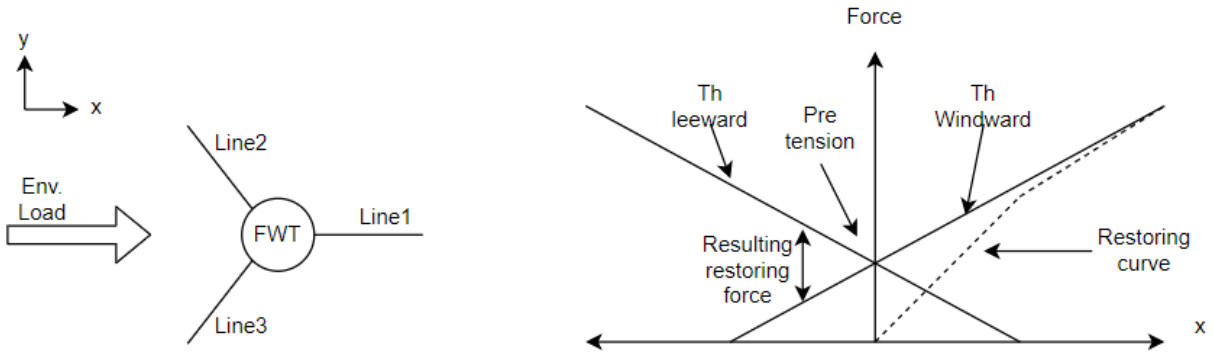

Figure 8.21: Simplified example figure of FWT and its resulting restoring force.

8.3.2 Dynamic analysis

The surge response for System I, II, V and VII are presented in Figure 8.22 for load case 1. The dynamic response containing the LF and WF response has been extrapolated to oscillate around zero line to easier compare the different systems.

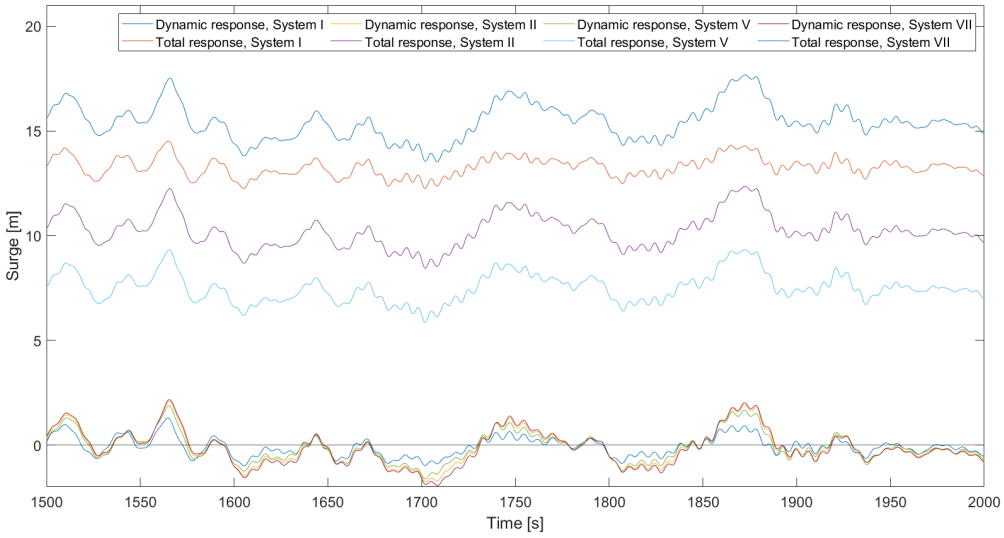

Figure 8.22: Surge response comparison for LC1

As expected will the time series of the dynamic responses demonstrate how the mooring systems in a large extent are unable to affect the dynamic response, which is seen in Figure 8.23a to be dominated by the LF motion. This substantiates the previous statement of inertia dominated systems in chapter 4 and how the mooring system should only affect the mean offset. Hence, an ideal system will therefore have a large steepness at the beginner of the restoring curve before it flattens at an acceptable mean offset for the expected mean environmental load. By further comparison of the surge energy spectrum, it is observed that all four systems will have the largest energy concentration at lower frequencies. The systems will also experiencing some effects from the resonance pitch motion where mean and extreme pitch motion in Figure 8.4 are presented as approximately the same for all systems. However, from Figure 8.23b it is only the chain catenary system who experiencing some wave frequent top end line tension response. This demonstrates one of the advantages of using synthetic lines, as it can absorb imposed dynamic motion trough extension without causing significant dynamic tension.

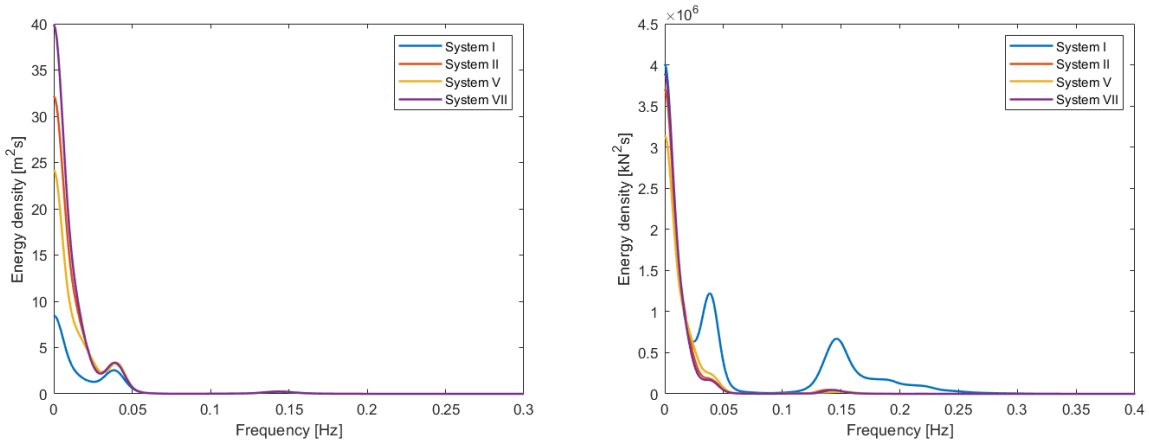

(a) Energy spectrum of surge response for LC1. **(b)** Energy spectrum of windward line tension for LC1.

Figure 8.23: Correlation between energy spectrum in surge and top end windward line tension for load case 1 with large smoothing factor.

8.4 Nylon system

The restoring curve for the nylon system is documented in Figure 8.24. The same drop in restoring increment are also observed for this system and the argumentation provided in the previous section also applies to some extent for this system. However, the horizontal contribution from the leeward line will never go to zero as the mooring lines never experiences ”slack” and the buoy prevent the angel between vertical axis and mooring line to go to zero.

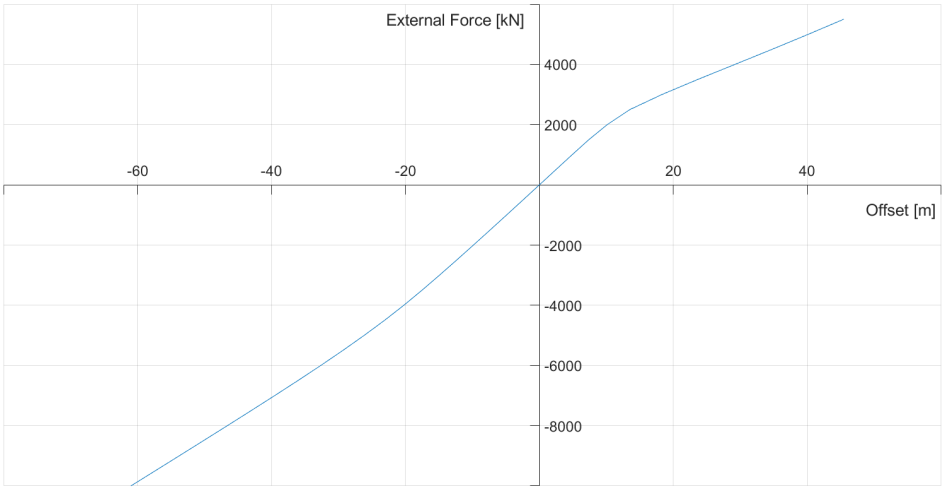

Figure 8.24: Restoring curve for nylon system, System VIII.

Figure 8.25-8.27 depicts the energy spectrum for the directional aligned environmental loads along one mooring line for better comparison of the energy peaks. A recap of the wave frequencies for the each loads case and natral frequency in surge heave and pitch are given in Table 8.6.

Table 8.6: Wave frequency and natural frequency of System VIII.

Load case#	Peak wave frequency [Hz]	Degree of freedom	Natural frequency [Hz]
1	0.12	Surge	0.015
2	0.10	Heave	0.05
3	0.08	Pitch	0.04
4	0.07		

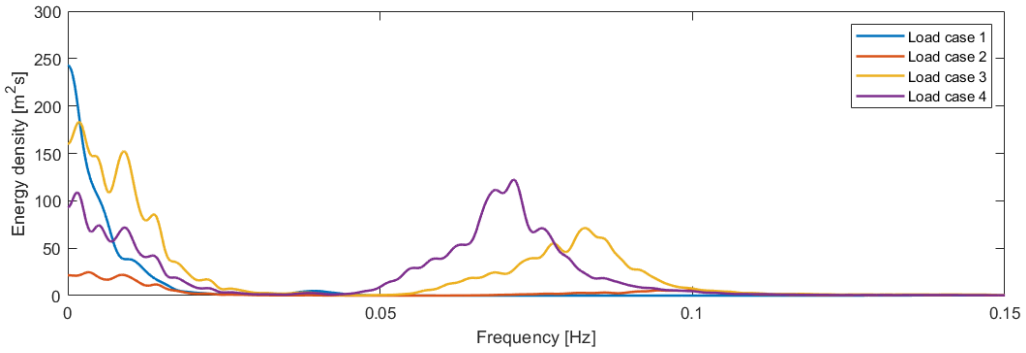

Figure 8.25: System VIII, Surge energy spectra

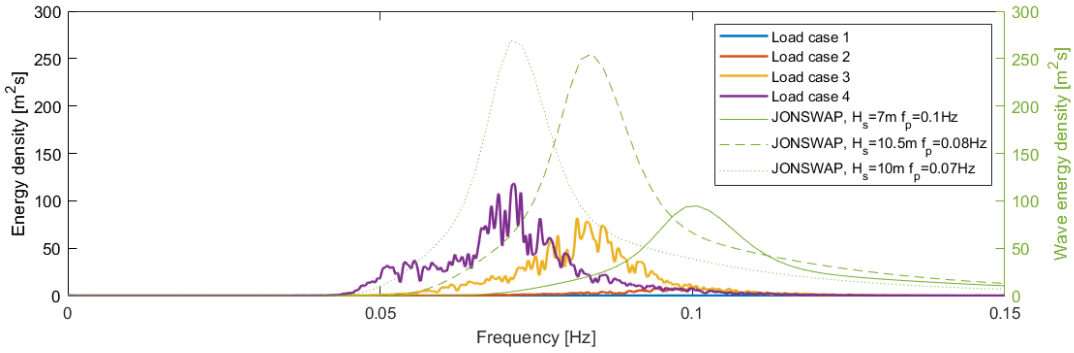

Figure 8.26: System VIII, Heave energy spectra

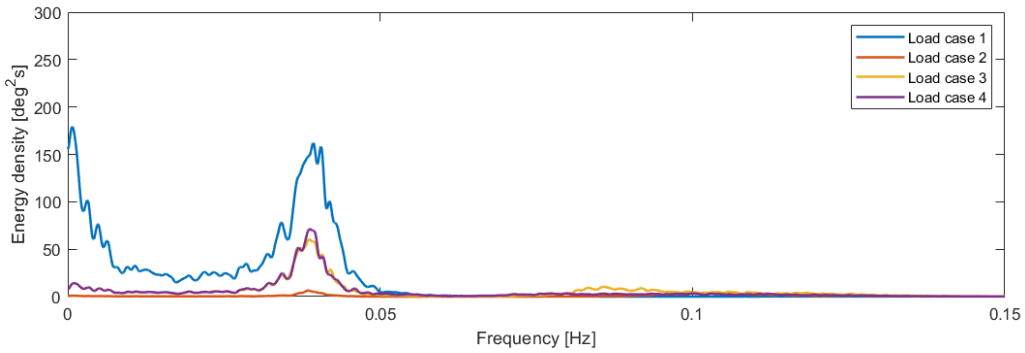

Figure 8.27: System VIII, Pitch energy spectra

Figure 8.25 presents the energy distribution in surge and gives a very good impression of surge response changes when the environmental conditions changes. For load case 1, the system is completely wind dominated similarly to the other systems, however, we do not observe what is assumed to be a coupling effect at pitch resonance. Load case 3 and 4 both uses the same 50-year mean wind speed and 10-year current, but different H_s and T_p combinations along the 50-year contour plot and is the reason the peak of the WF response shifts towards a higher frequency. The most interesting observations are the differences in WF response, and also the difference in the energy distribution for LC3 and LC4. While the peaks of load case 3 is largest at LF response, is the peaks for LC4 more evenly distributed between WF and LF response and is a result of longer waves for $f_p = 0.07$ versus $f_p = 0.08$. This is related to the dynamic load factor, exemplified in Figure 4.1, where lower ω/ω_0-ratio for inertia dominated systems will give a larger dynamic response.

Like for the chain catenary system, do Figure 8.26 very well visualize how the heave motion is concentrated inside the wave spectrum of its load case's respective JONSWAP spectrum. As expected will there be close to zero heave response for LC1, hence is this wave spectrum not depicted in the figure. Again is there more energy in the WF region of LC4 than for LC3, and the same argumentation of DLF used for surge applies in this case. Common for all four load cases is that the dynamic response is pulled toward lower frequencies, where resonance occurs.

Figure 8.27 depicts the dynamic pitch distribution where all load cases will create a peak at resonance pitch frequency. A large LF response is as expected observed for LC1 where the thrust force is at its peak and is implemented in the quadratic wind coefficients. It is also interesting to see how load case 3 is able to excite some WF response at 0.08 Hz. This is most likely due to the large significant wave height and the relatively short peak wave period, resulting in steeper waves which the structure to some extent will follow.

Chapter 9

Conclusion

In this thesis, four mooring configurations are proposed for a floating 10MW wind turbine operating in a water depth of 80m. In addition, four sub-systems of the polyester configuration with varying diameter and axial stiffness model is also given for comparison reasons. Through decay and pull-out tests, the natural period in all six degrees of freedom and restoring curves in surge has been successfully established for all systems. The dynamic behavior of the semi-submersible and top-end line tension for windward and leeward mooring lines was studied in detail. Metocean data from the Hywind Buchan Deep operation site was the basis for the load case definition. Prior to the analysis, a simplification of the CSC10MW SIMO/RIFLEX-model was achieved by removing the rotor blades, hub and tower, and implementing the wind loads by adding an estimated quadratic wind coefficient and modifying the kinematics of the semi-submersible. The report has also provided a review of relevant literature to strengthen the general understanding of the analysis performed.

Based on the results of this study, the following concluding remarks are made;

- An initial chain catenary system has successfully been included in the floating wind turbine model with references to the existing mooring systems used for Hywind Scotland.
- It has also been proven that feasible polyester mooring systems can be achieved when buoy and clump weights are applied to change the characteristics of the mooring lines.
- The systems have a negligible effect on resonance periods in heave and pitch.
- For a floating wind turbine, extreme conditions will be the most critical condition for surge and heave response, while weather conditions at rated wind speed will induce the most substantial pitch response.
- The maximum design line tension is found for the extreme weather condition and is mainly due to large wave frequency response. Furthermore, the advantage of using synthetic rope has been proven by its excellent ability to absorb the dynamic wave-frequency motion.
- The main technical issue with reducing the line diameter of polyester is found to be related to extreme offsets, as the line tension utilization factor only increased by 10% after a reduction of 20% in mooring line diameter.

- The choice of axial stiffness model will play an important part when modeling a polyester system dominated by elastic stiffness. This will have impact on both natural period and motion response in surge.

9.1 Recommendation for further work

1. The simplified model is only verified by a comparison of the static characteristic of the original model. Hence, the dynamic responses should be compared to the complete model where the turbine blades implement the thrust force. This would help to determine how accurate the quadratic wind coefficients are for the different operational regimes, and in general, quantifying the quality of the simulations.

2. This thesis only emphasized on the ultimate limit states, and for further analysis should the systems be tested for ALS and FLS.

3. Line tension utilization factor between 0.45 and 0.64 indicates that further optimizations of the synthetic rope systems is possible.

4. The 2. order wave loads from the potential theory have been neglected in the current model, and these should be estimated in order to determine whether or not they could excite any low-frequency response in surge due to resonance.

5. The non-linear stiffness model for polyester only includes the non-linear static stiffness model, and it should be looked at methods on how the linear dynamic stiffness could be added to the system.

6. More load cases along the 50-year Hs-Tp contour line should be tested.

Bibliography

[1] DNVGL-ST-0119. Floating Wind Turbine Structures, 2018.

[2] DNVGL-OS-E301. Position mooring, 2018.

[3] Qiang Wang. *Design of a Steel Pontoon-type Semisubmersible Floater Supporting the DTU 10MW Reference Turbine*. Master's thesis, NTNU, Norwegian University of Science and Technology, 2014.

[4] Lizer Ramirez, Daniel Fraile, and Brindley Guy. Offshore Wind in Europe, Key trends and statistics 2019. Technical report, WindEurope, February 2020.

[5] Subrata K. Chakrabarti. *Handbook of offshore engineering*, volume 2. Elsevier, 2005.

[6] Kjell Larsen. TMR4225-2of2 Lecture notes, 2019.

[7] Erik Falkenberg, Vidar Åhjem, and Limin Yang. Best Practice for Analysis of Polyester Rope Mooring Systems. In *Offshore Technology Conference*, Houston, Texas, USA, 2017. Offshore Technology Conference.

[8] Kjell Larsen. Axial Stiffness of Polyester Ropes - Proposed Stiffness Model. Technical report, 2018.

[9] Vryhof. Anchor manual 2005, July 2019.

[10] D Loukidis and V Vavourakis. Limit lateral resistance of vertical piles in plane strain. In Michael Hicks, Ronald Brinkgreve, and Alexander Rohe, editors, *Numerical Methods in Geotechnical Engineering*, pages 681–685. CRC Press, June 2014.

[11] DrillingFormulas.com. Suction Anchor Calculation, December 2019.

[12] Kun Xu, Kjell Larsen, Yanlin Shao, Min Zhang, Zhen Gao, and Torgeir Moan. Comparison of different mooring system concepts for a semi-submersible floating wind turbine in shallow water. *Department of Marine Technology, NTNU*, page 40, 2019.

[13] DNV-RP-C205. Environmental Conditions and environmental loads, 2010.

[14] David Johnson, Mingyao Gu, and Brian Gaunt. Wind Turbine Performance in Controlled Conditions: BEM Modeling and Comparison with Experimental Results. *International Journal of Rotating Machinery*, 2016:1–11, January 2016.

[15] Erin Bachynski. Integrated Dynamic Analysis of Wind Turbines TMR4505, 2019.

[16] Sintef Ocean. SIMO 4.10.3 User Guide, October 2019.

[17] Martin Marthiesen, Maja K Meyer, and Børge Kvingedal. Hywind Bunchan Deep Metocean Design Basis, March 2013.

[18] Christian Bak, Fredrik Zhale, Robert Bitsche, and Taeseong Kim. *Design and performance of a 10 MW wind turbine*. PhD thesis, DTU Wind Energy, Technical University of Denmark, 2013.

[19] Odd Magnus Faltinsen. *Sea Loads on Ships and Offshore Structures*. Cambridge University Press, 1998.

[20] D Myrhaug and W Lian. *Marine Dynamics, Lecture notes*. Akademika, 2009.

[21] Bjørnar Pettersen. *Marin Teknikk 3, Hydrodynamikk*. Akademika, 2017.

[22] Subrata K. Chakrabarti. Steady drift force on vertical cylinder - viscous vs. potential. *Applied Ocean Research*, 6(2):73–82, April 1984.

[23] Martin O.L Hansen. *Aerodynamics of Wind Turbines*. Earthscan, 2008.

[24] INC. WAMIT. WAMIT user manual version 7.3, May 2019.

[25] Kjell Larsen, Tjerand Vigesdal, Rune Bjørkli, and Oddgeir Dalane. Mooring of Semi Submersibles in Extreme Sea States: Simplified Models for Wave Drift Forces and Low Frequency Damping. American Society of Mechanical Engineers Digital Collection, September 2018.

[26] Sintef Ocean. Sima Manual, October 2019.

[27] Sintef Ocean. RIFLEX 4.16.1 User Guide, November 2019.

[28] Raymond A Serway. *Physics for scientists & engineers*. Philadelphia : Saunders College Pub., 2 edition, 1986.

[29] Ramnäs. Ramnäs Bruk Product Catalogue, December 2019.

[30] Bridon. Bridon Hardware Catalogue, August 2013.

[31] Mark B. Huntley. Fatigue and Modulus Characteristics of Wire-Lay Nylon Rope. *MTS Ocean Conference*, 2016.

Appendix A

Inital design

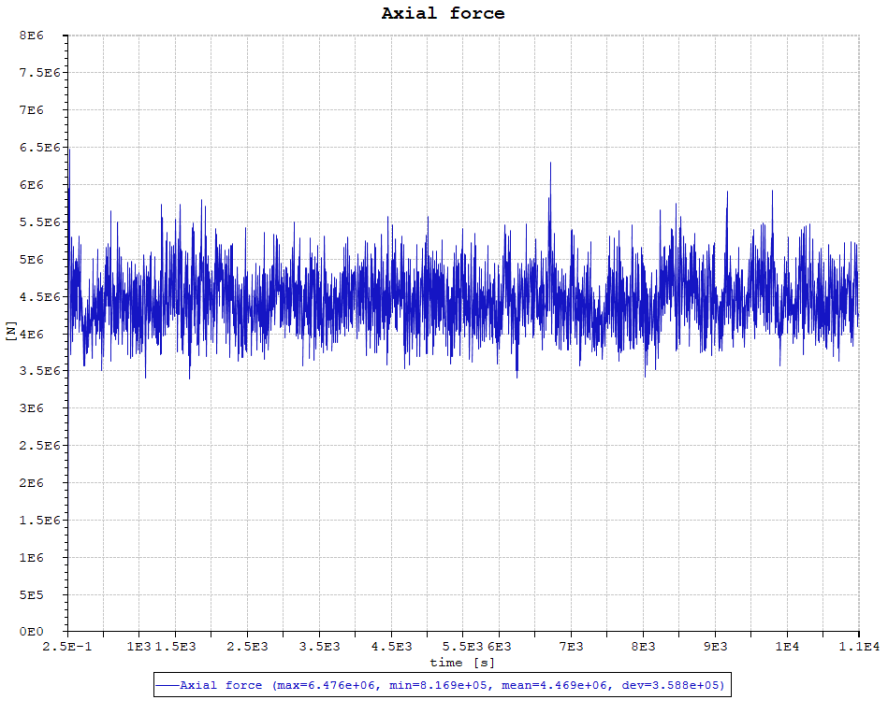

Figure A.1: Windward line tension, rated

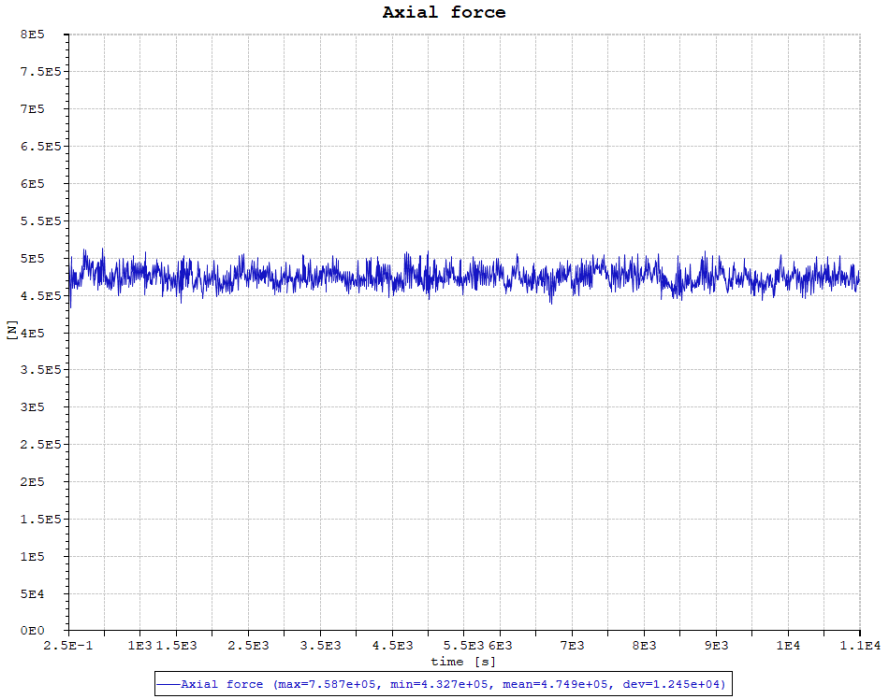

Figure A.2: Leeward line tension, rated

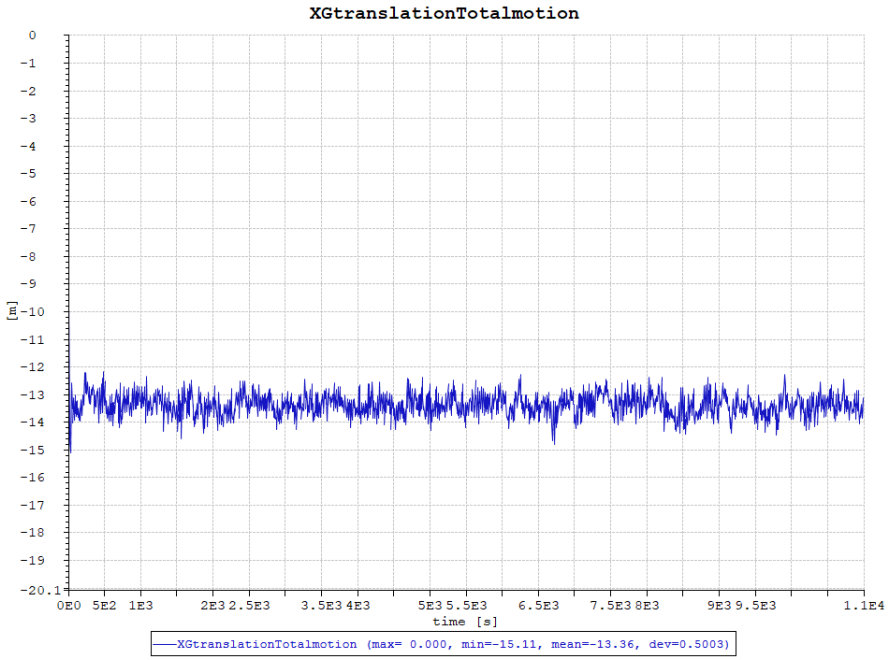

Figure A.3: Surge motion, rated

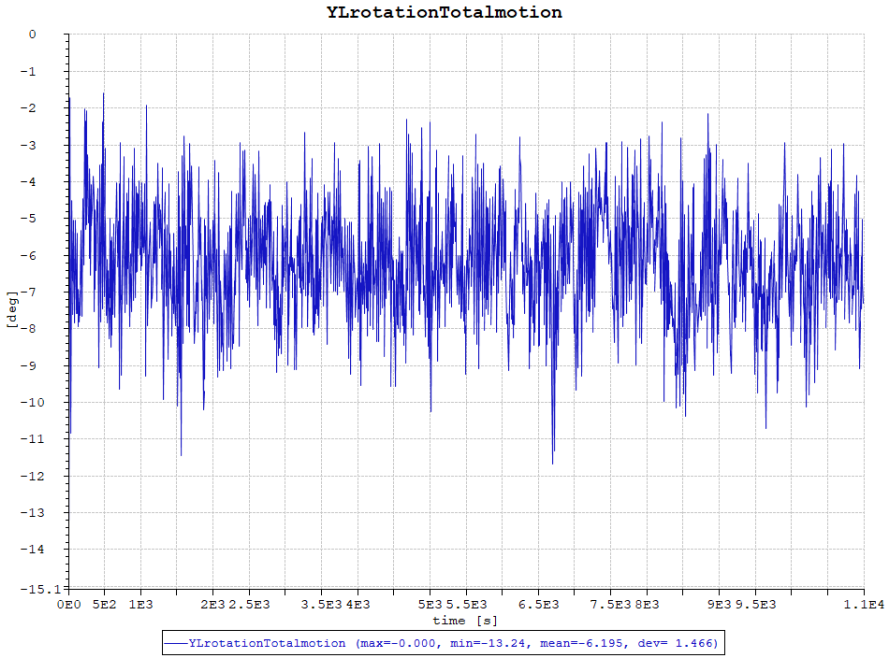

Figure A.4: Pitch motion, rated

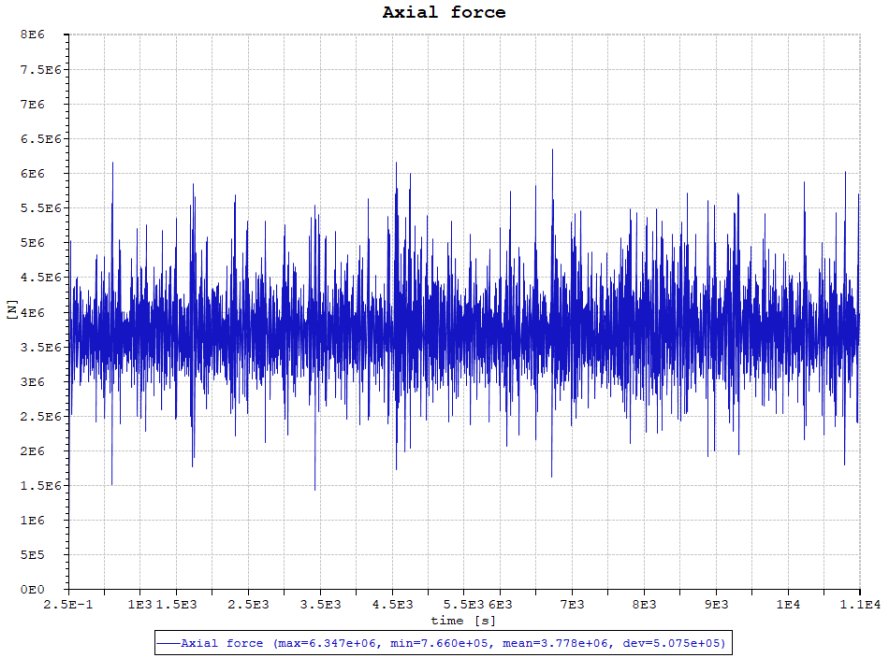

Figure A.5: Windward line tension, shutdown

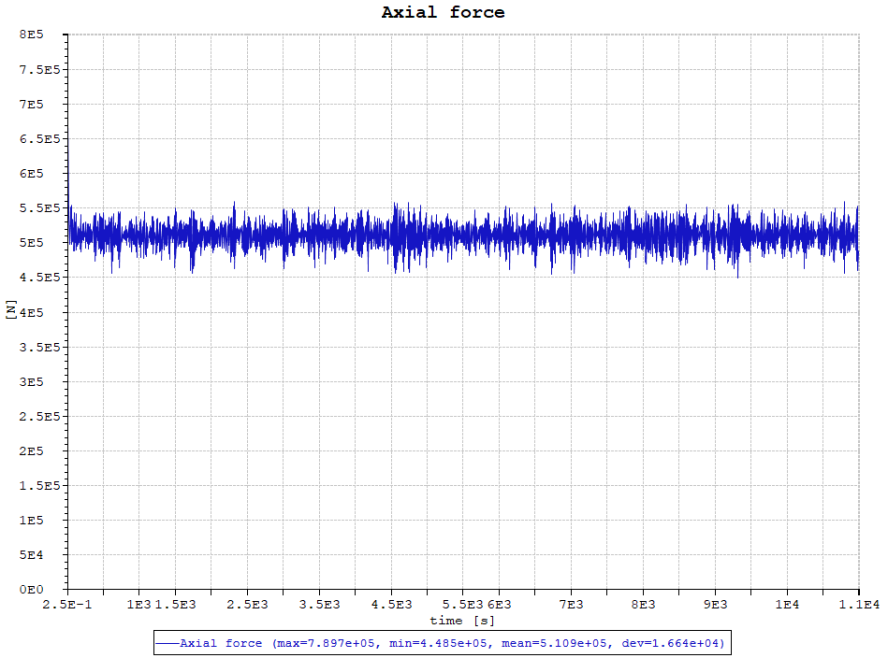

Figure A.6: Leeward line tension, shutdown

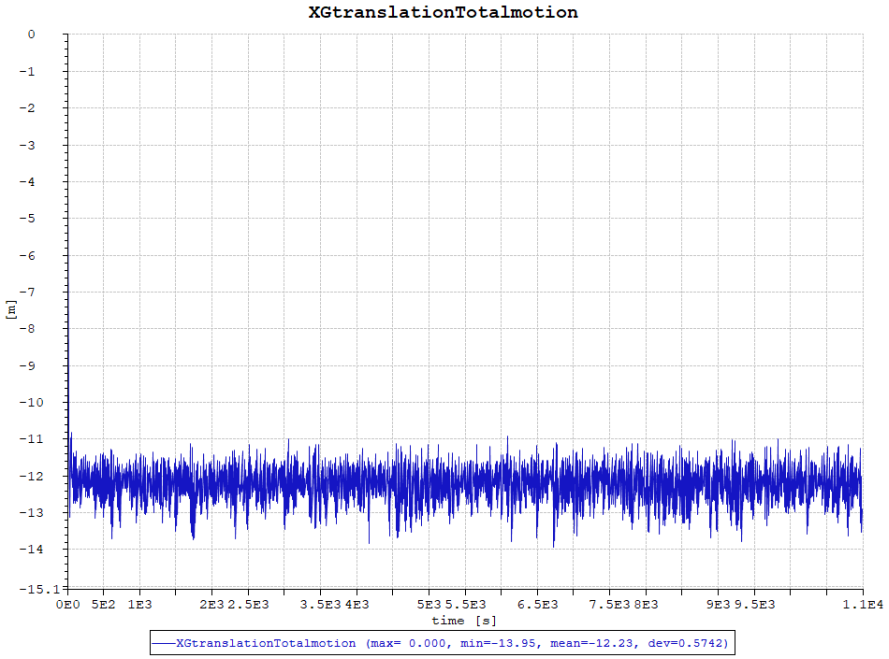

Figure A.7: Surge motion, shutdown

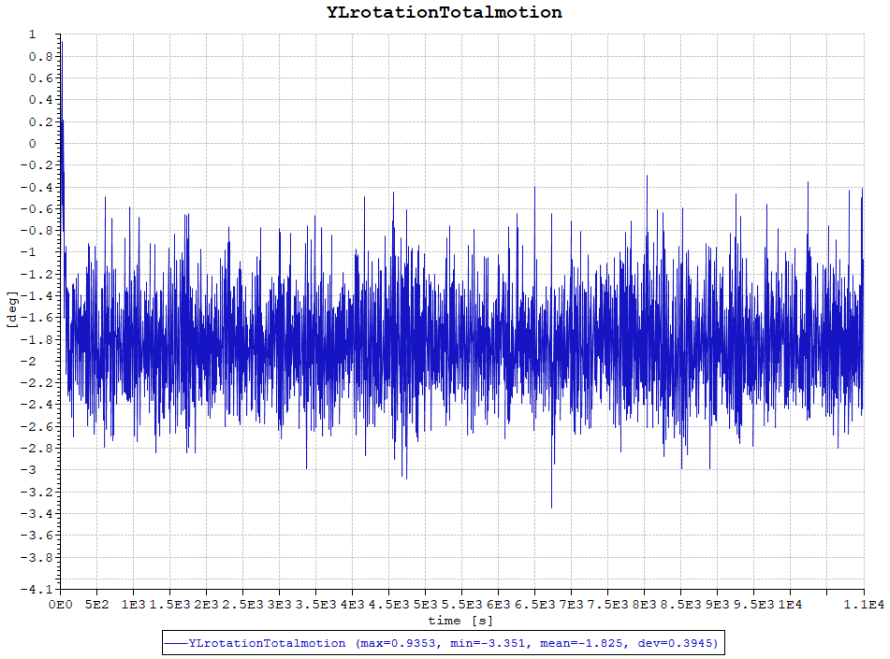

Figure A.8: Pitch motion, shutdown

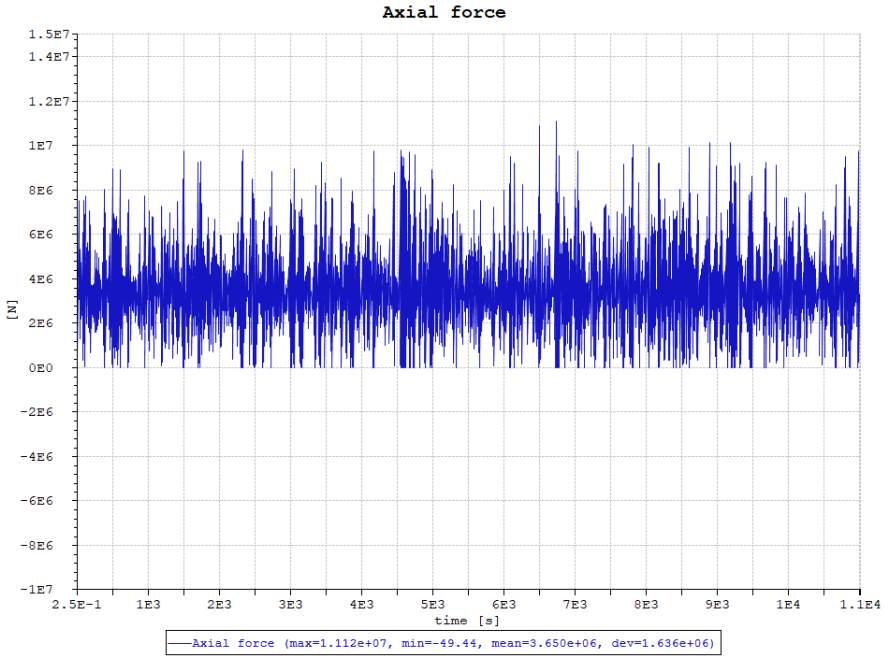

Figure A.9: Windward line tension, 50 year

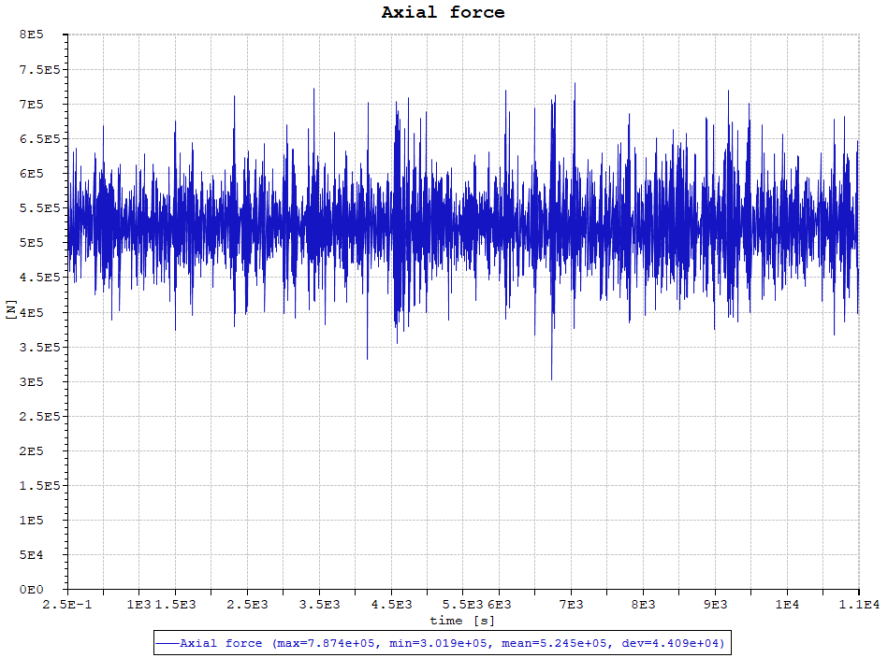

Figure A.10: Leeward line tension, 50 year

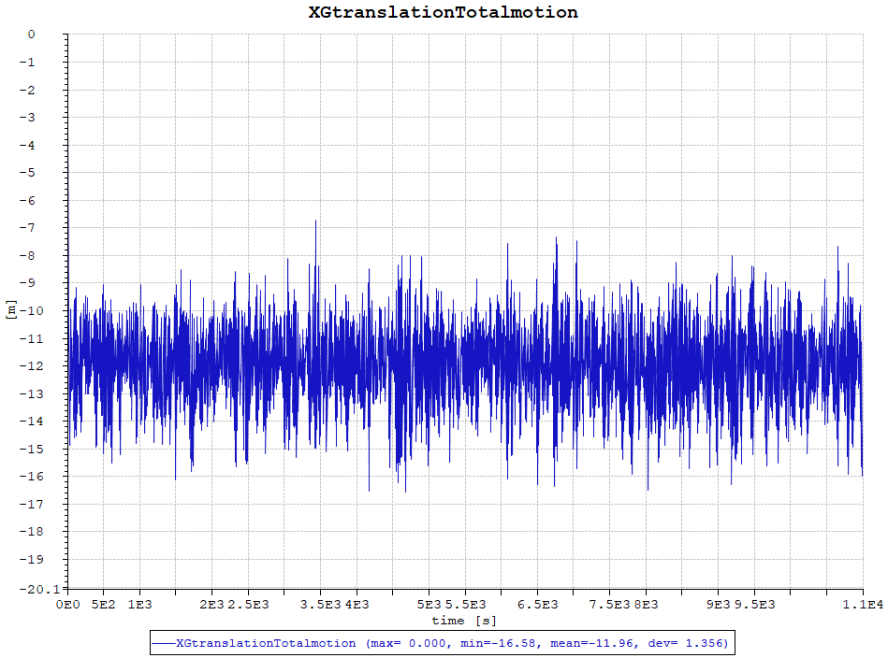

Figure A.11: Surge motion, 50 year

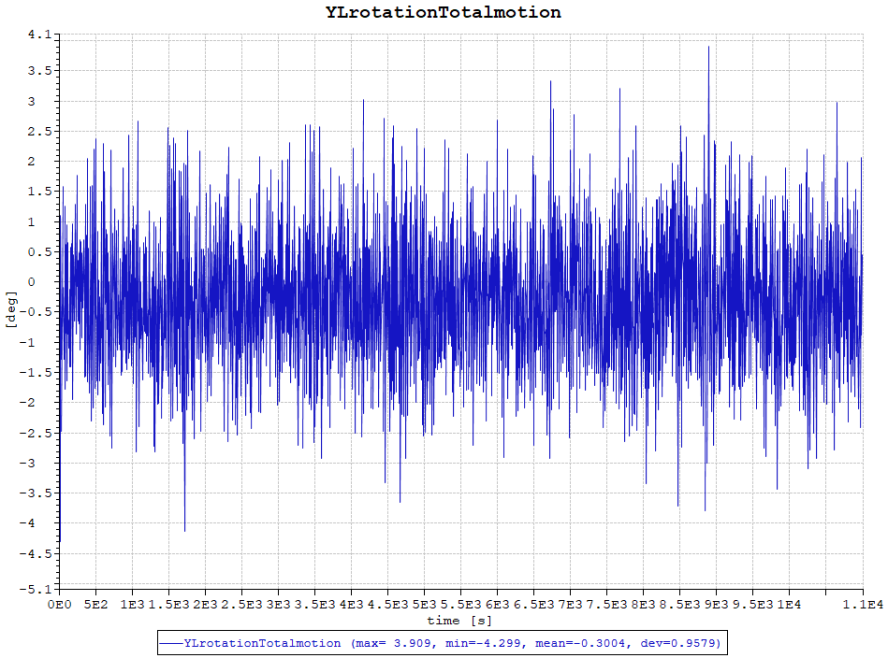

Figure A.12: Pitch motion, 50 year

Appendix B

ULS analysis

System I, Chain catenary

Table B.1: System I, LC1

Seed #	Max Surge	Mean Surge	Std Surge	Max heave	Mean Heave	Std heave	Max Pitch	Mean Pitch	Std pitch	Max Line1 [kN]	Mean Line1 [kN]	Std Line1 [kN]	Max Line2 [kN]	Mean Line2 [kN]	Std Line2 [kN]
1	-15.13	-13.19	0.39	0.51	-0.14	0.06	-13.39	-6.34	1.46	5938.14	4194.71	317.44	439.30	477.13	11.63
2	-15.16	-13.19	0.38	0.48	-0.14	0.06	-12.10	-6.34	1.43	5596.37	4194.08	313.15	439.11	477.12	11.41
3	-14.63	-13.16	0.37	0.38	-0.14	0.06	-11.98	-6.25	1.42	5708.12	4175.54	309.34	440.85	477.83	11.33
4	-15.28	-13.17	0.37	0.44	-0.14	0.06	-11.12	-6.27	1.41	5407.52	4179.49	305.92	445.48	477.63	11.33
5	-14.56	-13.17	0.38	0.38	-0.14	0.06	-12.09	-6.30	1.43	5724.45	4185.86	311.21	439.88	477.41	11.44
6	-14.59	-13.16	0.37	0.37	-0.14	0.06	-10.95	-6.24	1.39	5538.07	4174.41	307.92	444.45	477.84	11.16
7	-15.09	-13.18	0.37	0.36	-0.14	0.06	-11.43	-6.33	1.42	5640.46	4190.28	305.70	443.89	477.20	11.31
8	-15.23	-13.20	0.38	0.38	-0.14	0.06	-11.31	-6.37	1.46	5572.63	4201.55	316.17	442.84	476.87	11.59
9	-15.17	-13.19	0.38	0.39	-0.14	0.06	-11.66	-6.35	1.44	5798.68	4196.19	314.96	442.14	477.02	11.47
10	-14.87	-13.17	0.38	0.36	-0.14	0.06	-11.41	-6.29	1.44	5580.39	4183.49	313.18	443.19	477.55	11.51
11	-14.79	-13.18	0.37	0.36	-0.14	0.06	-12.34	-6.34	1.40	5442.11	4191.76	303.88	443.41	477.12	11.17
12	-14.98	-13.18	0.37	0.38	-0.14	0.06	-11.34	-6.31	1.41	5584.41	4187.00	309.45	441.87	477.35	11.26
Mean	-14.96	-13.18		0.40	-0.14		-11.76	-6.31		5627.61	4187.86		442.20	477.34	
Stand. Dev	0.26			0.05			0.67			147.92			2.06		
MPM	-15.07			0.38			-12.06			5561.05			441.27		
Tdyn										1377.00					
Td										7849.01					

Table B.2: System I, LC2

Seed #	Max Surge	Mean Surge	Std Surge	Max heave	Mean Heave	Std heave	Max Pitch	Mean Pitch	Std pitch	Max Line1 [kN]	Mean Line1 [kN]	Std Line1 [kN]	Max Line2 [kN]	Mean Line2 [kN]	Std Line2 [kN]
1	-13.70	-11.96	0.44	1.31	-0.05	0.41	-3.51	-1.97	0.36	5731.56	3492.88	431.73	454.30	513.94	14.80
2	-14.28	-11.95	0.43	1.41	-0.05	0.40	-3.17	-1.98	0.35	6312.32	3488.95	418.83	447.11	513.96	14.43
3	-14.14	-11.96	0.43	1.53	-0.05	0.41	-3.18	-1.97	0.36	6611.83	3492.77	429.75	435.76	513.93	14.67
4	-13.99	-11.96	0.43	1.32	-0.05	0.41	-3.12	-1.97	0.36	6009.22	3491.77	428.08	449.89	513.96	14.70
5	-13.95	-11.96	0.43	1.48	-0.05	0.41	-3.31	-1.98	0.36	6293.01	3493.81	428.60	448.20	513.90	14.70
6	-14.70	-11.97	0.45	1.88	-0.05	0.42	-3.57	-1.97	0.37	7298.37	3498.36	447.85	420.40	513.87	14.97
7	-13.93	-11.95	0.44	1.30	-0.05	0.41	-3.06	-1.97	0.36	5691.11	3488.78	431.05	442.40	514.03	14.73
8	-14.29	-11.96	0.43	1.55	-0.05	0.41	-3.18	-1.97	0.37	6539.92	3493.26	431.70	437.93	513.92	14.67
9	-14.19	-11.95	0.43	1.60	-0.05	0.40	-3.14	-1.98	0.36	6009.52	3488.19	430.19	441.03	513.94	14.38
10	-14.01	-11.96	0.44	1.61	-0.05	0.42	-3.14	-1.97	0.37	6612.95	3496.03	441.82	443.44	513.92	14.98
11	-14.27	-11.96	0.43	1.83	-0.05	0.41	-3.31	-1.97	0.36	6716.30	3489.60	425.20	434.21	513.96	14.69
12	-14.10	-11.96	0.44	1.61	-0.05	0.41	-3.09	-1.97	0.36	6588.75	3491.04	430.09	439.50	513.98	14.79
Mean	-14.13	-11.96		1.54	-1.31		-3.23	-1.97		6367.90	3492.12		441.18	513.94	
Stand. Dev	0.25			0.19			0.16			458.64			8.86		
MPM	-14.24			1.45			-3.31			6161.52			437.20		
Tdyn										2669.40					
Td										9211.20					

Table B.3: System I, LC3

Seed #	Max Surge	Mean Surge	Std Surge	Max heave	Mean Heave	Std heave	Max Pitch	Mean Pitch	Std pitch	Max Line1 [kN]	Mean Line1 [kN]	Std Line1 [kN]	Max Line2 [kN]	Mean Line2 [kN]	Std Line2 [kN]
1	-16.58	-11.98	1.31	4.37	-0.07	1.23	-4.30	-0.30	0.96	11116.76	3652.77	1635.04	301.94	524.28	43.71
2	-16.72	-11.97	1.29	4.57	-0.07	1.23	-3.75	-0.30	0.95	11352.82	3644.76	1618.17	324.00	524.21	43.01
3	-17.56	-11.98	1.30	5.01	-0.07	1.24	-3.54	-0.28	0.94	13272.68	3651.31	1645.39	312.69	524.33	43.91
4	-17.21	-11.97	1.31	4.05	-0.07	1.23	-4.21	-0.29	0.94	11784.77	3649.65	1639.71	334.97	524.38	43.53
5	-17.79	-11.98	1.31	5.32	-0.07	1.24	-3.72	-0.29	0.95	13374.49	3653.87	1649.18	322.24	524.31	43.84
6	-17.15	-12.00	1.32	5.12	-0.07	1.24	-3.73	-0.29	0.94	13013.89	3662.24	1684.60	317.08	524.12	44.08
7	-17.33	-11.98	1.31	4.28	-0.07	1.24	-4.11	-0.30	0.95	11972.42	3645.28	1652.11	342.43	524.32	43.25
8	-17.79	-11.98	1.30	4.83	-0.07	1.23	-4.19	-0.30	0.97	13555.17	3650.12	1639.71	296.40	524.17	43.31
9	-16.78	-11.97	1.30	5.45	-0.07	1.23	-3.58	-0.30	0.94	11944.62	3644.89	1644.07	319.10	524.12	43.28
10	-18.11	-11.98	1.32	5.57	-0.07	1.24	-3.38	-0.29	0.95	14388.09	3657.61	1671.51	300.62	524.29	44.27
11	-18.21	-11.97	1.30	5.79	-0.07	1.23	-3.93	-0.30	0.94	14669.83	3644.38	1643.30	242.24	524.35	44.25
12	-16.94	-11.97	1.32	4.80	-0.07	1.25	-3.78	-0.29	0.95	12104.58	3653.38	1666.95	346.70	524.40	44.39
Mean	-17.35	-11.98		4.93	-0.07		-3.85	-0.29		12712.51	3650.85		313.37	524.27	
Stand. Dev	0.55			0.55			0.30			1165.97			27.47		
MPM	-17.59			4.68			-3.98			12187.82			301.00		
Tdyn										8536.97					
Td										19685.80					

Table B.4: System I, LC4

Seed #	Max Surge	Mean Surge	Std Surge	Max heave	Mean Heave	Std heave	Max Pitch	Mean Pitch	Std pitch	Max Line1 [kN]	Mean Line1 [kN]	Std Line1 [kN]	in Line2 [kN]	Mean Line2 [kN]	Std Line2 [kN]
1	-16.46	-11.88	1.31	4.18	-0.07	1.23	-4.26	-0.30	0.94	11344.12	3656.59	1670.18	307.53	525.91	44.04
2	-16.59	-11.88	1.29	4.35	-0.07	1.23	-3.72	-0.30	0.94	11569.76	3648.61	1652.53	331.28	525.82	43.36
3	-17.37	-11.88	1.30	4.55	-0.07	1.24	-3.45	-0.28	0.93	13632.73	3655.26	1680.73	310.95	525.94	44.25
4	-17.06	-11.88	1.31	3.95	-0.07	1.23	-4.09	-0.29	0.93	12075.58	3653.57	1675.41	336.37	526.00	43.84
5	-17.62	-11.89	1.31	4.98	-0.07	1.24	-3.63	-0.29	0.94	13740.88	3657.89	1684.84	332.47	525.93	44.18
6	-16.95	-11.90	1.32	5.05	-0.07	1.25	-3.72	-0.29	0.93	13285.25	3666.27	1721.72	310.61	525.74	44.38
7	-17.19	-11.88	1.31	4.04	-0.07	1.24	-4.06	-0.30	0.93	12312.00	3649.35	1688.51	346.72	525.93	43.56
8	-17.62	-11.89	1.30	4.84	-0.07	1.23	-4.08	-0.30	0.96	13914.94	3653.95	1675.99	298.08	525.78	43.63
9	-16.61	-11.88	1.30	4.60	-0.07	1.23	-3.43	-0.30	0.93	12258.30	3648.72	1679.10	311.31	525.74	43.64
10	-17.93	-11.89	1.32	4.65	-0.07	1.25	-3.44	-0.29	0.93	14821.00	3661.51	1707.84	302.95	525.92	44.61
11	-18.03	-11.87	1.30	4.99	-0.07	1.23	-3.94	-0.30	0.93	15101.24	3648.25	1678.50	245.76	525.97	44.60
12	-16.80	-11.88	1.32	4.29	-0.07	1.25	-3.57	-0.29	0.93	12482.83	3657.33	1702.78	350.11	526.03	44.74
Mean	-17.19	-11.88		4.54	-0.07		-3.78	-0.29		13044.88	3654.77		315.34	525.89	
Stand. Dev	0.53			0.38			0.29			1225.03			27.95		
MPM	-17.43			4.37			-3.92			12493.62			302.76		
Tdyn										8838.84					
Td										20219.18					

Table B.5: System I, LC1 In between

Seed #	Max Surge	Mean Surge	Std Surge	Max heave	Mean Heave	Std heave	Max Pitch	Mean Pitch	Std pitch	Min Line1 [kN]	Mean Line1 [kN]	Std Line1 [kN]	Max Line2 [kN]	Mean Line2 [kN]	Std Line2 [kN]
1	27.39	21.62	1.45	4.17	-0.26	1.27	4.28	0.20	0.95	97.78	290.87	40.92	6508.56	3199.66	747.79
2	27.80	21.61	1.43	4.29	-0.26	1.27	3.63	0.20	0.96	118.17	290.80	40.38	7774.75	3195.99	734.37
3	28.02	21.61	1.43	4.52	-0.26	1.28	3.67	0.18	0.93	63.38	291.07	40.98	7792.17	3197.38	750.67
4	27.63	21.61	1.44	3.96	-0.26	1.27	3.95	0.18	0.94	123.46	290.92	40.70	7124.18	3196.90	739.58
5	28.26	21.62	1.45	4.98	-0.26	1.28	3.56	0.19	0.94	115.11	290.91	41.06	8096.69	3200.33	751.76
6	28.43	21.64	1.46	5.05	-0.26	1.28	3.49	0.18	0.92	68.67	290.66	41.22	8330.77	3204.28	760.96
7	28.29	21.61	1.45	3.96	-0.26	1.28	4.03	0.19	0.94	128.71	290.85	40.65	7275.10	3196.39	743.22
8	28.50	21.62	1.43	4.79	-0.26	1.27	4.22	0.20	0.99	78.32	290.73	40.85	8015.42	3199.84	742.74
9	27.40	21.61	1.45	4.58	-0.26	1.27	3.46	0.20	0.95	68.75	290.51	40.53	7390.09	3194.33	750.09
10	28.31	21.63	1.46	4.58	-0.26	1.29	3.72	0.18	0.94	98.24	290.95	41.24	7907.56	3202.28	765.80
11	28.21	21.61	1.44	4.86	-0.26	1.27	4.09	0.19	0.95	52.08	290.71	41.17	8335.41	3195.54	756.55
12	27.36	21.62	1.46	4.30	-0.26	1.29	3.48	0.19	0.94	107.37	290.97	41.29	7422.16	3201.47	764.31
Mean	27.97	21.62		4.50	-0.26		3.80	0.19		93.34	290.83		7664.41	3198.70	
Stand. Dev	0.43			0.37			0.30			26.16			539.81		
MPM	27.77			4.33			3.66			81.57			7421.49		
Tdyn													4222.79		
Td													11548.20		

System II

Table B.6: System II, LC1

Seed #	Max Surge	Mean Surge	Std Surge	Max heave	Mean Heave	Std heave	Max Pitch	Mean Pitch	Std pitch	Max Line1 [kN]	Mean Line1 [kN]	Std Line1 [kN]	Max Line2 [kN]	Mean Line2 [kN]	Std Line2 [kN]
1	-13.06	-10.03	0.66	0.05	-0.22	0.07	0.00	-7.55	1.60	5594.72	4685.91	227.36	974.86	1105.35	38.19
2	-12.65	-10.03	0.65	0.04	-0.22	0.07	0.00	-7.55	1.58	5574.09	4685.47	221.02	982.77	1105.33	38.87
3	-12.62	-9.98	0.64	0.04	-0.21	0.07	0.00	-7.46	1.56	5631.32	4667.92	220.00	971.13	1106.47	37.72
4	-13.02	-9.99	0.63	0.05	-0.21	0.07	0.00	-7.48	1.55	5393.85	4671.56	215.20	977.60	1106.21	37.39
5	-12.19	-10.01	0.65	0.09	-0.22	0.07	0.09	-7.51	1.57	5456.17	4677.37	220.36	966.68	1105.89	37.89
6	-12.21	-9.98	0.64	0.04	-0.21	0.07	0.00	-7.45	1.53	5499.28	4666.65	217.98	968.63	1106.48	38.22
7	-12.34	-10.02	0.64	0.05	-0.22	0.07	0.00	-7.54	1.55	5417.02	4682.06	218.79	962.02	1105.55	37.18
8	-12.55	-10.05	0.65	0.07	-0.22	0.07	0.00	-7.59	1.61	5502.47	4692.68	221.07	976.81	1104.91	37.20
9	-12.51	-10.04	0.65	0.05	-0.22	0.07	0.00	-7.56	1.58	5544.57	4687.44	223.60	969.85	1105.23	38.49
10	-12.32	-10.00	0.66	0.10	-0.21	0.07	0.00	-7.50	1.58	5472.00	4675.38	224.60	972.77	1106.03	39.44
Mean	-12.55	-10.01		0.06	-0.22		0.01	-7.52		5508.55	4679.25		972.31	1105.74	
Stand. Dev	0.30			0.02			0.03			77.34			5.99		
MPM	-12.68			0.05			0.00			5473.75			969.62		
Tdyn										798.48					
Td										7480.36					

Table B.7: System II, LC2

Seed #	Max Surge	Mean Surge	Std Surge	Max heave	Mean Heave	Std heave	Max Pitch	Mean Pitch	Std pitch	Max Line1 [kN]	Mean Line1 [kN]	Std Line1 [kN]	Max Line2 [kN]	Mean Line2 [kN]	Std Line2 [kN]
1	-10.15	-7.84	0.51	1.19	-0.14	0.40	-4.67	-3.14	0.36	5020.35	4014.79	208.44	918.27	1159.16	58.02
2	-10.78	-7.83	0.50	1.28	-0.14	0.39	-4.69	-3.14	0.35	5194.69	4011.45	201.51	918.71	1159.36	56.91
3	-10.58	-7.84	0.50	1.45	-0.14	0.40	-4.53	-3.14	0.36	5218.18	4014.67	204.27	926.80	1159.17	56.96
4	-10.53	-7.84	0.51	1.21	-0.14	0.40	-4.33	-3.14	0.36	5159.35	4013.76	205.29	903.74	1159.25	56.74
5	-10.45	-7.84	0.51	1.35	-0.14	0.40	-4.59	-3.14	0.36	5143.52	4015.70	206.80	922.51	1159.04	58.54
6	-11.52	-7.85	0.53	1.76	-0.14	0.41	-4.72	-3.14	0.36	5599.74	4019.41	214.78	888.68	1158.75	58.08
7	-10.35	-7.83	0.51	1.18	-0.14	0.40	-4.48	-3.14	0.35	5082.62	4011.00	208.64	924.78	1159.55	57.27
8	-10.80	-7.84	0.51	1.44	-0.14	0.40	-4.50	-3.14	0.36	5292.20	4015.26	207.99	909.44	1159.12	56.91
9	-10.62	-7.83	0.51	1.48	-0.14	0.39	-4.61	-3.14	0.35	5150.44	4010.56	205.35	902.13	1159.31	57.28
10	-10.40	-7.85	0.52	1.49	-0.14	0.41	-4.38	-3.14	0.36	5095.19	4017.38	210.76	914.33	1158.98	56.80
Mean	-10.618	-7.840		1.382	-0.141		-4.550	-3.142		5195.628	4014.399		912.939	1159.168	
Stand. Dev	0.373			0.181			0.130			160.831			11.970		
MPM	-10.785			1.301			-4.608			5123.254			907.553		
Tdyn										1110.127					
Td										7161.442					

Table B.8: System II, LC3

Seed #	Max Surge	Mean Surge	Std Surge	Max heave	Mean Heave	Std heave	Max Pitch	Mean Pitch	Std pitch	Max Line1 [kN]	Mean Line1 [kN]	Std Line1 [kN]	Max Line2 [kN]	Mean Line2 [kN]	Std Line2 [kN]
1	-13.86	-7.82	1.52	3.89	-0.14	1.15	-5.31	-1.60	0.94	6741.43	4120.62	620.15	651.79	1155.68	127.66
2	-14.55	-7.81	1.49	4.07	-0.14	1.15	-5.02	-1.60	0.93	7065.30	4114.76	606.00	588.89	1155.78	126.75
3	-15.58	-7.82	1.51	4.35	-0.14	1.16	-4.94	-1.58	0.92	7324.72	4119.79	614.55	578.23	1155.65	127.59
4	-14.44	-7.82	1.52	3.82	-0.14	1.15	-5.49	-1.59	0.94	6935.57	4118.19	618.37	574.92	1155.79	129.45
5	-15.95	-7.83	1.51	4.71	-0.14	1.16	-5.21	-1.59	0.94	7617.94	4121.97	618.39	611.88	1155.54	128.24
6	-15.78	-7.84	1.53	5.00	-0.14	1.16	-5.14	-1.59	0.92	7536.87	4128.57	625.54	546.77	1154.85	127.51
7	-14.83	-7.81	1.50	3.75	-0.14	1.16	-5.31	-1.60	0.94	6946.63	4113.56	613.63	601.25	1156.29	126.54
8	-16.29	-7.82	1.50	4.59	-0.14	1.15	-5.61	-1.60	0.97	7672.52	4119.54	613.36	579.16	1155.82	127.04
9	-14.99	-7.81	1.51	4.27	-0.14	1.15	-4.90	-1.60	0.94	7055.10	4114.44	616.69	646.05	1155.79	126.86
10	-15.93	-7.83	1.53	4.30	-0.14	1.16	-5.02	-1.59	0.93	7617.18	4123.95	622.72	577.37	1155.48	128.02
Mean	-15.28	-7.82		4.29	-0.14		-5.17	-1.59		7266.26	4119.05		589.28	1155.73	
Stand. Dev	0.81			0.40			0.22			357.88			33.97		
MPM	-15.65			4.11			-5.27			7105.21			573.99		
Tdyn										2988.23					
Td										10584.16					

Table B.9: System II, LC4

Seed #	Max Surge	Mean Surge	Std Surge	Max heave	Mean Heave	Std heave	Max Pitch	Mean Pitch	Std pitch	Max Line1 [kN]	Mean Line1 [kN]	Std Line1 [kN]	Max Line2 [kN]	Mean Line2 [kN]	Std Line2 [kN]
1	-13.98	-7.45	1.66	4.98	-0.15	1.35	-5.10	-1.60	0.89	6719.61	3976.80	667.19	772.14	1172.24	118.31
2	-14.82	-7.45	1.66	4.75	-0.15	1.37	-5.14	-1.60	0.88	7101.00	3976.11	668.89	789.69	1172.25	117.83
3	-15.17	-7.45	1.66	5.34	-0.15	1.37	-4.79	-1.59	0.88	7245.81	3976.30	668.97	748.81	1172.24	119.62
4	-13.98	-7.44	1.64	4.70	-0.15	1.34	-5.62	-1.59	0.88	6772.10	3974.21	660.99	714.64	1172.10	119.33
5	-15.63	-7.46	1.65	5.80	-0.14	1.36	-5.20	-1.59	0.89	7450.31	3979.26	667.90	760.81	1171.81	118.98
6	-13.88	-7.46	1.66	4.96	-0.15	1.36	-4.58	-1.59	0.87	6770.76	3982.35	670.61	694.55	1171.68	119.12
7	-14.34	-7.44	1.64	4.49	-0.15	1.35	-4.82	-1.60	0.87	6827.84	3971.95	662.42	787.59	1172.61	117.72
8	-15.08	-7.46	1.64	4.88	-0.15	1.34	-5.63	-1.60	0.93	7075.87	3978.03	660.45	697.91	1171.96	117.60
9	-15.15	-7.45	1.64	5.92	-0.15	1.35	-4.86	-1.60	0.89	7383.67	3974.97	664.05	727.20	1172.16	118.88
10	-15.78	-7.45	1.66	5.32	-0.15	1.36	-5.17	-1.59	0.88	7587.26	3977.39	668.83	751.55	1172.31	119.80
Mean	-14.78	-7.45		5.11	-0.15		-5.09	-1.59		7093.42	3976.74		744.49	1172.14	
Stand. Dev	0.70			0.47			0.35			315.65			34.73		
MPM	-15.09			4.90			-5.25			6951.38			728.86		
Tdyn										2975.92					
Td										10377.63					

Table B.10: System II, LC1IB

Seed #	Max Surge	Mean Surge	Std Surge	Max heave	Mean Heave	Std heave	Max Pitch	Mean Pitch	Std pitch	Max Line1 [kN]	Mean Line1 [kN]	Std Line1 [kN]	Max Line2 [kN]	Mean Line2 [kN]	Std Line2 [kN]
1	21.24	16.18	1.05	0.15	-0.26	0.07	15.40	8.43	1.78	577.00	659.92	24.22	4791.32	4108.67	182.86
2	21.23	16.18	1.02	0.17	-0.26	0.07	15.28	8.43	1.75	586.20	659.94	23.93	4691.95	4108.11	176.95
3	20.24	16.09	1.00	0.11	-0.26	0.07	15.39	8.33	1.72	584.27	661.60	23.52	4825.66	4092.00	174.34
4	20.71	16.11	0.98	0.09	-0.26	0.07	14.59	8.35	1.72	587.28	661.19	23.56	4642.37	4095.65	171.10
5	19.07	16.14	1.02	0.19	-0.26	0.07	15.16	8.38	1.74	586.65	660.69	23.93	4604.16	4100.68	176.71
6	19.70	16.08	0.99	0.13	-0.26	0.07	14.31	8.32	1.69	581.86	661.77	23.62	4735.33	4090.18	172.95
7	19.52	16.17	0.99	0.12	-0.26	0.07	14.59	8.41	1.72	577.22	660.10	23.11	4618.84	4106.10	173.11
8	19.80	16.22	1.01	0.16	-0.26	0.07	14.89	8.46	1.80	578.08	659.30	23.74	4717.48	4114.58	176.37
9	20.82	16.19	1.02	0.14	-0.26	0.07	14.58	8.44	1.76	585.21	659.70	23.94	4734.92	4110.35	177.85
10	20.46	16.13	1.04	0.13	-0.26	0.07	14.59	8.37	1.75	591.13	660.96	24.37	4663.25	4098.48	180.48
Mean	20.28	16.15		0.14	-0.26		14.88	8.39		583.49	660.52		4702.53	4102.48	
Stand. Dev	0.74			0.03			0.40			4.80			72.53		
MPM	19.95			0.13			14.70			581.33			4669.89		
Tdyn													567.41		
Td													6326.19		

System III

Table B.11: System III, LC1

Seed #	Max Surge	Mean Surge	Std Surge	Max heave	Mean Heave	Std heave	Max Pitch	Mean Pitch	Std pitch	Max Line1 [kN]	Mean Line1 [kN]	Std Line1 [kN]	Max Line2 [kN]	Mean Line2 [kN]	Std Line2 [kN]
1	-16.076	-12.387	0.763	0.486	-0.192	0.066	-15.031	-7.625	1.615	5345.347	4513.210	216.685	837.750	942.420	31.887
2	-16.168	-12.386	0.741	0.489	-0.192	0.065	-13.937	-7.623	1.593	5303.213	4512.763	210.040	846.449	942.411	31.989
3	-15.404	-12.325	0.735	0.458	-0.190	0.066	-14.184	-7.532	1.574	5432.634	4495.196	208.671	840.088	943.464	31.465
4	-16.230	-12.338	0.723	0.475	-0.191	0.065	-12.980	-7.552	1.569	5167.127	4498.916	204.037	834.797	943.218	31.203
5	-14.726	-12.358	0.742	0.483	-0.191	0.065	-14.110	-7.584	1.585	5181.845	4504.590	209.731	827.030	942.914	31.388
6	-14.940	-12.321	0.730	0.421	-0.190	0.065	-12.733	-7.523	1.541	5256.144	4493.890	207.116	834.701	943.503	31.250
7	-15.335	-12.375	0.731	0.427	-0.192	0.065	-13.428	-7.611	1.570	5156.602	4509.415	207.279	843.158	942.614	30.588
8	-15.792	-12.410	0.743	0.461	-0.193	0.066	-13.354	-7.656	1.633	5285.580	4520.037	209.914	842.913	942.001	30.190
9	-15.881	-12.393	0.748	0.470	-0.192	0.066	-13.376	-7.632	1.599	5322.530	4514.849	212.419	843.144	942.304	31.770
10	-15.722	-12.350	0.754	0.471	-0.191	0.066	-13.374	-7.569	1.597	5238.772	4502.670	213.711	826.165	943.046	32.851
Mean	-15.63	-12.36		0.46	-0.19		-13.65	-7.59		5268.98	4506.55		837.62	942.79	
Stand. Dev	0.51			0.02			0.67			87.31			6.94		
MPM	-15.86			0.45			-13.95			5229.69			834.50		
Tdyn										727.13					
Td										7131.00					

Table B.12: System III, LC2

Seed #	Max Surge	Mean Surge	Std Surge	Max heave	Mean Heave	Std heave	Max Pitch	Mean Pitch	Std pitch	Max Line1 [kN]	Mean Line1 [kN]	Std Line1 [kN]	Max Line2 [kN]	Mean Line2 [kN]	Std Line2 [kN]
1	-12.32	-9.78	0.55	1.22	-0.12	0.40	-4.72	-3.17	0.36	4736.13	3837.90	179.57	812.74	991.80	45.83
2	-12.89	-9.77	0.53	1.30	-0.12	0.39	-4.68	-3.17	0.35	4864.51	3834.61	172.54	814.95	991.97	45.35
3	-12.87	-9.78	0.53	1.47	-0.12	0.40	-4.54	-3.17	0.36	4930.90	3837.69	174.80	792.67	991.71	45.25
4	-12.73	-9.78	0.54	1.24	-0.12	0.40	-4.34	-3.17	0.36	4854.46	3836.95	176.39	787.00	991.86	45.14
5	-12.67	-9.78	0.54	1.38	-0.12	0.40	-4.62	-3.17	0.36	4836.53	3838.79	177.46	787.64	991.61	46.25
6	-13.74	-9.79	0.56	1.79	-0.12	0.41	-4.73	-3.17	0.36	5202.68	3842.56	185.34	782.09	991.38	46.49
7	-12.52	-9.77	0.55	1.21	-0.12	0.40	-4.52	-3.17	0.35	4792.41	3834.07	180.34	818.61	992.12	45.49
8	-13.21	-9.78	0.55	1.47	-0.12	0.40	-4.51	-3.17	0.36	5001.32	3838.39	178.91	798.23	991.68	45.58
9	-12.63	-9.77	0.54	1.51	-0.12	0.39	-4.64	-3.17	0.35	4791.35	3833.87	176.67	777.05	992.00	45.28
10	-12.50	-9.79	0.56	1.52	-0.12	0.41	-4.41	-3.17	0.36	4755.83	3840.52	182.44	780.71	991.58	44.65
Mean	-12.81	-9.78		1.41	-0.12		-4.57	-3.17		4876.61	3837.54		795.17	991.77	
Stand. Dev	0.41			0.18			0.13			139.74			15.26		
MPM	-12.99			1.33			-4.63			4813.73			788.30		
Tdyn										977.46					
Td										6699.35					

Table B.13: System III, LC3

Seed #	Max Surge	Mean Surge	Std Surge	Max heave	Mean Heave	Std heave	Max Pitch	Mean Pitch	Std pitch	Max Line1 [kN]	Mean Line1 [kN]	Std Line1 [kN]	Max Line2 [kN]	Mean Line2 [kN]	Std Line2 [kN]
1	-16.38	-9.83	1.60	3.92	-0.12	1.15	-5.37	-1.61	0.94	6078.69	3940.88	526.21	627.80	988.90	91.28
2	-17.14	-9.82	1.55	4.11	-0.12	1.15	-5.03	-1.61	0.94	6480.38	3935.15	510.59	557.29	988.97	90.84
3	-18.02	-9.83	1.57	4.38	-0.12	1.16	-4.93	-1.60	0.92	6621.91	3939.97	518.49	569.70	988.81	91.42
4	-17.22	-9.83	1.59	3.86	-0.12	1.15	-5.45	-1.60	0.94	6437.81	3938.73	523.32	590.79	989.10	92.03
5	-18.38	-9.84	1.58	4.74	-0.12	1.16	-5.22	-1.61	0.94	6860.81	3942.32	521.84	536.35	988.80	91.48
6	-18.70	-9.86	1.60	5.03	-0.12	1.16	-5.17	-1.60	0.92	6963.68	3948.93	529.36	565.15	988.20	92.12
7	-17.52	-9.81	1.57	3.78	-0.12	1.16	-5.34	-1.61	0.94	6418.29	3933.82	519.03	554.58	989.49	90.85
8	-18.93	-9.83	1.57	4.63	-0.12	1.15	-5.58	-1.62	0.97	6975.11	3939.90	518.80	530.21	988.87	91.44
9	-17.29	-9.82	1.58	4.29	-0.12	1.15	-4.93	-1.61	0.94	6375.95	3934.86	522.27	624.46	988.95	89.97
10	-18.33	-9.84	1.61	4.32	-0.12	1.17	-5.00	-1.60	0.94	6857.80	3944.23	529.63	498.31	988.75	90.29
Mean	-17.79	-9.83		4.30	-0.12		-5.20	-1.61		6607.04	3939.88		565.46	988.88	
Stand. Dev	0.81			0.41			0.23			298.71			40.57		
MPM	-18.15			4.12			-5.30			6472.62			547.21		
Tdyn										2534.83					
Td										9557.80					

Table B.14: System III, LC4

Seed #	Max Surge	Mean Surge	Std Surge	Max heave	Mean Heave	Std heave	Max Pitch	Mean Pitch	Std pitch	Max Line1 [kN]	Mean Line1 [kN]	Std Line1 [kN]	Max Line2 [kN]	Mean Line2 [kN]	Std Line2 [kN]
1	-16.12	-9.37	1.68	5.02	-0.12	1.35	-5.09	-1.61	0.89	6044.06	3795.45	548.41	723.64	1002.62	86.27
2	-17.15	-9.37	1.67	4.77	-0.12	1.37	-5.21	-1.61	0.89	6415.07	3794.83	547.54	695.34	1002.68	86.20
3	-17.28	-9.37	1.67	5.37	-0.12	1.37	-4.77	-1.60	0.89	6488.13	3794.87	548.03	675.21	1002.68	87.41
4	-16.27	-9.36	1.65	4.72	-0.12	1.34	-5.65	-1.60	0.89	6092.22	3793.32	542.70	681.55	1002.68	87.08
5	-17.80	-9.38	1.67	5.83	-0.12	1.36	-5.24	-1.61	0.89	6645.58	3798.02	547.69	695.88	1002.32	88.20
6	-15.95	-9.39	1.67	4.98	-0.12	1.36	-4.56	-1.60	0.88	6002.69	3801.01	549.24	639.51	1002.16	87.82
7	-16.51	-9.36	1.65	4.53	-0.12	1.35	-4.88	-1.61	0.88	6155.32	3790.68	543.00	739.28	1003.10	85.94
8	-17.28	-9.38	1.65	4.90	-0.12	1.34	-5.62	-1.62	0.93	6393.48	3796.85	542.03	646.41	1002.38	86.62
9	-17.21	-9.37	1.66	5.94	-0.12	1.35	-4.91	-1.61	0.89	6552.04	3793.75	545.70	673.39	1002.57	87.57
10	-17.97	-9.37	1.68	5.34	-0.12	1.36	-5.17	-1.60	0.88	6744.81	3796.19	550.02	655.91	1002.78	88.02
Mean	-16.95	-9.37		5.14	-0.12		-5.11	-1.61		6353.34	3795.50		682.61	1002.60	
Stand. Dev	0.70			0.47			0.35			264.10			32.07		
MPM	-17.27			4.93			-5.27			6234.50			668.18		
Tdyn										2440.26					
Td										9204.60					

Table B.15: System III, LC1IB

Seed #	Max Surge	Mean Surge	Std Surge	Max heave	Mean Heave	Std heave	Max Pitch	Mean Pitch	Std pitch	Max Line1 [kN]	Mean Line1 [kN]	Std Line1 [kN]	Max Line2 [kN]	Mean Line2 [kN]	Std Line2 [kN]
1	22.14	15.10	1.65	4.05	-0.15	1.20	5.43	1.77	0.98	439.85	652.73	63.50	4446.71	3323.73	254.07
2	22.66	15.08	1.60	4.16	-0.15	1.20	5.31	1.77	0.99	413.95	652.72	62.45	4546.44	3321.07	246.55
3	22.69	15.08	1.61	4.50	-0.15	1.21	5.41	1.75	0.96	344.08	652.98	63.59	4603.54	3321.79	248.52
4	22.55	15.08	1.62	3.95	-0.15	1.20	5.59	1.76	0.98	439.91	653.01	63.28	4570.02	3321.75	249.35
5	22.94	15.10	1.63	4.88	-0.15	1.21	5.20	1.76	0.97	364.40	652.80	63.48	4599.15	3323.94	251.30
6	23.84	15.12	1.64	5.08	-0.15	1.21	5.12	1.76	0.94	380.09	652.59	63.70	4775.69	3327.62	254.14
7	22.98	15.08	1.63	3.84	-0.15	1.21	5.53	1.77	0.97	401.54	653.11	62.72	4567.54	3320.83	251.37
8	23.11	15.10	1.61	4.70	-0.15	1.20	5.80	1.77	1.03	332.16	652.58	63.10	4649.81	3324.69	248.48
9	22.59	15.07	1.64	4.50	-0.15	1.20	5.17	1.77	0.98	367.31	652.93	62.45	4568.10	3320.33	252.48
10	22.79	15.10	1.67	4.41	-0.15	1.21	5.49	1.76	0.97	376.39	652.94	63.71	4598.96	3325.82	257.41
Mean	22.83	15.09		4.41	-0.15		5.40	1.76		385.97	652.84		4592.60	3323.16	
Stand. Dev	0.45			0.41			0.21			37.16			83.10	2.40	
MPM	22.63			4.22			5.31			369.25			4555.20	3322.07	
Tdyn													1233.13		
Td													6478.07		

System IV

Table B.16: System IV, LC1

Seed #	Max Surge	Mean Surge	Std Surge	Max heave	Mean Heave	Std heave	Max Pitch	Mean Pitch	Std pitch	Max Line1 [kN]	Mean Line1 [kN]	Std Line1 [kN]	Max Line2 [kN]	Mean Line2 [kN]	Std Line2 [kN]
1	-20.73	-15.77	0.90	0.24	-0.17	0.07	0.00	-7.69	1.63	5134.48	4358.98	205.72	729.04	799.49	19.31
2	-20.66	-15.77	0.88	0.11	-0.17	0.06	0.00	-7.69	1.61	5083.02	4358.48	198.95	732.77	799.49	19.34
3	-19.41	-15.69	0.87	0.10	-0.17	0.07	0.00	-7.60	1.59	5212.13	4340.89	197.02	730.23	800.45	18.98
4	-20.39	-15.71	0.85	0.10	-0.17	0.06	0.00	-7.62	1.58	4972.85	4344.69	192.61	732.68	800.22	18.92
5	-18.38	-15.73	0.88	0.23	-0.17	0.07	0.72	-7.65	1.60	4959.76	4350.28	198.92	731.81	799.95	19.13
6	-18.86	-15.69	0.86	0.11	-0.17	0.06	0.00	-7.59	1.55	5079.35	4339.54	196.18	730.31	800.49	19.38
7	-19.34	-15.75	0.86	0.10	-0.17	0.06	0.00	-7.68	1.58	4981.51	4355.21	195.48	732.59	799.66	18.78
8	-19.71	-15.80	0.88	0.15	-0.17	0.07	0.00	-7.72	1.65	5084.24	4365.84	198.59	732.53	799.10	18.93
9	-20.45	-15.78	0.88	0.17	-0.17	0.07	0.00	-7.70	1.61	5093.32	4360.69	200.78	737.64	799.37	19.34
10	-20.17	-15.72	0.89	0.12	-0.17	0.07	0.00	-7.63	1.61	5019.25	4348.43	202.67	736.64	800.06	19.61
Mean	-19.81	-15.74		0.14	-0.17		0.07	-7.66		5061.99	4352.30		732.63	799.83	
Stand. Dev	0.80			0.05			0.23			79.39			2.70		
MPM	-20.17			0.12			-0.03			5026.27			731.41		
Tdyn										677.97					
Td										6844.45					

Table B.17: System IV, LC2

Seed #	Max Surge	Mean Surge	Std Surge	Max heave	Mean Heave	Std heave	Max Pitch	Mean Pitch	Std pitch	Max Line1 [kN]	Mean Line1 [kN]	Std Line1 [kN]	Max Line2 [kN]	Mean Line2 [kN]	Std Line2 [kN]
1	-15.34	-12.55	0.60	1.24	-0.09	0.40	-4.77	-3.20	0.36	4433.22	3678.70	152.78	730.53	843.50	28.86
2	-15.92	-12.54	0.56	1.32	-0.09	0.40	-4.69	-3.20	0.35	4539.83	3675.47	145.06	727.00	843.67	28.22
3	-16.12	-12.55	0.57	1.50	-0.09	0.40	-4.57	-3.20	0.36	4644.51	3678.58	147.71	728.82	843.43	28.43
4	-15.72	-12.55	0.58	1.26	-0.09	0.40	-4.36	-3.20	0.35	4522.39	3677.84	149.19	720.44	843.55	28.29
5	-15.65	-12.55	0.58	1.40	-0.09	0.40	-4.65	-3.20	0.35	4502.74	3679.68	149.77	721.93	843.37	28.94
6	-16.84	-12.57	0.62	1.81	-0.09	0.41	-4.74	-3.20	0.36	4810.84	3683.46	157.98	718.50	843.14	29.07
7	-15.54	-12.53	0.60	1.23	-0.09	0.40	-4.56	-3.20	0.35	4483.27	3674.95	153.96	724.99	843.81	28.64
8	-16.53	-12.55	0.59	1.50	-0.09	0.40	-4.55	-3.20	0.36	4709.63	3679.39	152.12	713.55	843.43	28.79
9	-15.66	-12.53	0.58	1.53	-0.09	0.39	-4.67	-3.20	0.35	4506.84	3674.85	149.52	698.03	843.72	28.34
10	-15.41	-12.56	0.61	1.54	-0.09	0.41	-4.43	-3.20	0.36	4410.45	3681.42	155.85	704.08	843.31	28.49
Mean	-15.87	-12.55		1.43	-0.09		-4.60	-3.20		4556.37	3678.43		718.79	843.49	
Stand. Dev	0.49			0.18			0.13			126.74			10.71		
MPM	-16.09			1.35			-4.66			4499.34			713.97		
Tdyn										822.17					
Td										6220.76					

Table B.18: System IV, LC3

Seed #	Max Surge	Mean Surge	Std Surge	Max heave	Mean Heave	Std heave	Max Pitch	Mean Pitch	Std pitch	Max Line1 [kN]	Mean Line1 [kN]	Std Line1 [kN]	Max Line2 [kN]	Mean Line2 [kN]	Std Line2 [kN]
1	-20.06	-12.71	1.71	3.95	-0.10	1.16	-5.41	-1.63	0.94	5650.41	3778.96	440.87	593.29	840.63	59.64
2	-20.48	-12.68	1.63	4.14	-0.10	1.15	-5.03	-1.63	0.94	5871.08	3773.53	423.58	583.37	840.79	58.83
3	-21.29	-12.70	1.66	4.41	-0.10	1.16	-4.96	-1.61	0.93	6113.51	3778.14	430.96	568.39	840.62	59.32
4	-20.93	-12.70	1.68	3.89	-0.10	1.15	-5.41	-1.62	0.94	5940.07	3776.94	435.52	563.70	840.79	59.66
5	-21.74	-12.71	1.67	4.78	-0.10	1.16	-5.21	-1.62	0.94	6153.34	3780.40	433.30	569.48	840.59	59.57
6	-22.56	-12.74	1.71	5.06	-0.10	1.16	-5.19	-1.62	0.92	6370.82	3787.17	442.11	546.01	840.04	59.83
7	-21.11	-12.68	1.67	3.81	-0.10	1.16	-5.37	-1.63	0.94	5891.23	3772.04	433.13	575.18	841.19	59.08
8	-22.54	-12.70	1.67	4.66	-0.10	1.15	-5.57	-1.63	0.98	6313.58	3778.29	432.60	578.07	840.61	59.19
9	-20.47	-12.68	1.69	4.31	-0.10	1.15	-4.95	-1.63	0.94	5742.85	3773.36	435.75	600.55	840.81	58.41
10	-21.56	-12.72	1.72	4.35	-0.10	1.17	-4.97	-1.62	0.94	6130.43	3782.50	445.49	531.89	840.50	59.26
Mean	-21.27	-12.70		4.34	-0.10		-5.21	-1.62		6017.73	3778.13		570.99	840.66	
Stand. Dev	0.85			0.41			0.22			237.23	4.58		20.57		
MPM	-21.65			4.15			-5.31			5910.98	3776.07		561.74		
Tdyn										2134.91					
Td										8647.66					

Table B.19: System IV, LC4

Seed #	Max Surge	Mean Surge	Std Surge	Max heave	Mean Heave	Std heave	Max Pitch	Mean Pitch	Std pitch	Max Line1 [kN]	Mean Line1 [kN]	Std Line1 [kN]	Max Line2 [kN]	Mean Line2 [kN]	Std Line2 [kN]
1	-19.20	-12.11	1.72	5.05	-0.10	1.35	-5.11	-1.63	0.90	5459.97	3632.64	442.71	649.56	852.39	56.58
2	-20.23	-12.11	1.70	4.78	-0.10	1.37	-5.28	-1.63	0.89	5749.07	3631.98	439.58	667.27	852.39	56.38
3	-20.14	-12.10	1.70	5.40	-0.10	1.37	-4.76	-1.62	0.89	5753.50	3631.94	440.56	639.00	852.40	57.13
4	-19.74	-12.10	1.69	4.74	-0.10	1.34	-5.65	-1.62	0.89	5490.27	3630.64	436.01	653.87	852.45	56.80
5	-20.87	-12.12	1.70	5.85	-0.10	1.36	-5.27	-1.63	0.89	5920.30	3635.18	440.33	650.30	852.16	57.19
6	-19.21	-12.13	1.71	5.01	-0.10	1.36	-4.54	-1.62	0.88	5476.30	3638.18	441.96	626.38	851.98	57.08
7	-19.50	-12.09	1.69	4.56	-0.10	1.36	-4.95	-1.63	0.88	5542.79	3627.79	436.21	664.68	852.73	56.06
8	-20.51	-12.12	1.69	4.93	-0.10	1.34	-5.59	-1.63	0.94	5769.62	3634.18	436.52	646.20	852.15	56.32
9	-20.23	-12.10	1.70	5.96	-0.10	1.35	-4.97	-1.63	0.89	5848.52	3631.06	439.77	637.65	852.31	56.87
10	-21.03	-12.11	1.72	5.36	-0.10	1.36	-5.15	-1.62	0.89	5998.10	3633.42	444.45	637.95	852.48	57.11
Mean	-20.07	-12.11		5.16	-0.10		-5.13	-1.62		5700.85	3632.70		647.29	852.34	
Stand. Dev	0.65			0.47			0.34			196.05			12.68		
MPM	-20.36			4.95			-5.28			5612.62			641.58		
Tdyn										1981.19					
Td										8189.59					

Table B.20: System IV, LC1IB

Seed #	Max Surge	Mean Surge	Std Surge	Max heave	Mean Heave	Std heave	Max Pitch	Mean Pitch	Std pitch	Max Line1 [kN]	Mean Line1 [kN]	Std Line1 [kN]	Max Line2 [kN]	Mean Line2 [kN]	Std Line2 [kN]
1	27.37	19.89	1.75	4.06	-0.13	1.20	5.45	1.78	0.98	368.47	565.75	50.45	4158.62	3203.34	217.09
2	27.99	19.87	1.70	4.19	-0.13	1.20	5.36	1.78	0.99	385.52	565.71	49.78	4195.33	3200.89	209.32
3	28.16	19.87	1.70	4.52	-0.13	1.21	5.42	1.77	0.96	334.53	565.92	50.72	4281.91	3201.40	210.50
4	27.71	19.87	1.71	3.98	-0.13	1.20	5.63	1.77	0.98	385.75	566.05	50.46	4222.67	3201.47	212.14
5	28.20	19.89	1.73	4.90	-0.13	1.21	5.21	1.78	0.97	374.75	565.86	50.55	4262.25	3203.55	213.92
6	29.35	19.92	1.75	5.10	-0.13	1.21	5.16	1.77	0.94	298.16	565.67	50.98	4425.68	3207.52	216.55
7	28.13	19.87	1.73	3.86	-0.13	1.21	5.53	1.78	0.97	343.43	566.07	49.99	4207.88	3200.64	214.65
8	28.37	19.90	1.71	4.72	-0.13	1.20	5.81	1.79	1.03	345.22	565.63	50.28	4299.19	3204.39	211.74
9	28.09	19.86	1.74	4.52	-0.13	1.20	5.20	1.78	0.98	344.15	565.85	49.95	4271.72	3200.06	215.47
10	27.93	19.91	1.79	4.43	-0.13	1.22	5.52	1.77	0.97	366.33	565.89	51.08	4242.13	3205.62	221.01
Mean	28.13	19.89		4.43	-0.13		5.43	1.78		354.63	565.84		4256.74	3202.89	
Stand. Dev	0.51			0.41			0.21			27.02			73.33	2.43	
MPM	27.90			4.25			5.34			342.47			4223.74	3201.80	
Tdyn													1020.85		
Td													1786.49		

System V

Table B.21: System V, LC1

Seed #	Max Surge	Mean Surge	Std Surge	Max heave	Mean Heave	Std heave	Max Pitch	Mean Pitch	Std pitch	Max Line1 [kN]	Mean Line1 [kN]	Std Line1 [kN]	Max Line2 [kN]	Mean Line2 [kN]	Std Line2 [kN]
1	-10.68	-7.35	0.59	0.01	-0.27	0.07	0.00	-7.24	1.54	6358.10	5425.56	219.52	1635.15	1814.30	52.73
2	-10.07	-7.35	0.57	0.00	-0.27	0.07	0.00	-7.24	1.52	6332.43	5425.07	214.29	1602.77	1814.25	52.50
3	-9.67	-7.31	0.57	0.00	-0.27	0.07	0.00	-7.15	1.50	6362.38	5408.82	213.43	1608.87	1816.80	51.81
4	-10.23	-7.32	0.56	0.00	-0.27	0.07	0.00	-7.17	1.50	6127.59	5412.10	208.56	1612.49	1816.24	51.59
5	-9.39	-7.33	0.57	0.00	-0.27	0.07	0.00	-7.20	1.52	6244.86	5417.62	212.51	1635.22	1815.46	52.04
6	-9.20	-7.30	0.57	0.00	-0.27	0.07	0.00	-7.14	1.48	6152.28	5407.64	210.75	1613.40	1816.81	52.98
7	-9.26	-7.34	0.57	0.00	-0.27	0.07	0.00	-7.23	1.50	6142.12	5421.87	212.15	1616.14	1814.70	51.91
8	-9.39	-7.37	0.58	0.01	-0.27	0.07	0.00	-7.27	1.55	6177.89	5431.72	214.12	1634.75	1813.28	52.27
9	-9.88	-7.35	0.58	0.01	-0.27	0.07	0.00	-7.25	1.53	6228.69	5426.87	216.24	1608.81	1814.01	52.79
10	-9.94	-7.32	0.58	0.03	-0.27	0.07	0.00	-7.19	1.53	6217.63	5415.74	217.09	1615.55	1815.74	52.54
Mean	-9.77	-7.33		0.01	-0.27		0.00	-7.21		6234.40	5419.30		1618.32	1815.16	
Stand. Dev	0.48			0.01			0.00			89.18			12.16		
MPM	-9.99			0.00			0.00			6194.27			1612.84		
Tdyn										778.65					
Td										8407.73					

Table B.22: System V, LC2

Seed #	Max Surge	Mean Surge	Std Surge	Max heave	Mean Heave	Std heave	Max Pitch	Mean Pitch	Std pitch	Max Line1 [kN]	Mean Line1 [kN]	Std Line1 [kN]	Max Line2 [kN]	Mean Line2 [kN]	Std Line2 [kN]
1	-7.59	-5.52	0.50	1.12	-0.20	0.40	-4.43	-2.98	0.35	5845.61	4816.17	234.49	1523.08	1931.91	107.26
2	-8.37	-5.51	0.48	1.20	-0.20	0.39	-4.58	-2.98	0.35	6143.97	4813.31	227.44	1459.01	1932.68	104.97
3	-8.00	-5.52	0.49	1.38	-0.20	0.40	-4.36	-2.98	0.35	6063.70	4816.09	231.57	1480.21	1931.99	106.10
4	-8.03	-5.51	0.49	1.14	-0.20	0.40	-4.20	-2.98	0.35	6045.75	4815.27	232.15	1463.64	1932.24	106.93
5	-7.88	-5.52	0.49	1.29	-0.20	0.40	-4.41	-2.99	0.35	5964.14	4817.08	233.61	1473.53	1931.81	106.71
6	-8.86	-5.52	0.51	1.69	-0.20	0.40	-4.58	-2.98	0.36	6447.55	4820.29	239.75	1427.70	1930.91	108.26
7	-7.84	-5.51	0.49	1.11	-0.20	0.40	-4.23	-2.98	0.35	5972.65	4812.99	233.92	1527.44	1932.89	106.49
8	-8.27	-5.52	0.49	1.38	-0.20	0.40	-4.33	-2.99	0.36	6178.37	4816.51	234.07	1458.90	1931.83	107.01
9	-8.32	-5.51	0.49	1.42	-0.20	0.39	-4.40	-2.99	0.35	6163.74	4812.68	230.37	1449.81	1932.92	104.77
10	-7.92	-5.52	0.50	1.42	-0.20	0.40	-4.27	-2.98	0.36	5955.34	4818.33	236.09	1518.97	1931.30	107.30
Mean	-8.11	-5.51		1.32	-0.20		-4.38	-2.98		6078.08	4815.87		1478.23	1932.05	
Stand. Dev	0.36			0.18			0.13			167.56			34.05		
MPM	-8.27			1.23			-4.44			6002.68			1462.91		
Tdyn										1186.81					
Td										8337.54					

Table B.23: System V, LC3

Seed #	Max Surge	Mean Surge	Std Surge	Max heave	Mean Heave	Std heave	Max Pitch	Mean Pitch	Std pitch	Max Line1 [kN]	Mean Line1 [kN]	Std Line1 [kN]	Max Line2 [kN]	Mean Line2 [kN]	Std Line2 [kN]
1	-11.46	-5.49	1.49	3.83	-0.20	1.15	-5.02	-1.50	0.92	7943.39	4914.80	705.74	941.37	1915.58	235.14
2	-12.07	-5.47	1.46	4.01	-0.20	1.15	-4.78	-1.50	0.91	7989.36	4909.25	692.54	925.07	1916.51	229.98
3	-12.96	-5.48	1.48	4.29	-0.20	1.16	-4.91	-1.49	0.91	8361.99	4914.10	703.27	893.80	1915.91	232.56
4	-11.84	-5.48	1.49	3.76	-0.20	1.15	-5.42	-1.49	0.93	7945.49	4912.53	704.15	947.77	1916.44	234.62
5	-13.28	-5.49	1.49	4.66	-0.20	1.16	-5.14	-1.50	0.93	8683.65	4916.44	704.93	952.04	1915.78	234.02
6	-13.26	-5.50	1.50	4.93	-0.20	1.16	-4.90	-1.49	0.90	8753.12	4921.84	711.40	850.47	1913.87	235.82
7	-11.91	-5.47	1.47	3.69	-0.20	1.15	-5.04	-1.50	0.92	7846.80	4908.58	698.35	1031.45	1917.31	232.49
8	-13.31	-5.49	1.47	4.53	-0.20	1.15	-5.50	-1.51	0.94	8594.96	4913.40	698.42	866.84	1915.74	232.30
9	-12.53	-5.47	1.48	4.21	-0.20	1.14	-4.83	-1.50	0.92	8163.60	4909.13	700.75	906.48	1916.75	231.30
10	-13.34	-5.49	1.49	4.22	-0.20	1.16	-4.90	-1.49	0.91	8716.48	4917.33	707.77	887.67	1914.84	234.42
Mean	-12.60	-5.48		4.21	-0.20		-5.04	-1.50		8299.88	4913.74		920.29	1915.87	
Stand. Dev	0.72			0.41			0.24			363.65			51.94		
MPM	-12.92			4.03			-5.15			8136.24			896.92		
Tdyn										3222.50					
Td										12027.24					

Table B.24: System V, LC4

Seed #	Max Surge	Mean Surge	Std Surge	Max heave	Mean Heave	Std heave	Max Pitch	Mean Pitch	Std pitch	Max Line1 [kN]	Mean Line1 [kN]	Std Line1 [kN]	Max Line2 [kN]	Mean Line2 [kN]	Std Line2 [kN]
1	-12.02	-5.19	1.67	4.93	-0.20	1.36	-5.01	-1.50	0.86	8084.86	4787.28	782.45	1059.13	1952.71	222.83
2	-12.21	-5.19	1.68	4.70	-0.20	1.37	-4.75	-1.50	0.86	8138.47	4786.47	785.58	1085.02	1952.86	221.07
3	-13.11	-5.19	1.68	5.30	-0.20	1.37	-4.78	-1.49	0.86	8607.54	4786.93	787.28	953.68	1952.93	223.36
4	-11.68	-5.19	1.66	4.64	-0.20	1.34	-5.35	-1.49	0.86	7955.41	4784.61	775.01	1043.70	1952.97	220.80
5	-13.53	-5.20	1.67	5.74	-0.20	1.36	-5.02	-1.50	0.87	8770.96	4789.62	784.20	1091.53	1952.15	222.51
6	-11.86	-5.20	1.68	4.88	-0.20	1.36	-4.48	-1.50	0.86	8041.34	4792.07	787.84	949.28	1951.40	224.68
7	-11.98	-5.19	1.66	4.45	-0.20	1.36	-4.54	-1.50	0.85	7937.90	4782.79	778.24	1088.84	1953.60	220.12
8	-12.95	-5.20	1.65	4.82	-0.20	1.35	-5.39	-1.51	0.90	8122.37	4787.89	775.71	1000.58	1951.95	218.92
9	-13.15	-5.19	1.66	5.86	-0.20	1.35	-4.72	-1.50	0.87	8754.45	4784.92	778.65	1118.98	1952.50	219.25
10	-13.46	-5.19	1.67	5.25	-0.20	1.36	-4.94	-1.49	0.86	8787.79	4787.35	784.88	1082.27	1952.50	223.24
Mean	-12.59	-5.19		5.06	-0.20		-4.90	-1.50		8320.11	4786.99		1047.30	1952.56	
Stand. Dev	0.71			0.47			0.31			361.71			59.79		
MPM	-12.91			4.85			-5.04			8157.34			1020.39		
Tdyn										3371.53					
Td										12123.26					

Table B.25: System V, LC1IB

Seed #	Max Surge	Mean Surge	Std Surge	Max heave	Mean Heave	Std heave	Max Pitch	Mean Pitch	Std pitch	Max Line1 [kN]	Mean Line1 [kN]	Std Line1 [kN]	Max Line2 [kN]	Mean Line2 [kN]	Std Line2 [kN]
1	13.95	10.13	0.91	0.12	-0.30	0.09	14.92	8.21	1.75	841.47	1065.63	77.32	5287.21	4582.96	173.92
2	13.68	10.13	0.89	0.07	-0.30	0.08	14.94	8.21	1.72	847.68	1065.57	77.45	5127.98	4582.38	168.52
3	13.81	10.05	0.87	0.09	-0.30	0.08	15.13	8.11	1.70	842.85	1068.98	77.88	5295.80	4567.96	167.31
4	13.68	10.07	0.86	0.03	-0.30	0.08	14.07	8.13	1.69	842.62	1068.15	77.21	5101.19	4571.16	163.77
5	12.74	10.10	0.89	0.21	-0.30	0.08	14.98	8.17	1.71	843.78	1067.22	78.71	5110.30	4575.74	168.13
6	13.27	10.05	0.87	0.11	-0.30	0.08	13.69	8.10	1.66	830.85	1069.27	79.00	5178.23	4566.36	165.59
7	12.77	10.12	0.87	0.06	-0.30	0.08	14.47	8.20	1.70	828.35	1065.94	76.47	5113.00	4580.41	166.03
8	13.28	10.16	0.89	0.14	-0.31	0.09	14.39	8.24	1.77	857.88	1064.26	76.69	5168.99	4588.46	168.32
9	13.40	10.14	0.89	0.05	-0.30	0.08	14.16	8.22	1.73	840.59	1065.18	77.78	5213.00	4584.29	170.01
10	13.09	10.08	0.90	0.05	-0.30	0.09	14.26	8.15	1.72	846.01	1067.79	77.87	5164.29	4573.88	172.05
Mean	13.37	10.10		0.09	-0.30		14.50	8.17		842.21	1066.80		5176.00	4577.36	
Stand. Dev	0.42			0.05			0.47			8.28			70.29		
MPM	13.18			0.07			14.29			838.48			5144.37		
Tdyn													570.36		
Td													6948.70		

System VI

Table B.26: System VI, LC1

Seed #	Max Surge	Mean Surge	Std Surge	Max heave	Mean Heave	Std heave	Max Pitch	Mean Pitch	Std pitch	Max Line1 [kN]	Mean Line1 [kN]	Std Line1 [kN]	Max Line2 [kN]	Mean Line2 [kN]	Std Line2 [kN]
1	-12.87	-9.83	0.70	0.05	-0.24	0.07	0.00	-7.40	1.58	5801.00	4975.68	208.51	1163.97	1379.51	52.06
2	-12.66	-9.83	0.68	0.02	-0.24	0.07	0.00	-7.40	1.56	5762.63	4975.22	202.49	1179.38	1379.48	52.22
3	-12.61	-9.77	0.68	0.02	-0.24	0.07	0.00	-7.31	1.54	5863.77	4958.77	201.46	1213.44	1381.70	52.11
4	-12.90	-9.78	0.67	0.03	-0.24	0.07	0.00	-7.33	1.54	5610.21	4962.19	196.86	1194.95	1381.21	51.24
5	-12.05	-9.80	0.68	0.08	-0.24	0.07	0.13	-7.36	1.55	5645.04	4967.60	201.91	1158.46	1380.55	51.51
6	-12.15	-9.77	0.67	0.02	-0.24	0.07	0.00	-7.31	1.51	5669.25	4957.53	199.56	1185.71	1381.78	50.94
7	-12.19	-9.82	0.68	0.03	-0.24	0.07	0.00	-7.39	1.54	5615.85	4972.05	200.24	1195.13	1379.91	50.17
8	-12.46	-9.85	0.68	0.07	-0.24	0.07	0.00	-7.44	1.59	5722.75	4982.02	202.35	1166.57	1378.64	49.66
9	-12.48	-9.83	0.69	0.03	-0.24	0.07	0.00	-7.41	1.57	5739.70	4977.13	204.67	1207.67	1379.25	51.96
10	-12.21	-9.80	0.69	0.08	-0.24	0.07	0.00	-7.35	1.56	5691.46	4965.73	205.86	1206.59	1380.79	53.29
Mean	-12.46	-9.81		0.04	-0.24		0.01	-7.37		5712.17	4969.39		1187.19	1380.28	
Stand. Dev	0.30			0.03			0.04			82.15			19.61		
MPM	-12.59			0.03			-0.01			5675.20			1178.36		
Tdyn										709.55					
Td										7701.92					

Table B.27: System VI, LC2

Seed #	Max Surge	Mean Surge	Std Surge	Max heave	Mean Heave	Std heave	Max Pitch	Mean Pitch	Std pitch	Max Line1 [kN]	Mean Line1 [kN]	Std Line1 [kN]	Max Line2 [kN]	Mean Line2 [kN]	Std Line2 [kN]
1	-9.92	-7.51	0.53	1.17	-0.17	0.40	-4.53	-3.05	0.35	5262.94	4352.80	186.12	1195.94	1482.96	78.43
2	-10.54	-7.51	0.51	1.24	-0.17	0.39	-4.60	-3.06	0.35	5421.49	4349.89	179.81	1195.48	1483.55	78.13
3	-10.36	-7.51	0.52	1.43	-0.17	0.40	-4.42	-3.06	0.35	5421.78	4352.67	182.34	1191.43	1482.95	78.61
4	-10.33	-7.51	0.52	1.19	-0.17	0.40	-4.26	-3.05	0.35	5385.00	4351.90	183.71	1138.60	1483.14	78.94
5	-10.28	-7.52	0.52	1.32	-0.17	0.40	-4.52	-3.06	0.35	5370.37	4353.68	185.20	1204.42	1482.77	79.48
6	-11.32	-7.53	0.54	1.73	-0.17	0.40	-4.62	-3.05	0.36	5736.42	4357.07	191.95	1096.52	1482.09	78.97
7	-10.14	-7.50	0.53	1.16	-0.17	0.40	-4.35	-3.05	0.35	5308.66	4349.35	186.43	1177.88	1483.69	78.24
8	-10.71	-7.52	0.53	1.41	-0.17	0.40	-4.41	-3.06	0.36	5496.93	4353.24	186.17	1086.44	1482.87	78.24
9	-10.39	-7.50	0.52	1.44	-0.17	0.39	-4.49	-3.06	0.35	5389.60	4349.26	183.43	1141.13	1483.73	78.73
10	-10.18	-7.52	0.53	1.45	-0.17	0.40	-4.30	-3.05	0.36	5290.90	4355.21	188.51	1173.17	1482.54	77.87
Mean	-10.42	-7.51		1.35	-0.17		-4.45	-3.06		5408.41	4352.51		1160.10	1483.03	
Stand. Dev	0.38			0.18			0.12			134.60			42.50		
MPM	-10.59			1.27			-4.50			5347.84			1140.97		
Tdyn										996.47					
Td										7402.09					

Table B.28: System VI, LC3

Seed #	Max Surge	Mean Surge	Std Surge	Max heave	Mean Heave	Std heave	Max Pitch	Mean Pitch	Std pitch	Max Line1 [kN]	Mean Line1 [kN]	Std Line1 [kN]	Max Line2 [kN]	Mean Line2 [kN]	Std Line2 [kN]
1	-13.76	-7.57	1.56	3.85	-0.17	1.15	-5.19	-1.54	0.93	6745.42	4453.91	552.27	902.16	1473.80	174.06
2	-14.67	-7.55	1.52	4.04	-0.17	1.14	-4.87	-1.54	0.92	7062.19	4448.63	538.55	865.73	1474.54	171.30
3	-15.63	-7.56	1.54	4.32	-0.17	1.16	-4.90	-1.53	0.91	7239.91	4453.02	546.49	830.55	1473.78	173.16
4	-14.49	-7.56	1.56	3.80	-0.17	1.15	-5.45	-1.53	0.93	6938.25	4451.93	550.94	905.93	1474.49	173.69
5	-15.92	-7.57	1.55	4.67	-0.17	1.16	-5.15	-1.53	0.93	7463.17	4455.44	549.21	796.91	1473.74	173.59
6	-16.03	-7.59	1.57	4.96	-0.17	1.16	-4.97	-1.53	0.91	7507.00	4461.26	555.73	861.73	1472.44	172.83
7	-14.84	-7.55	1.54	3.70	-0.17	1.15	-5.15	-1.54	0.93	6938.21	4447.34	545.16	836.48	1475.10	171.66
8	-16.32	-7.56	1.54	4.57	-0.17	1.14	-5.53	-1.54	0.96	7539.35	4452.76	545.16	848.22	1473.90	170.78
9	-15.02	-7.55	1.55	4.22	-0.17	1.14	-4.85	-1.54	0.93	7025.78	4448.40	548.46	783.06	1474.71	172.79
10	-15.95	-7.58	1.56	4.25	-0.17	1.16	-4.93	-1.53	0.92	7496.90	4456.85	554.65	831.58	1473.36	172.84
Mean	-15.26	-7.56		4.24	-0.17		-5.10	-1.53		7195.62	4452.95		846.23	1473.99	
Stand. Dev	0.83			0.41			0.24			290.83			39.85		
MPM	-15.64			4.05			-5.21			7064.74			828.30		
Tdyn										2613.70					
Td										10362.82					

Table B.32: System VII, LC2

Seed #	Max Surge	Mean Surge	Std Surge	Max heave	Mean Heave	Std heave	Max Pitch	Mean Pitch	Std pitch	Max Line1 [kN]	Mean Line1 [kN]	Std Line1 [kN]	Max Line2 [kN]	Mean Line2 [kN]	Std Line2 [kN]
1	-15.17	-12.57	0.56	1.21	-0.13	0.40	-4.71	-3.15	0.36	4716.83	3773.20	171.36	801.75	935.39	35.29
2	-15.72	-12.56	0.54	1.29	-0.13	0.39	-4.65	-3.15	0.35	4862.71	3769.88	163.67	787.34	935.52	35.02
3	-15.72	-12.57	0.54	1.46	-0.13	0.40	-4.52	-3.15	0.36	4952.61	3773.07	166.64	791.68	935.32	35.19
4	-15.58	-12.57	0.55	1.23	-0.13	0.40	-4.30	-3.15	0.36	4850.65	3772.31	168.06	794.96	935.47	35.07
5	-15.53	-12.58	0.55	1.37	-0.13	0.40	-4.60	-3.15	0.36	4849.54	3774.16	168.67	781.54	935.24	35.17
6	-16.52	-12.59	0.58	1.77	-0.13	0.41	-4.70	-3.15	0.36	5248.21	3778.01	177.50	786.15	935.08	36.39
7	-15.38	-12.56	0.56	1.19	-0.13	0.40	-4.50	-3.15	0.35	4789.50	3769.38	172.34	791.58	935.69	34.87
8	-16.03	-12.58	0.56	1.46	-0.13	0.40	-4.48	-3.15	0.36	5029.72	3773.86	171.23	784.60	935.36	35.00
9	-15.44	-12.56	0.55	1.50	-0.13	0.39	-4.62	-3.15	0.35	4752.51	3769.22	168.48	795.24	935.58	35.14
10	-15.34	-12.58	0.57	1.50	-0.13	0.41	-4.39	-3.15	0.36	4748.33	3775.93	174.78	798.55	935.26	35.22
Mean	-15.64	-12.57		1.40	-0.13		-4.55	-3.15		4880.06	3772.90		791.34	935.39	
Stand. Dev	0.39			0.18			0.13			161.16			6.44		
MPM	-15.82			1.32			-4.61			4807.54			788.44		
Tdyn										1035.92					
Td										6717.64					

Table B.29: System VI, LC4

Seed #	Max Surge	Mean Surge	Std Surge	Max heave	Mean Heave	Std heave	Max Pitch	Mean Pitch	Std pitch	Max Line1 [kN]	Mean Line1 [kN]	Std Line1 [kN]	Max Line2 [kN]	Mean Line2 [kN]	Std Line2 [kN]
1	-16.19	-9.32	1.69	4.97	-0.15	1.35	-5.02	-1.56	0.88	5979.39	4042.17	475.01	826.68	1237.67	118.33
2	-17.35	-9.32	1.68	4.73	-0.15	1.36	-5.09	-1.56	0.88	6305.67	4041.54	473.13	829.60	1237.74	118.25
3	-17.35	-9.32	1.68	5.32	-0.15	1.36	-4.77	-1.55	0.88	6349.35	4041.54	473.77	766.80	1237.68	118.21
4	-16.47	-9.31	1.67	4.67	-0.15	1.34	-5.56	-1.55	0.88	6020.69	4040.28	469.31	822.02	1237.91	118.59
5	-17.93	-9.33	1.68	5.78	-0.15	1.35	-5.15	-1.56	0.88	6482.17	4044.64	473.24	765.24	1237.25	119.17
6	-16.19	-9.34	1.69	4.94	-0.15	1.36	-4.52	-1.55	0.87	5972.17	4047.53	474.78	820.40	1236.95	119.81
7	-16.59	-9.30	1.67	4.48	-0.15	1.35	-4.76	-1.56	0.87	6063.81	4037.47	468.78	812.63	1238.25	117.73
8	-17.48	-9.33	1.67	4.86	-0.15	1.34	-5.54	-1.57	0.93	6291.20	4043.42	468.57	826.37	1237.27	118.22
9	-17.35	-9.31	1.68	5.88	-0.15	1.35	-4.78	-1.56	0.88	6410.01	4040.34	472.18	797.50	1237.55	118.24
10	-18.15	-9.32	1.69	5.29	-0.15	1.36	-5.07	-1.55	0.88	6571.22	4042.82	476.15	816.08	1237.68	118.04
Mean	-17.11	-9.32		5.09	-0.15		-5.02	-1.56		6244.57	4042.18		808.33	1237.60	
Stand. Dev	0.70			0.47			0.34			219.78			24.09		
MPM	-17.42			4.88			-5.18			6145.67			797.49		
Tdyn										2104.72					
Td										8938.08					

Table B.30: System VI, LC1IB

Seed #	Max Surge	Mean Surge	Std Surge	Max heave	Mean Heave	Std heave	Max Pitch	Mean Pitch	Std pitch	Max Line1 [kN]	Mean Line1 [kN]	Std Line1 [kN]	Max Line2 [kN]	Mean Line2 [kN]	Std Line2 [kN]
1	19.48	14.53	1.10	0.18	-0.28	0.08	15.20	8.34	1.77	667.97	795.60	38.59	4908.82	4263.74	166.97
2	19.22	14.52	1.07	0.12	-0.28	0.08	15.19	8.34	1.74	670.88	795.59	37.80	4783.70	4263.08	161.44
3	18.98	14.42	1.05	0.14	-0.28	0.08	15.31	8.24	1.72	669.21	798.37	37.40	4929.44	4248.29	159.19
4	18.84	14.45	1.04	0.04	-0.28	0.08	14.39	8.26	1.71	680.05	797.67	37.42	4763.77	4251.67	156.14
5	17.58	14.48	1.07	0.26	-0.28	0.08	15.14	8.30	1.73	688.60	796.90	38.22	4719.91	4256.31	161.29
6	18.29	14.41	1.05	0.15	-0.28	0.08	14.01	8.23	1.68	680.22	798.61	37.68	4856.90	4246.66	158.25
7	17.63	14.51	1.04	0.11	-0.28	0.08	14.58	8.33	1.72	660.99	795.93	37.02	4744.43	4261.22	157.74
8	18.33	14.56	1.07	0.18	-0.28	0.08	14.76	8.38	1.80	689.28	794.47	38.02	4829.96	4269.35	160.76
9	18.99	14.54	1.07	0.11	-0.28	0.08	14.44	8.35	1.75	665.97	795.23	37.79	4829.02	4265.16	162.22
10	18.57	14.46	1.09	0.10	-0.28	0.08	14.32	8.28	1.74	671.11	797.34	38.45	4791.11	4254.46	164.80
Mean	18.59	14.49		0.14	-0.28		14.74	8.31		674.43	796.57		4815.71	4258.00	
Stand. Dev	0.64			0.06			0.45			9.61			68.53		
MPM	18.30			0.11			14.53			670.10			4784.87		
Tdyn													530.32		
Td													6463.45		

System VII

Table B.31: System VII, LC1

Seed #	Max Surge	Mean Surge	Std Surge	Max heave	Mean Heave	Std heave	Max Pitch	Mean Pitch	Std pitch	Max Line1 [kN]	Mean Line1 [kN]	Std Line1 [kN]	Max Line2 [kN]	Mean Line2 [kN]	Std Line2 [kN]
1	-19.31	-15.22	0.71	0.21	-0.20	0.07	-15.07	-7.60	1.61	5354.90	4460.90	227.06	818.56	897.35	25.31
2	-19.43	-15.22	0.69	0.10	-0.20	0.07	-14.10	-7.60	1.59	5342.38	4460.43	220.13	812.75	897.31	26.12
3	-18.01	-15.16	0.69	0.09	-0.20	0.07	-14.14	-7.51	1.57	5436.38	4442.44	219.06	811.88	897.98	25.77
4	-19.45	-15.17	0.68	0.07	-0.20	0.07	-12.96	-7.53	1.57	5148.13	4446.24	213.91	808.81	897.84	25.98
5	-17.67	-15.19	0.70	0.22	-0.20	0.07	-14.07	-7.56	1.58	5229.98	4452.14	219.44	808.71	897.68	25.67
6	-17.74	-15.16	0.68	0.09	-0.20	0.07	-12.67	-7.50	1.54	5260.89	4441.15	216.89	803.80	898.02	26.70
7	-18.59	-15.21	0.68	0.06	-0.20	0.07	-13.39	-7.59	1.57	5175.20	4456.95	217.70	813.73	897.43	24.72
8	-19.08	-15.24	0.69	0.14	-0.21	0.07	-13.30	-7.63	1.63	5274.55	4467.88	220.48	815.68	897.07	26.44
9	-19.14	-15.22	0.70	0.12	-0.20	0.07	-13.48	-7.61	1.60	5335.82	4462.55	222.72	810.54	897.27	25.90
10	-19.01	-15.18	0.70	0.11	-0.20	0.07	-13.32	-7.55	1.59	5257.63	4450.13	223.86	806.76	897.75	25.44
Mean	-18.74	-15.20		0.12	-0.20		-13.65	-7.57		5281.59	4454.08		811.12	897.57	
Stand. Dev	0.70			0.06			0.70			87.45			4.35		
MPM	-19.06			0.10			-13.96			5242.24			809.17		
Tdyn										792.24					
Td										7176.72					

Table B.33: System VII, LC3

Seed #	Max Surge	Mean Surge	Std Surge	Max heave	Mean Heave	Std heave	Max Pitch	Mean Pitch	Std pitch	Max Line1 [kN]	Mean Line1 [kN]	Std Line1 [kN]	Max Line2 [kN]	Mean Line2 [kN]	Std Line2 [kN]
1	-19.00	-12.61	1.59	3.90	-0.13	1.15	-5.35	-1.59	0.94	6241.05	3877.58	522.38	666.68	934.01	72.50
2	-19.63	-12.59	1.54	4.09	-0.13	1.15	-5.00	-1.58	0.94	6761.13	3871.69	504.32	571.47	933.93	71.50
3	-20.58	-12.61	1.56	4.36	-0.13	1.16	-4.90	-1.57	0.93	7038.96	3876.51	514.00	585.24	933.87	72.47
4	-19.85	-12.60	1.58	3.84	-0.13	1.15	-5.41	-1.58	0.94	6725.27	3875.33	518.45	609.03	934.10	72.94
5	-21.03	-12.62	1.57	4.73	-0.13	1.16	-5.18	-1.58	0.94	7446.39	3878.93	518.65	597.05	933.85	73.05
6	-20.97	-12.63	1.59	5.02	-0.13	1.16	-5.16	-1.58	0.92	7415.22	3885.89	527.48	541.89	933.48	72.96
7	-20.18	-12.59	1.56	3.77	-0.13	1.16	-5.32	-1.58	0.94	6779.86	3870.40	515.31	575.06	934.44	72.25
8	-21.47	-12.61	1.56	4.62	-0.13	1.15	-5.54	-1.59	0.97	7561.22	3876.73	517.30	536.40	933.99	71.48
9	-19.80	-12.59	1.57	4.28	-0.13	1.15	-4.89	-1.58	0.94	6635.74	3871.43	518.48	599.78	933.93	71.31
10	-20.91	-12.62	1.60	4.31	-0.13	1.16	-4.97	-1.58	0.94	7393.70	3881.11	528.18	566.71	933.95	72.28
Mean	-20.34	-12.61		4.29	-0.13		-5.17	-1.58		6999.86	3876.56		584.93	933.96	
Stand. Dev	0.77			0.41			0.23			438.79			37.19		
MPM	-20.69			4.11			-5.28			6802.40			568.19		
Tdyn										2927.98					
Td										10163.49					

Table B.34: System VII, LC4

Seed #	Max Surge	Mean Surge	Std Surge	Max heave	Mean Heave	Std heave	Max Pitch	Mean Pitch	Std pitch	Max Line1 [kN]	Mean Line1 [kN]	Std Line1 [kN]	Max Line2 [kN]	Mean Line2 [kN]	Std Line2 [kN]
1	-18.72	-12.12	1.67	5.01	-0.13	1.35	-5.06	-1.59	0.89	6166.90	3727.66	530.05	671.68	943.74	73.65
2	-19.65	-12.11	1.66	4.75	-0.13	1.37	-5.22	-1.59	0.89	6671.74	3726.88	528.45	686.44	943.63	73.07
3	-19.76	-12.11	1.66	5.36	-0.13	1.37	-4.76	-1.58	0.89	6785.01	3726.90	529.76	661.02	943.64	73.72
4	-19.49	-12.11	1.65	4.72	-0.13	1.34	-5.62	-1.58	0.89	6196.10	3725.36	522.97	658.90	943.57	73.76
5	-20.29	-12.12	1.66	5.82	-0.13	1.36	-5.22	-1.59	0.89	7024.59	3730.20	530.56	663.36	943.40	72.88
6	-18.46	-12.13	1.67	4.97	-0.13	1.36	-4.52	-1.58	0.88	6124.30	3733.21	531.12	609.38	943.26	73.95
7	-19.23	-12.10	1.65	4.52	-0.13	1.35	-4.88	-1.59	0.88	6409.28	3722.74	524.46	667.08	944.01	72.08
8	-19.90	-12.12	1.65	4.88	-0.13	1.34	-5.59	-1.59	0.94	6724.03	3729.18	525.31	624.26	943.51	72.39
9	-19.67	-12.11	1.66	5.93	-0.13	1.35	-4.91	-1.59	0.89	6849.19	3725.97	528.43	653.48	943.64	72.90
10	-20.47	-12.12	1.67	5.33	-0.13	1.36	-5.13	-1.58	0.88	7187.87	3728.35	532.90	637.10	943.77	72.89
Mean	-19.56	-12.12		5.13	-0.13		-5.09	-1.58		6613.90	3727.64		653.27	943.62	
Stand. Dev	0.63			0.47			0.35			373.30			23.22		
MPM	-19.85			4.92			-5.25			6445.92			642.82		
Tdyn										2719.56					
Td										9605.17					

Table B.35: System VII, LC1IB

Seed #	Max Surge	Mean Surge	Std Surge	Max heave	Mean Heave	Std heave	Max Pitch	Mean Pitch	Std pitch	Max Line1 [kN]	Mean Line1 [kN]	Std Line1 [kN]	Max Line2 [kN]	Mean Line2 [kN]	Std Line2 [kN]
1	31.40	25.43	1.12	0.30	-0.23	0.08	15.31	8.40	1.75	303.56	468.97	55.86	4465.42	3862.20	152.06
2	31.33	25.43	1.08	0.22	-0.23	0.08	15.21	8.40	1.73	320.19	469.47	55.01	4361.86	3861.82	146.18
3	29.93	25.33	1.06	0.23	-0.23	0.08	15.32	8.30	1.70	289.54	474.78	53.23	4504.49	3848.28	144.37
4	30.46	25.35	1.05	0.11	-0.23	0.08	14.45	8.32	1.69	312.63	472.87	53.01	4352.99	3850.97	141.51
5	28.56	25.38	1.09	0.35	-0.23	0.08	15.12	8.35	1.71	317.46	471.03	54.29	4270.45	3855.03	146.72
6	29.25	25.32	1.06	0.22	-0.23	0.08	14.09	8.29	1.66	309.09	475.03	53.17	4418.53	3846.68	143.77
7	28.64	25.42	1.05	0.20	-0.23	0.08	14.53	8.38	1.70	319.37	470.22	54.25	4305.62	3860.14	142.21
8	29.27	25.47	1.08	0.24	-0.23	0.08	14.91	8.43	1.78	310.16	467.21	54.71	4396.35	3867.45	145.88
9	30.69	25.44	1.09	0.22	-0.23	0.08	14.50	8.41	1.73	309.72	468.73	54.58	4396.40	3863.70	147.37
10	30.12	25.37	1.11	0.21	-0.23	0.08	14.36	8.34	1.72	312.57	472.07	55.03	4336.16	3853.60	149.67
Mean	29.97	25.39		0.23	-0.23		14.78	8.36		310.43	471.04		4380.83	3856.99	
Stand. Dev	1.02			0.06			0.45			8.94			70.96		
MPM	29.51			0.20			14.58			306.40			4348.89		
Tdyn										-163.45			495.08		
Td										326.30			[HTML]C6EFCE5880.48		

System VIII

Table B.36: System VIII, LC1

Seed #	Max Surge	Mean Surge	Std Surge	Max heave	Mean Heave	Std heave	Max Pitch	Mean Pitch	Std pitch	Max Line1 [kN]	Mean Line1 [kN]	Std Line1 [kN]	Max Line2 [kN]	Mean Line2 [kN]	Std Line2 [kN]
1	-24.81	-19.34	1.17	0.39	-0.03	0.07	-14.72	-7.38	1.63	4923.09	4365.60	154.52	574.57	745.37	51.51
2	-24.61	-19.34	1.13	0.31	-0.03	0.07	-13.81	-7.38	1.61	4886.48	4365.00	149.07	592.10	745.44	49.78
3	-24.06	-19.23	1.11	0.29	-0.02	0.07	-14.02	-7.29	1.59	5004.52	4350.78	146.60	565.49	750.05	49.06
4	-24.30	-19.26	1.09	0.30	-0.03	0.07	-12.79	-7.31	1.58	4849.66	4353.90	143.28	606.16	748.96	48.47
5	-22.66	-19.29	1.13	0.33	-0.03	0.07	-13.95	-7.34	1.60	4813.70	4358.35	148.87	616.52	747.63	50.03
6	-23.31	-19.23	1.11	0.26	-0.02	0.07	-12.54	-7.28	1.56	4899.94	4349.68	146.83	576.26	750.32	49.52
7	-22.70	-19.32	1.10	0.26	-0.03	0.07	-13.27	-7.37	1.59	4818.25	4362.49	145.44	604.13	746.22	48.86
8	-23.24	-19.38	1.12	0.31	-0.03	0.07	-13.21	-7.41	1.65	4894.80	4371.05	148.18	586.40	743.51	49.82
9	-24.27	-19.35	1.13	0.31	-0.03	0.07	-13.21	-7.39	1.62	4889.98	4366.93	149.75	582.35	744.82	50.19
10	-23.75	-19.28	1.15	0.27	-0.03	0.07	-13.19	-7.32	1.61	4846.08	4357.08	151.73	601.58	748.05	50.87
Mean	-23.77	-19.30		0.30	-0.03		-13.47	-7.35		4882.65	4360.09		590.56	747.04	
Stand. Dev	0.77			0.04			0.65			56.10			16.33		
MPM	-24.12			0.28			-13.76			4857.40			583.21		
Tdyn										500.58					
Td										6544.12					

Table B.37: System VIII, LC2

Seed #	Max Surge	Mean Surge	Std Surge	Max heave	Mean Heave	Std heave	Max Pitch	Mean Pitch	Std pitch	Max Line1 [kN]	Mean Line1 [kN]	Std Line1 [kN]	Max Line2 [kN]	Mean Line2 [kN]	Std Line2 [kN]
1	-18.37	-15.05	0.68	1.38	0.04	0.40	-4.45	-2.93	0.35	4304.07	3820.65	102.38	749.36	938.92	38.58
2	-18.98	-15.03	0.64	1.47	0.04	0.40	-4.42	-2.93	0.35	4387.38	3818.21	96.49	717.01	939.81	36.07
3	-19.46	-15.05	0.65	1.64	0.04	0.40	-4.29	-2.93	0.35	4453.44	3820.67	98.38	695.65	938.89	36.67
4	-18.66	-15.04	0.66	1.40	0.04	0.40	-4.10	-2.93	0.35	4348.26	3820.11	99.55	731.75	939.13	37.27
5	-18.35	-15.05	0.66	1.55	0.04	0.40	-4.40	-2.93	0.35	4300.14	3821.43	99.62	756.85	938.61	37.28
6	-20.02	-15.08	0.71	1.95	0.04	0.41	-4.44	-2.93	0.36	4537.88	3824.44	106.18	669.79	937.36	39.92
7	-18.38	-15.03	0.70	1.37	0.04	0.40	-4.27	-2.93	0.35	4311.67	3817.84	104.01	749.46	940.08	39.03
8	-19.83	-15.05	0.68	1.64	0.04	0.40	-4.27	-2.93	0.36	4513.43	3821.33	101.73	684.32	938.67	38.18
9	-18.74	-15.03	0.66	1.68	0.04	0.39	-4.37	-2.93	0.35	4351.99	3817.72	99.51	733.82	939.97	37.21
10	-18.28	-15.07	0.71	1.68	0.04	0.41	-4.16	-2.93	0.36	4309.80	3822.90	105.03	753.58	938.07	39.57
Mean	-18.91	-15.05		1.58	0.04		-4.32	-2.93		4381.81	3820.53		724.16	938.95	
Stand. Dev	0.65			0.18			0.12			89.24			31.21		
MPM	-19.20			1.50			-4.37			4341.65			710.11		
Tdyn										521.12					
Td										5878.64					

Table B.38: System VIII, LC3

Seed #	Max Surge	Mean Surge	Std Surge	Max heave	Mean Heave	Std heave	Max Pitch	Mean Pitch	Std pitch	Max Line1 [kN]	Mean Line1 [kN]	Std Line1 [kN]	Max Line2 [kN]	Mean Line2 [kN]	Std Line2 [kN]
1	-23.97	-15.44	1.92	4.10	0.04	1.16	-5.12	-1.36	0.94	5109.76	3890.09	287.46	504.05	908.92	99.91
2	-24.20	-15.41	1.80	4.30	0.04	1.15	-4.73	-1.36	0.94	5118.83	3885.76	273.65	513.34	910.02	94.30
3	-25.99	-15.43	1.84	4.56	0.04	1.17	-4.71	-1.35	0.92	5422.50	3889.37	279.15	452.75	909.02	95.38
4	-24.53	-15.43	1.87	4.06	0.04	1.16	-5.17	-1.35	0.94	5202.18	3888.47	281.76	497.77	909.39	97.68
5	-25.09	-15.45	1.86	4.94	0.04	1.17	-4.97	-1.35	0.94	5283.75	3890.92	280.59	491.73	908.50	96.34
6	-27.01	-15.49	1.92	5.21	0.04	1.17	-4.92	-1.35	0.91	5559.37	3896.69	288.37	423.94	906.36	99.10
7	-24.67	-15.40	1.88	3.97	0.04	1.16	-5.05	-1.36	0.94	5192.47	3884.80	282.51	495.38	911.06	97.24
8	-26.50	-15.44	1.87	4.82	0.04	1.15	-5.34	-1.36	0.97	5468.92	3889.81	281.26	448.02	909.11	96.84
9	-24.15	-15.41	1.89	4.67	0.04	1.15	-4.63	-1.36	0.94	5189.72	3886.01	283.32	497.26	910.34	97.83
10	-25.17	-15.46	1.96	4.83	0.04	1.17	-4.68	-1.35	0.93	5298.75	3893.36	292.58	485.57	908.13	101.50
Mean	-25.13	-15.43		4.55	0.04		-4.93	-1.35		5284.63	3889.53		480.98	909.08	
Stand. Dev	1.05			0.42			0.24			153.12			29.08		
MPM	-25.60			4.36			-5.04			5215.72			467.90		
Tdyn										1326.19					
Td										7377.22					

Table B.40: System VIII, LC1IB

Seed #	Max Surge	Mean Surge	Std Surge	Max heave	Mean Heave	Std heave	Max Pitch	Mean Pitch	Std pitch	Max Line1 [kN]	Mean Line1 [kN]	Std Line1 [kN]	Max Line2 [kN]	Mean Line2 [kN]	Std Line2 [kN]
1	32.53	26.06	1.97	0.53	-0.09	0.08	15.48	8.35	1.81	182.82	224.92	11.78	4052.54	3607.64	136.39
2	31.78	26.05	1.88	0.54	-0.09	0.08	15.34	8.35	1.79	185.27	224.88	11.29	4003.80	3606.72	130.38
3	32.96	25.84	1.82	0.45	-0.09	0.08	15.41	8.25	1.75	188.00	225.92	11.06	4091.71	3591.89	126.12
4	32.46	25.89	1.81	0.45	-0.09	0.08	14.73	8.27	1.75	191.51	225.65	11.29	4043.53	3595.58	125.24
5	31.19	25.95	1.89	0.44	-0.09	0.08	15.14	8.31	1.77	185.64	225.42	11.55	3960.69	3599.69	130.78
6	32.11	25.82	1.85	0.42	-0.09	0.08	14.36	8.24	1.72	188.85	226.07	11.40	4032.70	3590.53	128.22
7	31.60	26.03	1.81	0.38	-0.09	0.08	14.56	8.34	1.75	189.00	224.93	10.91	3996.24	3605.10	125.39
8	31.57	26.14	1.84	0.40	-0.09	0.08	15.29	8.39	1.84	189.16	224.40	11.39	4001.25	3613.05	127.46
9	32.99	26.08	1.87	0.54	-0.09	0.08	14.66	8.36	1.79	188.35	224.72	11.31	4090.47	3608.76	129.88
10	31.82	25.94	1.92	0.44	-0.09	0.08	14.52	8.29	1.77	191.20	225.54	11.66	4005.87	3598.68	133.10
Mean	32.10	25.98		0.46	-0.09		14.95	8.31		187.98	225.25		4027.88	3601.76	
Stand. Dev	0.61			0.06			0.43	0.05		2.70			42.37		
MPM	31.83			0.43			14.76	8.29		186.77			4008.81		
Tdyn													407.05		
Td													5394.63		

Table B.39: System VIII, LC4

Seed #	Max Surge	Mean Surge	Std Surge	Max heave	Mean Heave	Std heave	Max Pitch	Mean Pitch	Std pitch	Max Line1 [kN]	Mean Line1 [kN]	Std Line1 [kN]	Max Line2 [kN]	Mean Line2 [kN]	Std Line2 [kN]
1	-21.94	-14.58	1.81	5.20	0.04	1.36	-4.81	-1.37	0.89	4853.81	3775.05	278.84	612.30	954.34	95.22
2	-22.99	-14.58	1.77	5.16	0.04	1.37	-4.99	-1.37	0.90	4988.91	3774.45	275.20	572.05	954.42	93.17
3	-23.32	-14.58	1.78	5.58	0.04	1.37	-4.60	-1.36	0.89	4992.77	3774.47	275.93	582.36	954.50	93.21
4	-22.08	-14.57	1.76	4.91	0.04	1.34	-5.35	-1.36	0.89	4854.73	3773.39	272.81	614.30	954.74	92.77
5	-24.03	-14.60	1.78	6.02	0.04	1.36	-5.01	-1.37	0.89	5124.96	3776.90	275.85	542.48	953.47	93.31
6	-22.44	-14.61	1.79	5.16	0.04	1.37	-4.37	-1.36	0.88	4921.05	3779.28	277.14	584.39	952.55	94.05
7	-22.95	-14.55	1.77	4.72	0.04	1.36	-4.64	-1.37	0.88	4982.66	3771.29	273.02	577.76	955.75	92.55
8	-23.90	-14.59	1.78	5.67	0.04	1.35	-5.33	-1.38	0.94	5105.43	3776.49	273.91	556.25	953.81	93.02
9	-23.21	-14.57	1.79	6.13	0.04	1.35	-4.64	-1.37	0.89	5087.50	3774.15	276.27	576.95	954.71	94.01
10	-24.15	-14.59	1.82	5.52	0.04	1.37	-4.83	-1.36	0.89	5213.31	3775.81	280.02	523.55	954.12	95.45
Mean	-23.10	-14.58		5.41	0.04		-4.86	-1.37		5012.51	3775.13		574.24	954.24	
Stand. Dev	0.78			0.46			0.32			119.03			28.18		
MPM	-23.45			5.20			-5.00			4958.95			561.56		
Tdyn										1183.82					
Td										6979.35					

Olav Røthe Kyte

Design of Mooring Systems For Floating Wind Turbines in Shallow Wate

NTNU
Norwegian University of
Science and Technology